A STUDY OF THE USE OF STATISTICAL TURBULENCE PARAMETERS IN CORRELATING AXIAL DISPERSION DATA IN THE CENTRAL CORE OF AIR FLOWING IN A PIPE.

by

DOUGLAS IAN EXALL M.Sc.(Eng.) (Natal)

Submitted in partial fulfilment of the requirements for the degree of Doctor of Philosophy in the Department of Chemical Engineering at the University of Natal, Durban.

October, 1970.

ACKNOWLEDGEMENTS.

I would like to express my sincere gratitude to Professor E.T. Woodburn for his guidance and continued interest in supervising this project.

Thanks are also expressed to Dr. R.P. King for many helpful discussions and suggestions.

The willing co-operation of Messrs. D. Penn, E. Magnus, J. Botha, A. Achurch, N. Brokensha and G. Vath in constructing the apparatus is much appreciated.

The financial support of this project by the South African Atomic Energy Board is gratefully acknowledged.

Finally, special thanks are due to my wife, Birgit, for her patience and encouragement in the course of this work.

The work described in this dissertation was performed in the Department of Chemical Engineering at the University of Natal, Durban during the period September, 1967 to September, 1970.

D.I. EXALL.

LIST OF CONTENTS.

LIST OF CONTENTS (contd.)

LIST OF FIGURES.

LIST OF TABLES.

LIST OF PLATES.

SYNOPSIS

The longitudinal fluctuations at a point in the core of air flowing through a 15 cm. diameter pipe at a mean centerline velocity of 13.4 and 29.5 m/sec. were measured with a hot-wire anemometer. This signal, after analog to digital conversion, was stored in the form of digital samples on an ICT computer drum storage device. This method of data recording includes the effect of all eddy frequencies from DC upwards and the presence of large, slow eddies in the longitudinal direction became apparent in the subsequent autocorrelations.

The longitudinal dispersion of a tracer material injected on the axis of the pipe was measured over short distances with pulses of approx. 20 msecs. duration of radio-active Krypton-85, detected at two downstream stations by small surface-barrier radiation detectors. By varying the separation of these two stations, an asymptotic mixing coefficient was established which was very much greater than the corresponding transverse mixing coefficient measured by other workers.

The method proposed by Philip(4) for the prediction of the Lagrangian time autocorrelation from the Eulerian velocity measurements was examined with the correlation data of Baldwin and the data obtained in this investigation. The method applied to the unfiltered correlation data in the present measurements in a non-isotropic field to predict a longitudinal turbulent Peclet no. was found to predict a value in the region measured experimentally. When the present velocity data was filtered to remove the low-frequency components and give a turbulence intensity equal to that measured in a radial direction in previous dispersion measurements, the mixing coefficient predicted with Philip's method was found to agree very well with the transverse mixing coefficient reported in these investigations. A value is also suggested for the longitudinal Peclet number in the absence of the low-frequency fluctuations.

CHAPTER 1.

1.1 Introduction.

The study of the dispersion of a passive scalar in near-isotropic turbulence fields has been of interest for some considerable time. Taylor, in 1921 (1), developed his theory of diffusion by continuous movements and obtained an expression for the rate of dispersion of a marking property such as heat or a tracer material introduced into the isotropic turbulence field. This expression is most usually written in the form:

$$\overline{X^2}(t) = 2\overline{u^2} \int_0^t \int_0^{\tau_1} R(\tau) d\tau d\tau_1 \qquad (1.1)$$

where $R(\tau)$ is the Lagrangian autocorrelation function on the velocity obtained by following one particular fluid particle on its meandering path while it is subjected to the random velocity fluctuations in the turbulence field, repeating this for many particle releases, and then taking the mean of the velocity covariance $u_i(0)u_i(\tau)$ over all realizations to give

$$R(\tau) = \frac{\overline{u(0)u(\tau)}}{\overline{u^2}} \qquad (1.2)$$

The direct measurement of this function poses many practical difficulties if it is, in fact, even possible.

A more fruitful approach, lacking an exact theoretical treatment, is to examine experimentally the time dependence of the variance $\overline{X^2}(t)$ which is physically more susceptible to measurement. Many workers have

adopted this approach and have measured the radial dispersion of a tracer material injected continuously from a near-point source, or the dispersion of heat from a line source normal to the direction of mean flow in a pipe. These measurements have established a Peclet number based on the radial mixing coefficient ranging between approximately 600 and 1200, with the majority around 850.

It is usually assumed that the turbulence field in the core of a medium flowing at high velocity in a pipe is nearly isotropic and homogeneous in the longitudinal direction. It has, however, been found that the statistical properties of the turbulence in the radial and longitudinal directions under these conditions show some discrepancies. Laufer (2), for instance, found that the measured spectra of the velocity fluctuations at a fixed point showed a low frequency deficiency in the radial direction compared with the longitudinal fluctuation spectrum or the radial fluctuation spectrum calculated using isotropic relations, even at very high Reynolds numbers of 500 000 : Baldwin (17) measured a turbulence intensity about 20% higher in the longitudinal direction than the radial direction.

An investigation of the assumption of the approach to isotropy in the core of pipe flow would thus appear to be of value, particularly as the contribution of turbulent mixing to the longitudinal dispersion in flow through a pipe has usually been regarded as negligibly small compared with the effect of the velocity profile, mainly on the basis of the radial dispersion measurements described.

1.2 Scope of this Investigation.

The aims of this investigation may be stated as:

a) To measure the longitudinal velocity fluctuations at a fixed point on the centerline of a pipe through which air is flowing at a high velocity, and to record these fluctuations without loss of any frequency component present in the signal up to the maximum frequency expected to be significant at the level of turbulence considered. This has been estimated to be of the order of 5000 Hz. for the velocities in the region considered (49).

b) To measure the longitudinal dispersion of a tracer material, introduced into the pipe on the centerline, over a distance short enough that the velocity profile in the pipe does not affect the longitudinal mixing, and to establish a value for the longitudinal turbulent mixing coefficient and hence a true longitudinal Peclet number, which may be compared with that measured by previous workers in the radial direction.

c) To examine the relationship postulated by Philip (4) to predict the form of the Lagrangian velocity auto-correlation from Eulerian measurements in an isotropic, homogeneous turbulence field and to compare the value predicted for the longitudinal mixing coefficient by this model with the value experimentally measured.

1.3 Review of Previous Work.

The large volume of theoretical and experimental work in the field of turbulence precludes an exhaustive general survey: only those publications of particular

relevance to the present investigation will be discussed here. The definition of turbulence terms such as isotropy, homogeneity, integral scales etc. are included in the Appendix.

The two flow regions which have been thought to most closely approach isotropy have been the region behind grids arranged normal to the direction of flow, and the core of high velocity flow through a pipe, The former region is complicated by the decay of the turbulence with increasing distance from the grid and the preference in the measurement of Lagrangian parameters has been for the central core of the flow in a pipe.

Much work has been done in determining the rate of dispersion of tracer materials in a direction transverse to the direction of mean flow - essentially a Lagrangian measurement. Hot-wire anemometer data has also been established for a single-point measurement and the two-point measurement where the two probes are separated in space. There appears, however, to have been little progress in establishing a general relationship between the two types of measurement: the practical approach of Mickelsen (16) and Baldwin (17) provides a method for estimation of the transverse Lagrangian parameters from the longitudinal Eulerian measurements. Philip's theoretical relationship between the Eulerian and Lagrangian measurements, if confirmed, would provide a very useful general method for the estimation of Lagrangian parameters.

1.3.1 Previous Dispersion Measurements.

Taylor's work in the theory of turbulence (1, 5) has formed the basis for much of the subsequent work. As will be shown in the following chapter, his expression for the variance, equation (1.1), may for large times be written as $\overline{X^2}(t) = 2Et$ where E is a mixing coefficient analogous to the molecular diffusivity D in the Einstein expression describing the Brownian motion, $\overline{S^2} = 2Dt$, where S is the particle displacement. This simplification is most convenient in practical descriptions of turbulent dispersion and considerable effort has been devoted to the determination of the parameter E. The two methods generally used have, as far as is known, both considered dispersion in a direction normal to that of the mean flow: the first method has been to release a marking substance continuously from a point source on the axis of the channel and determine the steady-state radial dispersion $\overline{Y^2}$ as a function of the distance from the point of release which, besides giving the approximate form of $\overline{Y^2}$ for short times, has also for large times yielded a value for E. The second method, basically identical and used in the flow of air, has been to study the dispersion of heat behind a heated wire stretched across the channel normal to the direction of flow: this method is not suitable for dispersion measurements at large time due to the rapid dissipation of the heated air. Both these methods have been confined to what has been believed to be the isotropic turbulence field in the core of the channel.

Towle and Sherwood (6), in 1939, injected carbon dioxide and hydrogen continuously on the centerline of a

duct through which air was flowing and sampled at various distances from the source with a series of 21 sampling tubes arranged on a diameter: they found a Peclet number at large separation from the source of 750 for the case of a velocity of 11.77 m/sec. in a 15.24 cm. diameter duct, and an average value for high Reynolds number of N_{Pe} = 850. (Peclet no. UL/E is to be considered calculated based on the centerline velocity and the pipe diameter). Their measurements under these conditions extended to a distance of 216 cm. from the injector with no apparent increase in the dispersion due to the velocity profile in the pipe. They also noted no measurable difference in the rate of dispersion of the two gases.

Kalinske and Pien (7) studied the transverse dispersion of droplets of immiscible liquid injected into water flowing in an open channel and obtained values for $\overline{Y^2}(t)$ from a series of photographs, but the method was abandoned as too laborious in favor of a continuous injection of a mixture of hydrochloric acid and alcohol with sampling on a cross-stream traverse downstream. From the measured curve of the displacement variance as a function of distance downstream, the second derivative was calculated to give $R(\tau)$ which was shown to agree quite well with the form $R(\tau) = e^{-\tau/T}$ where T= a constant. The variance versus distance curve showed appreciable variation and the errors in calculating $\frac{d^2\overline{Y^2}}{dX^2}$ are probably large.

Townsend (8) developed a method for the almost instantaneous production of heat spots in air in a turbulence field in a square channel behind a grid, but the

method could only be used for short distances from the source and low Reynolds numbers due to the rapid dissipation of the small quantities of heat.

Uberoi and Corrsin (10) examined the transverse dispersion behind a line source of heat in air in a square channel behind a grid. Following Taylor (5), they assumed that the molecular and turbulent diffusion were statistically independent processes and the displacement variances due to the two effects were additive. Townsend (11) made similar measurements behind a line source of heat and presented data on the displacement variance as a function of distance, concluding that..... "the behavior of the single-particle Lagrangian correlation function for appreciable time intervals cannot be obtained with any accuracy from measurements of the heat-wake." He was able to show that the high values of the turbulent intensity $\overline{(v^2)}^{\frac{1}{2}}/U$ obtained by Uberoi and Corrsin from the heat wake were probably due to oscillation of the wire stretched across the pipe. He examined in some detail the relationship between the dispersion of a fluid particle and the dispersion as measured behind a line source, and showed that the mechanisms of molecular and turbulent dispersion were not statistically independent, obtaining an expression which showed the interaction for small times increases the dispersion over that obtained if the effect on the displacement variance were additive:

$$S^2 = \overline{Y^2} + 2D(t-t_o) + \frac{28}{45} D\omega^2 (t-t_o)^3 \text{ to } O(t-t_o)^3$$

where ω is the vorticity of the turbulence.

Although the treatment was for small times only, Townsend and Batchelor and Townsend (13) suggested that even for larger times, the accelerated diffusion would have an effect which was appreciable. Mickelsen (14) examined this region in Townsend's actual apparatus by injecting carbon dioxide and helium into air in a manner similar to Towle and Sherwood, and he found that, within the experimental error, the simple correction for molecular diffusion

$$\overline{Y^2} = S^2 - 2Dt$$

was sufficient to bring both sets of data into agreement. It should be noted, however, that his injection velocity for the carbon dioxide experiments was a factor of 4 or 5 times the stream velocity in order to obtain measurable quantities of tracer.

On the basis of these results, Saffman (12) re-examined the problem of accelerated diffusion and showed that there was a fallacious assumption in Townsend's derivation in that the instantaneous centroid of the marking substance actually lags behind the fluid particle originally coincident with it, and even though the interaction increases the dispersion relative to the centroid, the net effect is to reduce the dispersion relative to the origin:

$$S^2 = \overline{Y^2} + 2D(t-t_o) - \frac{1}{9}D\omega^2(t-t_o)^3 \quad \text{to} \quad O(t-t_o)^3$$

It should be emphasized that both analyses were for small time only. Saffman postulates a relationship for large time which shows that for high Reynolds number

the effect of the interaction term becomes greater than the molecular diffusion term, but this has not been experimentally verified. The data of Flint, Kada and Hanratty (25) supports the idea that for practical purposes in the region considered in tracer experiments and for tracer materials with Schmidt numbers no smaller than considered in these cases, the mechanisms of turbulent and molecular diffusion are statistically independent.

Flint, Kada and Hanratty (25) studied the lateral dispersion of carbon dioxide and hydrogen in air, and potassium chloride in water, in a 3-in. diameter pipe. It was found that the displacement variance for the two gases in air could be brought into approximate agreement by the correction $\overline{Y^2} = S^2 - 2Dt$. By assuming three different forms for the Lagrangian correlation coefficient

$$R(\tau) = \exp(-\tau/T_L)$$

$$R(\tau) = \exp(-\frac{\pi}{4}\,\tau^2/T_L{}^2)$$

and $$R(\tau) = 1 - \frac{\tau}{2}\,T_L \qquad \text{for} \quad 0 \leq \tau \leq 2T_L$$

$$R(\tau) = 0 \qquad \text{for} \quad \tau \geq 2T_L$$

they showed that all forms closely predicted the short time behavior of the measured diplacement variance. Fitting these forms to the experimental data resulted in values for the intensity $(\overline{v^2})^{\frac{1}{2}}/U$ which were all higher than previously found with hot-wire anemometers, which they attributed to injector interference of the flow field. Their results also showed that the linear dependence of $\overline{Y^2}$ with distance downstream extended to a distance of

8 pipe diameters from the source before the velocity profile in the pipe appeared to have an effect on the results; these being obtained in the range $9700 \leqslant N_{Re} \leqslant 87\ 000$. From the asymptotic slope, values for the turbulent diffusivity E were calculated, and presented on a plot of reciprocal Peclet number as a function of Reynolds number. This showed that above a N_{Re} of approximately 50 000, the Peclet number was a constant at a value of about 1200.

Malengé and Gosse (27) examined the lateral dispersion of potassium permanganate solution in water flow in a 10.2 cm. diameter Pyrex glass pipe in the range $10\ 000 \leqslant N_{Re} \leqslant 100\ 000$. Their work differed from that of Towle and Sherwood, and Flint et al, in that the injector consisted of four 0.96 mm. diameter tubes arranged in the form of a cross, all directed towards the axis, the position of each tube and the injection pressure being varied to give a near-point source with a relatively small disturbance of the flow by the injector. The dispersion coefficient E obtained was found by a method which was, in effect, $\overline{Y^2} = 2EX/U$, neglecting the correction term for small time, and was hence slighly low. The Peclet number for the higher Reynolds number was about 780. These values were later corrected by Groenhof (28) to obtain values of $N_{Pe} = 630$.

Becker, Rosensweig and Gwozdz (18) used the light-scattering properties of an oil-fog injected continuously on the axis of an 8-in. diameter pipe to measure radial dispersion at very high Reynolds numbers from 480 000 to 684 000 in air. The optical probe directed

a beam of light across the channel and measured, at right-angles to the beam, the light scattered by the fog, the only disturbance of the flow thus coming from the small 2.8 mm. diameter injector. From the data for small time, a value of the radial intensity $(\overline{v^2})^{\frac{1}{2}}/U$ of 0.0284 was obtained which agreed very well with the published values of Baldwin and Walsh (20). The value of the Peclet number they obtained from the data at large times as $N_{Pe} = 852$.

Boothroyd (34) used hydrogen as tracer material in studying the radial dispersion in air in 2-in. and 3-in. diameter pipes in the range $35\ 000 \leqslant N_{Re} \leqslant 80\ 000$, and obtained a radial intensity from the displacement curve at short time of 0.041 at $N_{Re} = 80\ 000$, but the results were scattered. The Peclet number was found to be approximately 760 at $N_{Re} = 80\ 000$.

Groenhof (28) measured the radial dispersion of sodium chloride solution in water in a 2-in. diameter pipe with an injection and detection apparatus similar to Malengé and Gosse, in the range $25\ 800 \leqslant N_{Re} \leqslant 74\ 900$. No correction for molecular diffusion was necessary and the average Peclet number based on the centerline velocity was about 620 at $N_{Re} = 74\ 900$. The results were presented as a reduced eddy diffusivity of mass

$$a_D = \frac{E_D}{U^* d}$$

where U^* is the friction velocity calculated from the Blasius equation for the wall shear stress τ_w where $U^* = (\tau_w/\rho)^{\frac{1}{2}}$, and this function a_D retained an essentially

constant value over the range of Reynolds numbers studied. Analogous to a_D, a reduced eddy kinematic viscosity and reduced eddy thermal diffusivity

$$a_M = \frac{E_M}{U^*d} \qquad \text{and} \qquad a_H = \frac{E_H}{U^*d}$$

respectively, were defined and values were obtained from the data of previous workers (6,20,27,2, etc.). This showed that in the central portion of steady turbulent flow in a pipe or channel a_M, a_H, and a_D were independent of N_{Re} for $N_{Re} > 20\,000$.

Defining eddy Prandtl and Schmidt numbers as

$$Pr_T = \frac{E_M}{E_H} = \frac{a_M}{a_H} \qquad \text{and} \qquad Sc_T = \frac{E_M}{E_D} = \frac{a_M}{a_D} \quad ,$$

these parameters are assumed equal to 1 as a consequence of the assumption of complete analogy of eddy momentum transfer and heat or mass transfer. The independence of a_M, a_D, and a_H with Reynolds number is evidence for this analogy. Groenhof showed that based on experimental data, values in water and air flows of $a_M = 3.2 \cdot 10^{-2}$, and values in air flows for a_H and a_D of the same value, indicated that Pr_T and Sc_T were equal to 1 in the central region of gas flow in a pipe when the Prandtl and Schmidt numbers, N_{Pr} and N_{Sc} , were close to 1. Based on the values of a_D found in water flow in a pipe by Malengé and Gosse, and Groenhof of $3.9 \cdot 10^{-2}$ and $4.0 \cdot 10^{-2}$ respectively, the value of Sc_T under these conditions is found to be 0.8 .

Assuming that the eddy diffusivities measured in water in these cases were not affected by molecular diffusion (N_{Sc} of tracers approx. 750), Groenhof postulates

that these measured values of E_D are in fact equal to the true eddy diffusivity of the fluid, E, and that $\frac{E_M}{E}$ would have the same value in liquid or gas flow. The apparent complete analogy of momentum and heat or mass transfer with the combined effect of eddy and molecular diffusion would then be due to the fact that the N_{Sc} and N_{Pr} numbers are in general about 1 in a gas.

There would appear, however, to be an inconsistency in this argument if one considers the results of Becker, Rosensweig and Gwozdz (18) who used an oil fog with very high Schmidt number to obtain a value of $a_D = 3.2 \cdot 10^{-2}$ in air.

1.3.2 Previous Eulerian or Anemometer Measurements.

Laufer (2) conducted hot-wire anemometer measurements in a 10-in. diameter pipe at Reynolds numbers of 50 000 and 500 000 in an apparatus carefully designed to establish stable flow conditions. The frequency analysis of this data showed a marked low frequency deficiency in the radial direction spectrum measured when compared with that calculated from the longitudinal spectrum using isotropic relations. Laufer concluded that closer examination of the turbulent energy equations, and particularly of the pressure terms, for turbulent flow with considerable experimental work would be necessary to examine the reasons for this deficiency.

Martin and Johanson (26) obtained single-point hot-film anemometer data in water flow in a 6-in. diameter pipe in the range $19\,000 \leq N_{Re} \leq 160\,000$ by photographing

samples of the fluctuations on an oscilloscope screen and reading directly the values of the instantaneous velocity from the photographs. This method overcame the insensitivity of most conventional electronic instrumentation to the low frequency fluctuations encountered at N_{Re} less than 200 000, if it is accepted that the average of the autocorrelations performed on the discontinuous samples was a close approximation to the true correlation coefficient. Difficulty was experienced with anemometer drift and the individual data was scattered. Eulerian integral length scales were presented as a function of N_{Re}, and the single result on the spectral energy of Sandborn at N_{Re} = 25 000 was used to calculate a value for this parameter: the value was in approximately the same range, if slightly low.

Patterson and Zakin (29) measured hot-film anemometer data in organic solvents in 1-in. and 2-in. diameter pipes in the range $8\,000 \leqslant N_{Re} \leqslant 200\,000$. Corrections were made for non-linear frequency response of the electronic and recording apparatus in the range 10 Hz. to 10 000 Hz. and no difficulty was found with anemometer drift in the non-conducting fluids. The longitudinal intensity $(\overline{u^2})^{\frac{1}{2}}/U$ obtained was higher than that obtained in air by Laufer (2) and Sandborn (30) and considerably higher than the values obtained by Martin and Johanson: the average at N_{Re} = 100 000 of 0.035 was in the range measured by Baldwin in air (17). The diameter of the pipe was also found to influence the result with lower intensities in the smaller pipe. Turbulent energy spectra were presented which were checked

with the spectra measured directly without recording, which showed good agreement except for attenuation below 15 Hz. Integral length scales were calculated from the spectra using the relationship $U = 0.8U_{\Sigma}$ for the convection velocity, and it was shown that the signal attenuation below 15 Hz. caused a deficiency in the integral length scale of 10 to 20%.

Frenkiel and Klebanoff (31) have developed a method for the digital recording of turbulence data which they used for the study of higher-order correlations in the turbulence field behind a grid in a large 1.37 m. wind-tunnel, and obtained correlation curves on 160 020 data points recorded at a time interval of approximately 80 μsecs. over 12.5 secs. The signal from the hot-wire anemometer was recorded in analog form on a tape together with a 12 800 Hz. timing signal; the tape was then replayed at a lower speed, allowing digitising of the signal. The autocorrelation performed on this signal was found to approach more closely the monotonic asymptote to the zero axis expected for this function. Despite the long (12.5sec) recording time for each sample, some scatter was found in the amplitude of this function which led the authors to speculate on a possible non-stationarity of the turbulence field:

> "..... the very precision of the analysis of digital techniques brings out what appears to be a "meteorology" of the wind-tunnel flow which cannot easily be observed with the conventional hot-wire anemometer."

The space correlation coefficient obtained with the transformation $X = Ut$ corresponded very well with the

experimental values measured by Favre et al (32) and Stewart (33), also in grid-generated turbulence.

1.3.3 Previous Work Relating Eulerian and Lagrangian Measurements.

Mickelsen (16) described a method of correlating hot-wire anemometer measurements of the fluctuating velocity with radial dispersion data of helium in air. Considering the double integral on the Eulerian correlation function $R(\xi)$ where ξ = separation distance,

$$E_{DI} = \int_0^{\xi} \int_0^{\xi'} R(\xi'')d\xi'' \, d\xi'$$

it is seen that E_{DI} and the displacement variance $\overline{Y^2}(\tau)$ both have the units of (distance)^2. Comparing the value of E_{DI} at a distance of ξ_i with an equal value of $\overline{Y^2}$ at time τ_i it is possible to obtain a relationship between ξ and τ: if $\xi = B(\overline{v^2})^{\frac{1}{2}} \cdot \tau$, a value of $B = 0.7$ provided a satisfactory correlation of the data.

Baldwin (17,20), in an extensive study, examined the dispersion of heat behind a line source in an 8-in. diameter pipe with various diameters of the source, extrapolating to zero diameter to obtain heat wake measurements. Single-point hot-wire anemometer data was obtained and, based on his previous work on heat transfer from fine wires, Baldwin showed that a more accurate estimation of the exponent at high velocities in King's equation describing heat transfer from a cylinder:

$$N_{Nu} = A + B\sqrt{N_{Re}}$$

leads to a wire voltage dependence on the velocity of

$U^{0.18}$ rather than the dependence $U^{0.25}$ used by previous workers. The assumption of a linearized response of the wire fluctuating voltage to the velocity fluctuations i.e. $(\overline{e^2})^{\frac{1}{2}} = K_1(\overline{u^2})^{\frac{1}{2}}$ where K_1 = a const. was, however, retained. Baldwin's method of data handling was to find a value for K as a function of distance ξ in the expression:

$$\int_0^{K\xi} \int_0^{K\xi'} f(K\xi'')d(K\xi'')\, d(K\xi')$$

which makes this expression equal to the measured displacement variance $\frac{1}{2}\overline{Y^2}$ from the heat wake measurements. This was done by dividing the curve of $\frac{1}{2}\overline{Y^2}(\tau)$ into a convenient number of intervals between the time $\tau = 0$ and the time where a linear time dependence is established, assuming that this time may be accurately determined. The correlation curve $R(\xi)$ was divided into the same number of intervals between $\xi = 0$ and the first zero of $R(\xi)$. Numerical integration then established K as a function of ξ and hence the Lagrangian correlation coefficient is given by $R(\tau) = f(K\xi)$.

This procedure gave Lagrangian correlation functions which should be quite reliable, limited by the accuracy of the measured $\frac{1}{2}\overline{Y^2}(\tau)$, and also established a simple relationship between the hot-wire anemometer measurements and the turbulent dispersion data. The average value of the Peclet number calculated (18) for these results was 910.

The results showed that the similarity of shape of the Eulerian and Lagrangian curves is probably true

over a large portion of the curves, but is not true near the origin. Baldwin also found that the lateral Lagrangian intensities inferred from the diffusion results, as well as the lateral intensities from the anemometer measurements, were consistently less than the longitudinal anemometer intensities.

The relationship suggested by Burgers was also examined, viz. that to the same approximation as the Lagrangian derivative of the transverse velocity is given by:

$$\frac{dv}{dt} = \frac{\partial v}{\partial t} + U \frac{\partial v}{\partial x}$$

the two-point time correlation

$$R_v(\xi,\tau) = \frac{\overline{v_b(x,t)v_c(x+\xi,t+\tau)}}{\overline{v^2}}$$

for two particles b and c, the average being taken over many pairs of such particles, approximates the Lagrangian correlation coefficient $R(\tau)$ in isotropic, homogeneous, stationary turbulence, where $\xi = Ut$, U being the mean flow velocity. Baldwin measured these two-point correlation coefficients in the longitudinal direction with two hot-wire anemometers and found that the peak of the correlation curve occurred consistently later than the value predicted by $\tau = \xi/U$: the Lagrangian correlation coefficient $R(\tau)$ inferred from the lateral heat diffusion was found to resemble the general Eulerian correlation function evaluated at $R_u(\xi,\tau)_{\xi=Ut}$, the deviation being relatively large for increasing time. The lag in time

of the correlation peak was found to be represented by $\xi = 0.93U_{\mathfrak{L}}\tau$. Bass found a similar discrepancy, $\xi = 0.985U_{\mathfrak{L}}\tau$ in the work of Favre in grid-generated turbulence where no effect would be expected from excursions into slower-moving adjacent regions. Baldwin and Mickelsen (19) subsequently used this data for the approximation to $R(\tau)$ to estimate the predicted behavior of the displacement variance $\overline{Y^2}$ with time for the two cases of $\xi = U_c \cdot \tau$ where $U_c = 0.93\ U_{\mathfrak{L}}$ and $U_c = U_{\mathfrak{L}}$. It was found that for large times, the predicted slope of the plot of $\overline{Y^2}$ as a function of time, and hence the mixing coefficient E, was larger than the measured transverse value by a factor of 1.5 at $U_{\mathfrak{L}}$ = 73 ft/sec. to a factor of 3.6 at $U_{\mathfrak{L}}$ = 160 ft/sec. for the first case, and corresponding factors of 1.03 and 2.3 in the second. Corrsin (21), examining the relationship at high Reynolds numbers between the Lagrangian integral time scale T_L and the general Eulerian integral time and space scales measured at a point moving with the mean fluid velocity, presented an heuristic proof that the Eulerian and Lagrangian integral time scales were approximately equal and that the Eulerian integral length scale was given approximately by the expression

$$L = (\overline{u^2})^{\frac{1}{2}} \cdot T_L$$

Kraichnan (22) confirmed this expectation for high Reynolds numbers but postulated a different result for small N_{Re}. Saffman (23), following a conjectural relationship for large times proposed by Corrsin (24) for the Lagrangian and Eulerian space-time correlations, and

making certain assumptions of the form of the spectrum function based on the Eulerian space-time correlation coefficient, obtained the relationship $L = 2.5(\overline{u^2})^{\frac{1}{2}} \cdot T_L$. The assumptions were basic to the development, however, and Saffman stresses the qualitative nature of the result.

Philip (4) has recently presented a non-rigorous derivation of the Lagrangian correlation function in terms of the Eulerian correlation function. The model assumes a Gaussian displacement probability density function (pdf) θ for particles marked at the origin, and also a general form for the Eulerian correlation coefficient in cylindrical coordinates $R(x,r,t)$. The assumption that the pdf applying to those particles which arrive at the point (x,r,t) from the point $(0,0,0)$, may be replaced by the general Gaussian form for θ, leads to an expression for the Lagrangian correlation function in terms of the general Eulerian correlation coefficient. As it is proposed to examine this model with the results of the present investigation, it will be considered in more detail in the following chapter.

1.3.4 Atmospheric Turbulence

Besides the results determined in the laboratory, much work has been performed on turbulent dispersion in the atmosphere. Matters are complicated in this case by the fact that the spectrum of eddy sizes in the atmosphere extends up to the large scales causing the general disturbances. A second complication is that the turbulence is usually neither stationary nor homogeneous. Tracer

experiments have been performed, however, and analyzed in terms of Taylor's analysis. Hay and Pasquill (35) studied the crosswind spread of lycopodium spores 100 m. from the continuously emitting source and measured the wind velocity and direction fluctuations at the source. By assuming similar shapes for the Eulerian and Lagrangian correlation functions, they established a rough empirical transformation between the time axes in the two cases of $t_L = 4t_E$, but the values varied from 1.1 to 8.5 in different experiments. This large scatter is typical of the difficulties experienced in the study of a stochastic system in which one has little or no control over the parameters.

A good review of the study of atmospheric turbulence is provided by Pasquill (36).

CHAPTER 2.

THEORETICAL TREATMENT.

2.1 Treatment of Dispersion Data.

The results obtained by previous workers reviewed in Section 1.3 indicate that the technique of measuring dispersion in a turbulence field in the central core of air flowing through a pipe has been well established in the radial direction. The methods used to infer a Lagrangian autocorrelation coefficient from an Eulerian measurement, have however been based on Eulerian measurements made in the direction of mean flow, although practically every investigator has found that this region is not an isotropic field. It would thus be much more satisfactory if one could obtain Lagrangian data determined by the same velocity fluctuation components which determine the Eulerian data. The closest approach to this measurement would appear to be the mixed space-time correlation function determined in a preliminary measurement by Baldwin (17) from which an approximate Lagrangian correlation function may be inferred. This data was, however, obtained by recording the fluctuating signal from the hot-wire anemometer signal on a tape-recorder with a frequency response ± 1dB in the range 30 to 15 000 Hz. and with a correlator ± 3dB in the range 30 to 4 000 Hz. Eulerian data measured in this range would possibly partially exclude the effect of the slow, low-frequency eddies which are dominant in the production of dispersion.

The technique for the measurement of dispersion in a longitudinal direction would obviously differ from that

in the radial dispersion measurement, as it becomes necessary to use a discontinuous marking of the fluid particles in the form of pulses of tracer material. This introduces the complication that the dispersion produced by a turbulence field on these pulses released from a near-point source is dependent on the linear dimensions of the individual clouds. The effect may be visualized by considering the dispersion of puffs of smoke released from a chimney into the atmosphere: if the dimensions of the clouds are much smaller than the energy-containing dispersing eddies in the atmospheric turbulence field, the individual clouds will be transported as a whole in a certain direction and the dispersion within the cloud is effected by the smaller eddies of a size comparable with that of the cloud. There then exists a spatial distribution of concentration about the center of gravity for an individual pulse which in general does not correspond with the mean distribution about the mean position of the center of gravity, the mean being taken over many individual realizations. Although the importance of this effect was realized a long time ago and discussed in papers by Richardson (9) and Brier (3), and a formal treatment was developed by Batchelor (37,38), the difficulty in the determination of the necessary statistical parameters has made further material progress difficult and it appears that the survey article by Batchelor and Townsend in 1956 (13) still represents basically the present position.

The treatment developed by Taylor (1) is based on the movement of a single particle and the Lagrangian

correlation function on this particle at various times in its flight. In the averaging over many particles, we effectively release one particle at a time and follow it on its path, plotting the displacement X from the origin (or some point fixed in the direction of displacement), repeat this for many particles, and take the average over all realizations. This establishes a mean concentration at any point at time t which will be equivalent to the function $P(x,y,z,t)$, which is the probability that a single particle released from the origin will be at the point (x,y,z) at time t. The virtually instantaneous release of a small cloud of particles from the origin will result in a spatial distribution at time t which is generally not the same as $P(x,y,z,t)$. If the results of Taylor's theoretical treatment are to be applicable, it must be ensured that the individual clouds produce as uniform a distribution as possible i.e. approximate $P(x,y,z,t)$ for each realization. For a time-distributed release of a cloud, this means that the impulse response extracted from the measurements of the distribution at two points should show little variation. This may be done by increasing the dimensions of the cloud released until it is of a size comparable with the largest eddy present in the turbulence field. The constraint on this action is the decreasing accuracy with which the dispersion within a cloud may be measured between two fixed points as the initial linear dimensions of the cloud increase. In the present case, where it is proposed to measure the longitudinal dispersion, the length of the pulse in this direction must thus be a compromise. For these reasons,

it might be expected that the impulse responses extracted from the pulse measurements would show some variation: a better approximation to the time average temporal variation at a fixed point may be obtained by averaging the individual contributions for each time over a large number of realizations. From this average impulse response, a value for the mixing coefficient E compatible with Taylor's treatment may be extracted.

2.2 Validity of the Axial Mixing Model.

Batchelor and Townsend (13) have shown that the dispersion of a series of marked particles of fluid released from X_o at time t_o into a homogeneous turbulence field where the velocity fluctuations u(t) are a stationary, random function of time, would for large values of time be expected to be Gaussian distributed in the space variables. Previous experimental work (17,18,8) has, in fact, established that the distribution transverse to the mean flow may be described within the limits of experimental error by a Gaussian distribution function for practically all times in the (wide) velocity ranges studied by these workers in the wind-tunnel or central core of air flowing in a pipe. This useful result that X(t) has an asymptotically normal distribution for all times, implies that the probability density function $\theta(X_1,t|X_o,t)$ of the displacement $X(t) = X_1-X_o$ of a cloud of particles released instantaneously from a point source is normally distributed in the transverse direction

$$\Theta(X,t|t_o) = \frac{1}{(2\pi\overline{X^2})^{\frac{1}{2}}} \exp\{ -X^2/2\overline{X^2} \} \quad .... \quad (2.1)$$

where $X(t)$ is a one-dimensional scalar. Thus Θ obeys the classical diffusion equation

$$\frac{\partial\Theta}{\partial t} = E'\frac{\partial^2\Theta}{\partial X^2} \quad ..... \quad (2.2)$$

where in general E' will be a function of time

$$E'(t) = \tfrac{1}{2}\frac{d\overline{X^2(t)}}{dt} \quad ,$$

where $\overline{X^2}(t)$ is given by equation (1.1)

$$\overline{X^2}(t) = 2\overline{u^2}\int_o^t\int_o^{\tau_1} R(\tau)d\tau d\tau_1 \quad ..... \quad (1.1)$$

$$= 2\overline{u^2}\int_o^t R(\tau)d\tau\cdot t - 2\overline{u^2}\int_o^t \tau R(\tau)d\tau$$

and for large time when the second term becomes negligible when compared with the first

$$\overline{X^2}(t) = 2\overline{u^2}\int_o^t R(\tau)d\tau\cdot t = 2Et \quad .... \quad (2.3)$$

where E is now a constant for large values of t, and

$$E = \tfrac{1}{2}\frac{d\overline{X^2(t)}}{dt} \quad , \text{ (t large)} \quad ..... \quad (2.4)$$

The generalization of these expressions to 3-dimensions, assuming isotropy, results in a probability density function

$$\Theta(X,t) = \frac{1}{(4\pi Et)^{3/2}} \exp\{-(X^2/4Et)\} \quad .... \quad (2.1b)$$

where $X(t)$ is now a vector displacement.

The mean concentration $C(X,t)$ of a marking substance at any point is then equal to the probability of finding marked fluid at that point (13) i.e.

$$C(X,t) = \int_{-\infty}^{\infty} C(X_o,t_o)\ \theta(X_1,t|X_o,t_o)\ dX_o \quad \ldots\ldots (2.5)$$

When $C(X_o,t_o) = \delta(X_1-X_o)$, i.e. with a unit concentration Dirac impulse of marking substance at X_o at time t_o, this becomes, from equation (2.1b)

$$C(X,t) = \theta(X,t|t_o)$$

$$= \frac{1}{(4\pi Et)^{3/2}}\ \exp(-X^2/4Et)$$

or, if $X(t)$ is measured from a fixed point in a fluid flowing with mean velocity U in the x-direction, where $X^2 = x^2+y^2+z^2$,

$$C(x,y,z,t) = \frac{1}{(4\pi Et)^{3/2}}\ \exp\left[-\left\{(x-Ut)^2+y^2+z^2\right\}/4Et\right] \ldots(2.6)$$

If now the source is arbitrarily time-distributed, $Q(t)$ [gm/sec], and the concentration is measured at two fixed points downstream x_1 and x_2, these are given by the convolution integral

$$C(x_1,y,z,t) = \int_o^t \frac{1}{(4\pi Et)^{3/2}} \exp\left[-\left\{(x_1-Ut)^2+y^2+z^2\right\}/4Et\right] Q(t-\tau)\,d\tau \quad \ldots\ldots(2.8)$$

with a similar expression for $C(x_2,y,z,t)$, or expressed as a Laplace transform,

$$C(x_1,y,z,s) = H_1(s)Q(s) \quad \ldots\ldots\ldots(2.9a)$$

and $$C(x_2,y,z,t) = H_2(s)Q(s) \quad \ldots\ldots\ldots(2.9b)$$

Hence, in the s-domain, the second distribution

is given in terms of the first by

$$C(x_2,y,z,s) = \frac{H_2(s)}{H_1(s)}\, C(x_1,y,z,s) \quad = H_3(s)\,C(x_1,y,z,s) \quad \ldots(2.10)$$

The Laplace transform $H_1(s)$ is given by

$$L\left[\frac{1}{(4\pi Et)^{3/2}}\, \exp\left[-\left\{(x_1-Ut)^2+y^2+z^2\right\}/4Et\right]\right]$$

$$= \frac{1}{4\pi E^{3/2}}\, \exp\left(\frac{Ux_1}{2E}\right)\cdot L\left[\frac{1}{2(\pi t^3)^{\frac{1}{2}}}\cdot \exp\left(-\frac{x_1^2+y^2+z^2}{4Et}\right)\exp\left(-\frac{U^2t}{4E}\right)\right]$$

$$\ldots\ldots\ldots(2.11)$$

and this is given by, (39),

$$\frac{1}{4\pi E^{3/2}}\cdot \exp\frac{Ux_1}{2E}\cdot \exp\left[-\left(s+\frac{U^2}{4E}\right)^{\frac{1}{2}}\left(\frac{x_1^2+y^2+z^2}{E}\right)^{\frac{1}{2}}\right]\cdot\left[\frac{E}{x_1^2+y^2+z^2}\right]^{\frac{1}{2}} \quad \ldots.(2.12)$$

with a similar expression for $H_2(s)$. Hence $H_3(s)$ is obtained by dividing two expressions of the form of equation (2.12), and reverse-transforming (39), then with y=z=0 for measurement on the axis of the pipe, one obtains finally the impulse response between the stations 1 and 2:

$$H_3(t) = \frac{x_1}{x_2}\,\frac{x_2-x_1}{(4\pi Et^3)^{\frac{1}{2}}}\cdot \exp\left[-(x_2-x_1-Ut)^2/4Et\right] \quad \ldots\ldots(2.13)$$

and it is obvious that this is the same impulse response obtained from the axial mixing model often used to describe flow patterns in chemical reactor systems (43).

The factor x_1/x_2 would be difficult to determine, as it is based on the distance from a virtual origin, but as the sensitivity of the two detectors at stations 1 and 2

will generally be different and the pulse curves will be normalized, this factor may be included in the normalization. The impulse response, equation (2.13) then reduces to the same form as the expression for molecular diffusion in one-dimension from an area source (50)

$$H_D(t) = \frac{x_2 - x_1}{(4\pi Dt^3)^{\frac{1}{2}}} \cdot \exp\left[-(x_2 - x_1 - Ut)^2/4Dt\right]$$

In fact, the above derivation of $H_3(t)$ could have been restricted to the one-dimensional case if it were assumed that as far as the two detectors were concerned, the source was space-distributed normal to the direction of mean flow, Q(t) $(gm/cm^2 sec)$. The normalizing of the two pulses implies this assumption.

With a suitable regression technique it is then possible to obtain values of U and E from the convolution integral

$$C(x_2,t) = \int_0^t H_3(\tau)C(x_1,t-\tau)d\tau \quad \ldots\ldots(2.14)$$

The regression is actually performed on three parameters: U, E and a parameter normalizing the two pulses. This parameter occurs as a pre-exponential factor in the impulse response. As the two pulses were normalized before the regression, this factor was always very close to 1.

Law and Bailey (41) have presented a non-linear regression technique with a least-squares criterion which ensures convergence for any starting value of the parameters. King and Woodburn (42) have written computer

programs based on this technique for the axial mixing model for use on the IBM 1130 computer which were adapted for use in the present investigation. The convergence of the parameters was found, however, to be slow if the starting values were far from the correct values. Starting values of U and E were thus estimated by the method of moments described by Sater and Levenspiel (43,44) which were then used in the regression program.

It is appropriate to stress here that the derivation of the impulse response in equation (2.13) relies on the fact that the coefficients in the differential equation describing the dispersion of the tracer material between the two measurement stations are constants. The case where these parameters are time-varying is considerably more complicated as Laplace-transform techniques are in general not applicable (40). Equation (2.13) will therefore not describe the dispersion produced by the turbulence field on a cloud of particles released instantaneously from a point source at the first measurement station as one might expect from the definition of an impulse response. It should rather be regarded as a mathematically convenient expression describing the dispersion of tracer material between the two stations where the dimensions of the tracer cloud at the first station are such that the average rate of increase of displacement of the elements of the cloud about its center of gravity is already linear with time. i.e. equation (2.3) is applicable. By varying the distance between the two measurement stations, the compliance with this condition may be examined.

2.3 Hot-Wire Anemometer Treatment.

2.3.1 Digital Sampling.

The proposed method, described in detail in the following chapter, of digitally sampling the fluctuating voltage signal from the hot-wire anemometer before recording the signal, provides more freedom in the subsequent processing of the data: one is not dependent on the commercially-available linearizers or correlators which almost inevitably produce some attenuation of the signal. Provided that no signal component is lost in the hot-wire anemometer instrument itself, or the sampling technique, one obtains a set of "raw data" which is a permanent record of the voltage fluctuations. The method of digital sampling is known, however, to produce "aliasing" of higher frequencies in the signal if the sample interval is not carefully chosen (45). As the sampling interval in the present investigation had a lower limit of 100 μsecs., this question becomes of some relevance.

2.3.2 Evaluation of the Fluctuating Velocity.

Baldwin (17) has shown that the King equation (48) which leads to a relationship between the air velocity U and the current I flowing through the hot-wire in a constant-temperature anemometer circuit

$$U = U_o \left[\left(\frac{I}{I_o} \right)^2 - 1 \right]^2 \qquad \ldots\ldots\ldots\ldots (2.14)$$

where U_o and I_o are calibration constants, does not accurately describe the heat transfer from fine wires in a high velocity airstream. This relationship is usually used to describe the steady-state mean values of U and I,

and a linear relationship is assumed between the instantaneous fluctuating velocity and current (or voltage across a standard resistor in series with the probe)(49). In the present investigation, calibration of the signal could be performed with a Pitot tube for each mean velocity and the digitally sampled data could conveniently be converted to velocities on the computer in the course of the direct calculation of the autocorrelation functions. It was thus not necessary to assume a linear relationship between the instantaneous values of U and I. A direct comparison between the mean value of I measured for each case of a mean velocity determined with a Pitot tube and the value of U calculated with equation (2.14) based on the value at U = 13.4 m/sec. is shown in Table 1. In the present case, with a fairly small range in velocity fluctuation,equation (2.14) is apparently quite capable of correlating the data, and over the small range in velocity fluctuation even a linear relationship would not have resulted in a great error.

From Baldwin's curves for the present case of a 0.00015-in. diameter wire in a mean flow of 13.4 m/sec., corresponding to a Knudsen number of about 0.016 and a Mach number of 0.04, the error in using equation (2.14) is not very great. This function was thus used to convert the recorded voltage fluctuations to velocities on the computer.

TABLE 1.

Hot-wire anem. voltage (I) :	0.305	0.468	0.478	0.490	0.508	0.525
Pitot tube (mm H_2O) :	0	5.10	8.0	10.82	17.72	25.80
U from Pitot tube (m/sec) :	0	9.47	11.52	13.40	17.15	20.75
$U = U_o(I^2/I_o^2 - 1)^2$:	0	9.87	11.46	13.40	16.98	20.70

2.3.3 The Effect of Aliasing of High Frequencies (45,46)

The sampling theorem of random noise theory states that if F(f) is a function restricted to the band of frequencies between -B and +B where

$$F(f) = \int_{-\infty}^{\infty} p(t)\, e^{-j2\pi ft} dt$$

then

$$p(t) = \sum_{n=-\infty}^{\infty} p\left(\frac{n}{2B}\right) \frac{\sin\pi(2Bt-n)}{\pi(2Bt-n)} \qquad .....(2.15)$$

which shows how the function p(t) is reconstructed from its samples taken $^1/_{2B}$ secs. apart. The derivation of this result implies that p(t) contains no frequencies at absolute values $\geq$ B Hz. If now q(t) is another function which does contain frequencies > B Hz., where q(t) is the input to a low-pass filter cutting off at ± B Hz. and the output from the filter is p(t), by sampling p(t) at points $^1/_{2B}$secs. apart, we have

$$p(t) = \sum_{n=-\infty}^{\infty} q\left(\frac{n}{2B}\right) \frac{\sin\pi(2Bt-n)}{\pi(2Bt-n)} \qquad .....(2.16)$$

since

$$p\left(t=\frac{m}{2B}\right) = \sum_{n=-\infty}^{\infty} q\left(\frac{n}{2B}\right) \frac{\sin\pi(m-n)}{\pi(m-n)} = q\left(\frac{m}{2B}\right)$$

Thus the output wave p(t) can be determined by input samples of q(t) at $\tau = \frac{n}{2B}$; however, the input wave q(t) cannot be reproduced in this way.

The autocorrelation which is obtained on the band-limited signal p(t) may be written

$$R_{pp}(\tau) = \overline{p(t)p(t+\tau)}$$

$$= \sum_{n=-\infty}^{\infty} \sum_{m=-\infty}^{\infty} q(\frac{n}{2B}) q(\frac{m}{2B}) \frac{\sin\pi(2Bt-n)\sin\pi(2Bt-2B\tau-m)}{\pi(2Bt-n)\pi(2Bt-2B\tau-m)}$$

$$= \sum_{k=-\infty}^{\infty} R_{qq}(\frac{k}{2B}) \frac{\sin\pi(k+2B\tau)}{\pi(k+2B\tau)} \qquad \text{where } k = n-m$$

.....(2.17)

Also, for $\tau = 0$,

$$R_{pp}(0) = \sum_{k=-\infty}^{\infty} R_{qq}(\frac{k}{2B}) \frac{\sin\pi k}{\pi k} = R_{qq}(0) \quad ....(2.17b)$$

There is no way of separating the contributions of $R_{qq}(\frac{k}{2B})$ to the measured autocorrelation $R_{pp}(\tau)$ and hence once the signal has been sampled with an interval $1/2B$ secs., the true autocorrelation $R_{qq}(\tau)$ cannot be regenerated. One is then forced to adopt an aesthetically less satisfactory approach of sampling the signal with various sample intervals and examining the results for deviations. As aliasing is expected to produce a distortion of the higher frequency components of the signal, it is more convenient to examine the frequency spectrum of the signal obtained from the autocorrelation using the relationship developed by Taylor (47)

$$F(n) = 4\int_0^{\infty} R_{pp}(t)\cos(2\pi nt)dt \quad .....(2.18)$$

If the power spectrum function F(n) is approximately constant for the curves obtained with various sample times up to a frequency of about 5 000 Hz., it is very probable that there is very little power in fluctuations of a higher frequency.

It may be noted, from equation (2.17b), that possible aliasing has no effect on the zero lag value of an autocorrelation function.

2.3.4 Lagrangian Autocorrelation Function Postulated by Philip.

One of the comparatively recent proposals for the evaluation of a Lagrangian autocorrelation function in terms of the Eulerian measurements is the non-rigorous derivation suggested by Philip (4) for the case of homogeneous, isotropic, stationary turbulence. The essentials of Philip's treatment are as follows.

The case of zero mean flow is first considered with velocity component u parallel to the direction x, with r the radial coordinate. The Eulerian correlation function is defined as

$$\mathcal{R}(x,r,t) = \frac{\overline{u(0,0,0)u(x,r,t)}}{\overline{u^2}}$$

with the Eulerian integral length scale $L = \int_0^\infty \mathcal{R}(x,0,0)dx$ with an analogous expression for the integral time scale T. The assumption that the probability density distribution function $\Theta(x,r,t)$ of a particle released at (0,0,0) is Gaussian in the space variables is

$$\Theta(x,r,t) = \frac{2\pi r}{(2\pi\overline{X^2})^{3/2}} \exp -\left(\frac{x^2+r^2}{2\overline{X^2}}\right) \quad \ldots.(2.19)$$

where $\overline{X^2}(t)$ is given by the Taylor expression, equation (1.1).

By defining a sub-ensemble Eulerian correlation function $\mathcal{R}'(x,r,t)$, which applies only to those particles arriving at (x,r,t) which were the same particles at (0,0,0), a relationship for the Lagrangian autocorrelation function R(t) is obtained by integrating over all possible positions of the particle after its release, with weighting by the probability density $\Theta(x,r,t)$.

$$R(t) = \int_{-\infty}^{\infty} \int_{0}^{\infty} \Theta(x,r,t)\, \mathcal{R}'(x,r,t)\, dr dx \quad \ldots\ldots (2.20)$$

The assumption that $\mathcal{R}'(x,r,t)$ may be replaced by $\mathcal{R}(x,r,t)$ is not rigorously justified but has some plausibility.

$$R(t) = \int_{-\infty}^{\infty} \int_{0}^{\infty} \Theta(x,r,t)\, \mathcal{R}(x,r,t)\, dr dx \quad \ldots\ldots (2.21)$$

A convenient form examined by Philip

$$\mathcal{R}(x,r,t) = \exp\left[-\frac{\pi}{4}\left(\frac{x^2+3.138r^2}{L^2} + \frac{t^2}{T^2}\right)\right] \quad \ldots\ldots (2.22)$$

satisfies quite well most of the conditions imposed on an Eulerian correlation function (4). Combining equations (1.1), (2.19), (2.21) and (2.22) gives

$$R_*(t_*) = \frac{\exp(-\frac{1}{4}\pi t_*^2)}{\left(1+3.138\pi\alpha^2 \int_0^{t_*}\int_0^{\tau_1} R_*(\tau)\, d\tau d\tau_1\right)\left(1+\pi\alpha^2 \int_0^{t_*}\int_0^{\tau_1} R_*(\tau)\, d\tau d\tau_1\right)^{\frac{1}{2}}} \quad \ldots\ldots\ldots (2.23)$$

where $t_* = \frac{t}{T}$, $\alpha = (\overline{u^2})^{\frac{1}{2}}\frac{T}{L}$ and $R_*(t_*)$ is the function R(t) in terms of t_*.

No theoretical estimate of α is available, although the work of Corrsin (21), and Kraichnan (22) and Saffman (23) has shown that it should be of the order of 1 for high levels of turbulence. It might also be expected that α is approximately 1 to satisfy a possible transformation between the space and time axes of the Eulerian correlation function.

With the assumption that $\alpha = 1$, equation (2.23) may be solved on the computer by iteration for $R_*(t_*)$. To obtain R(t), an estimate of T is needed from the single-point Eulerian correlation function measured in the present investigation with a mean flow U in the x-direction. Defining a new variable x_U by the transformation $x = x_U - Ut$, the apparent Eulerian correlation function

$$\mathcal{R}_U(x_U,r,t) = \mathcal{R}(x_U-Ut,r,t)$$

and the apparent Eulerian integral time scale

$$T_U = \int_0^\infty \mathcal{R}_U(0,0,t)dt = \int_0^\infty \mathcal{R}(-Ut,0,t)dt$$

Using the form of $\mathcal{R}$ in equation (2.22), Philip finally obtained

$$\frac{T_U}{T} = \left(1+\frac{U^2T^2}{L^2}\right)^{-\frac{1}{2}} = \left(1+\frac{\alpha^2}{I^2}\right)^{-\frac{1}{2}} \quad .....(2.24)$$

and so the Lagrangian autocorrelation function R(t) is obtained from equations (2.23) and (2.24).

By assuming that the Lagrangian and Eulerian mean squares of the x-component of the velocity fluctuations are equal (21), the mixing coefficient predicted by this method may be obtained from

$$E = \overline{u^2}\int_0^\infty R(t)dt \ .$$

CHAPTER 3.

EXPERIMENTAL DESIGN.

3.1 General Description.

The investigation was conducted in a rigid, opaque, seamless PVC pipe 9.2 meters long, 154 mm I.D. and 160 mm O.D., which was supported from the steel girders in the roof and the brick walls of the building to prevent possible vibrations being transmitted to it. A general view of the apparatus is shown in Plates 1 and 2, with a schematic representation in Fig. 1. The inlet end of the pipe was fitted with a contraction nozzle of spun aluminium whose surface was left in the rough, unpolished state and this was enclosed in a box closed at the end, with an inlet on each side panel covered with a fibrous filter material. This arrangement reduced the effect of draughts and encouraged the rapid attainment of steady-state conditions in the flow. The other end of the pipe was connected through a large volume vessel (1.22 X 1.71 X 2.09 m.) to a 100cm. diameter centrifugal type fan driven by a 15 kW motor. The purpose of the large vessel was to minimize possible surging in the system. Throttles were located as shown in Fig. 1 before the surge tank and fan with a pressure drop across the first "Maltese-cross" type throttle of about 10 mm. Hg, and across the second of about 75 mm Hg for the case of U_E = 13.4 m/sec. The test section comprised the last 12 diameters of the pipe before the flexible right-angled bend into the anti-surge vessel.

Direct velocity measurements in the pipe were made

PLATE 1.

General View of the Apparatus.

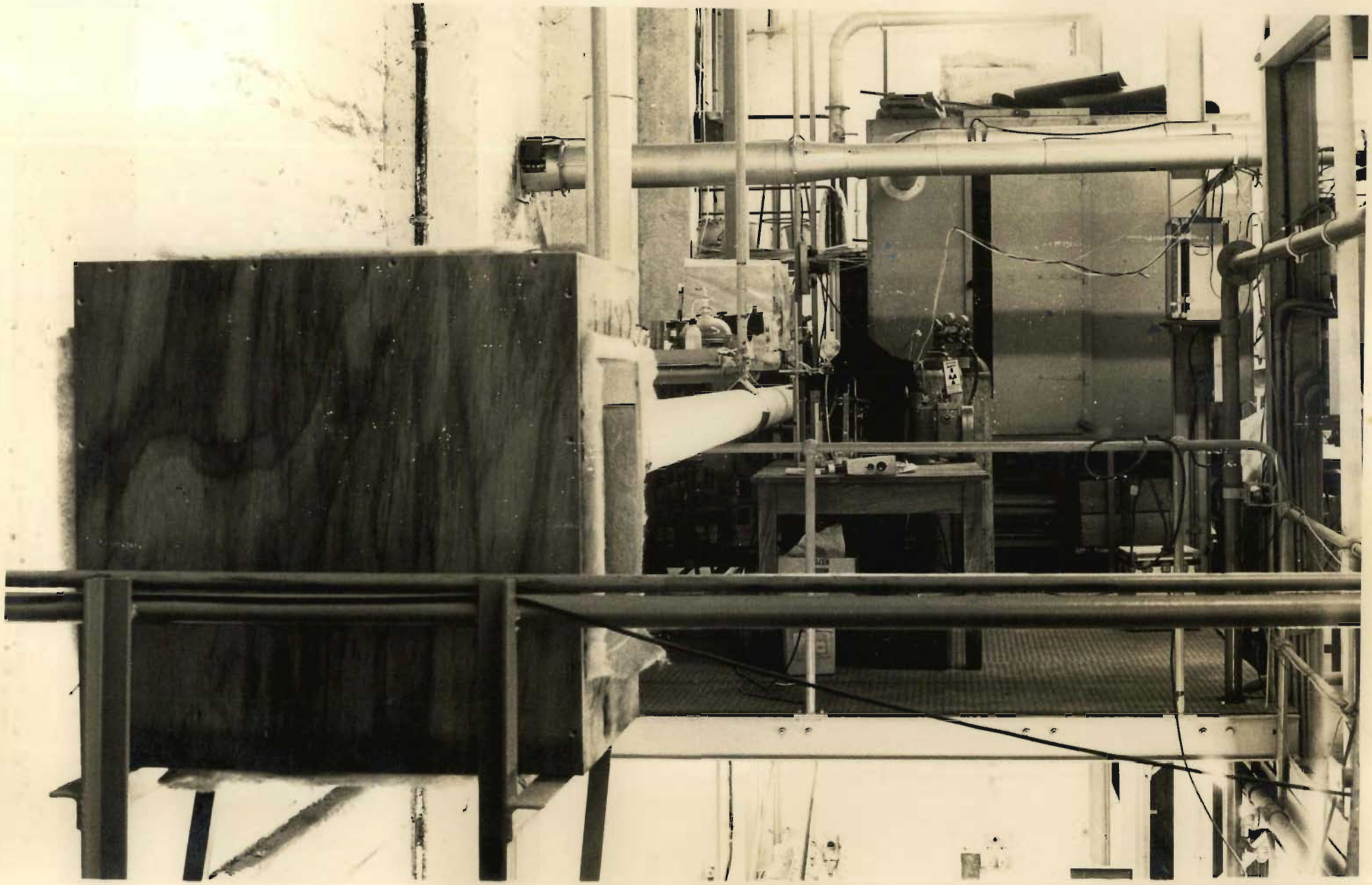

PLATE 2.

The Test-section

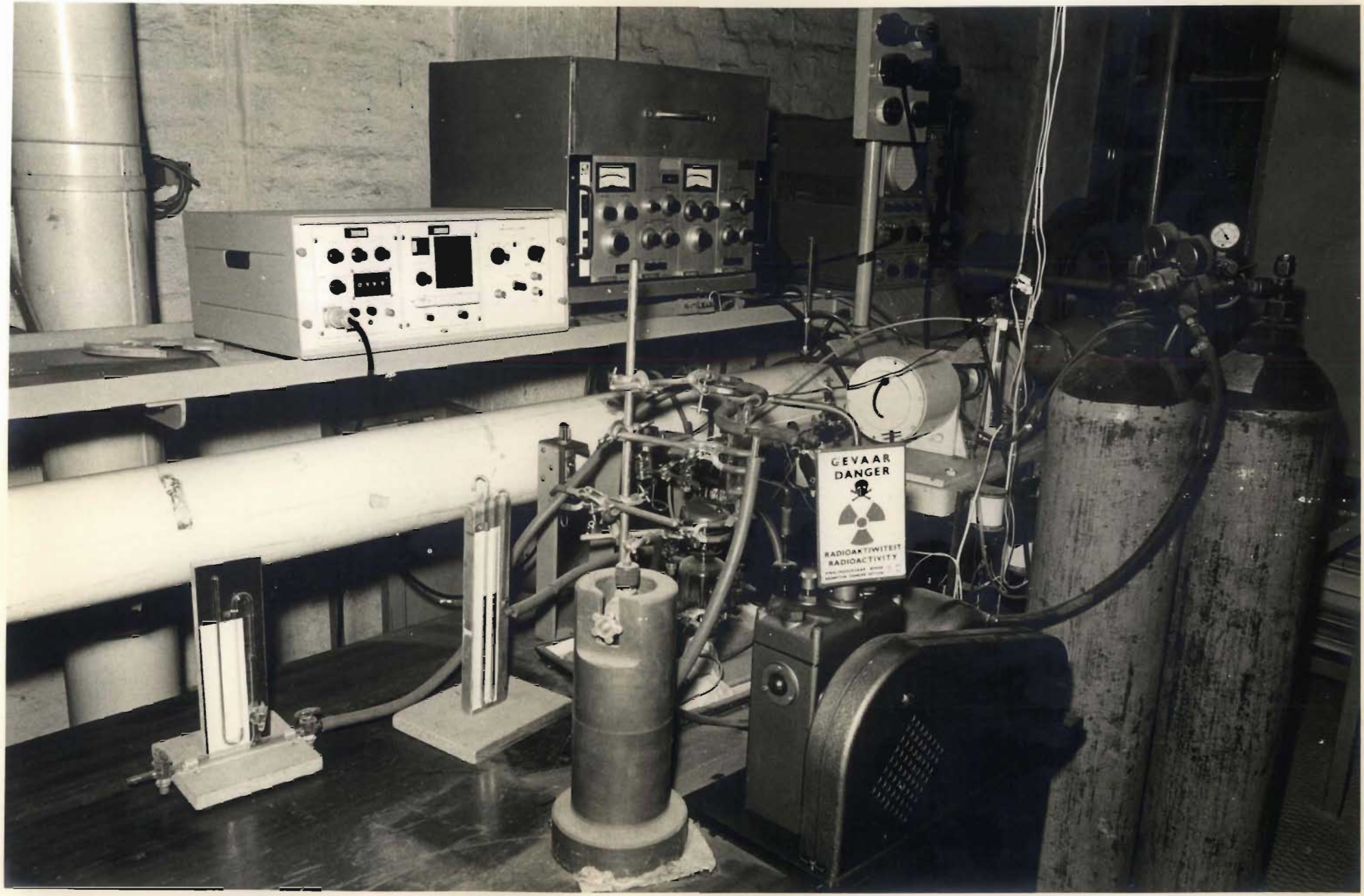
GEVAAR
DANGER
RADIOAKTIWITEIT
RADIOACTIVITY

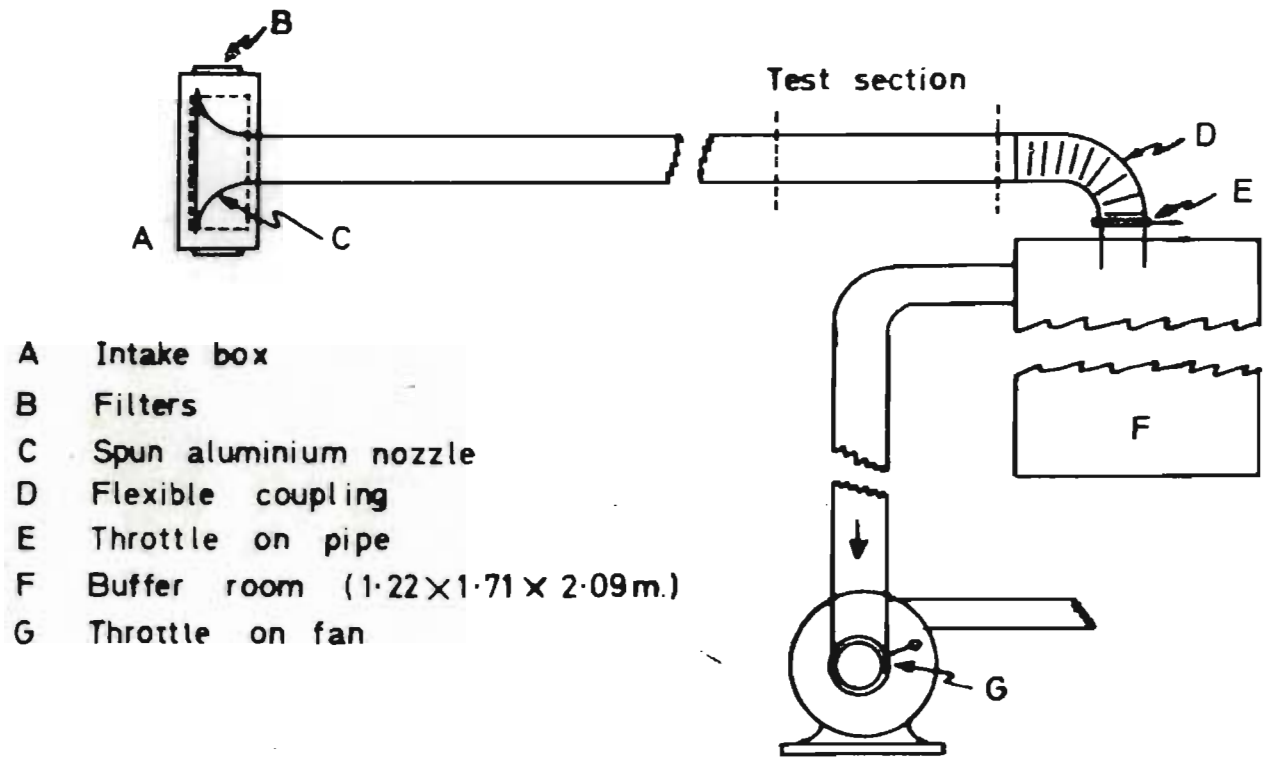

A Intake box
B Filters
C Spun aluminium nozzle
D Flexible coupling
E Throttle on pipe
F Buffer room (1·22×1·71×2·09m.)
G Throttle on fan

FIG.1 Schematic layout of apparatus

with a small 2.5 mm diameter Pitot static tube and a Casella water micromanometer which allowed readings to within 0.05 mm H_2O and this was used to set the flowrates in the pipe. Velocity profiles in the pipe were obtained from vertical traverses with the Pitot tube at two stations 7.7 m and 9.0 m. from the entrance of the pipe, and the results are shown in Fig.2. the maintained shape of the velocity profile shows that the flow may be considered fully-developed in the central portion of the pipe over this region, for the two values of the mean centerline velocity studied here. A small degree of asymmetry is noticeable in Fig. 2 but this could equally well have been due to a slight mis-positioning of the Pitot tube as a horizontal traverse showed the same asymmetry.

3.2 The Hot-Wire Anemometer.

The material used in the construction of the hot-wire probe was 0.00015-inch (approx 4μ) diameter tungsten wire. The wire was copper-plated on each side of the sensitive region of about 1 mm. length using the apparatus shown in Plate 3, with a pure copper anode, the wire forming the cathode, in a practically saturated solution of copper sulphate with 10% by volume concentrated sulphuric acid (48). The plated region of the wire had a diameter 3 to 4 times the diameter of the wire, the length to diameter ratio of the sensitive region being about 250. The wire was then soldered to the tips of two fine sewing needles mounted about 2 mm. apart in a ceramic insulator in the end of an L-shaped, rigid, stainless steel tube as shown in Plate 4 and Fig. 3. Slight tension was applied

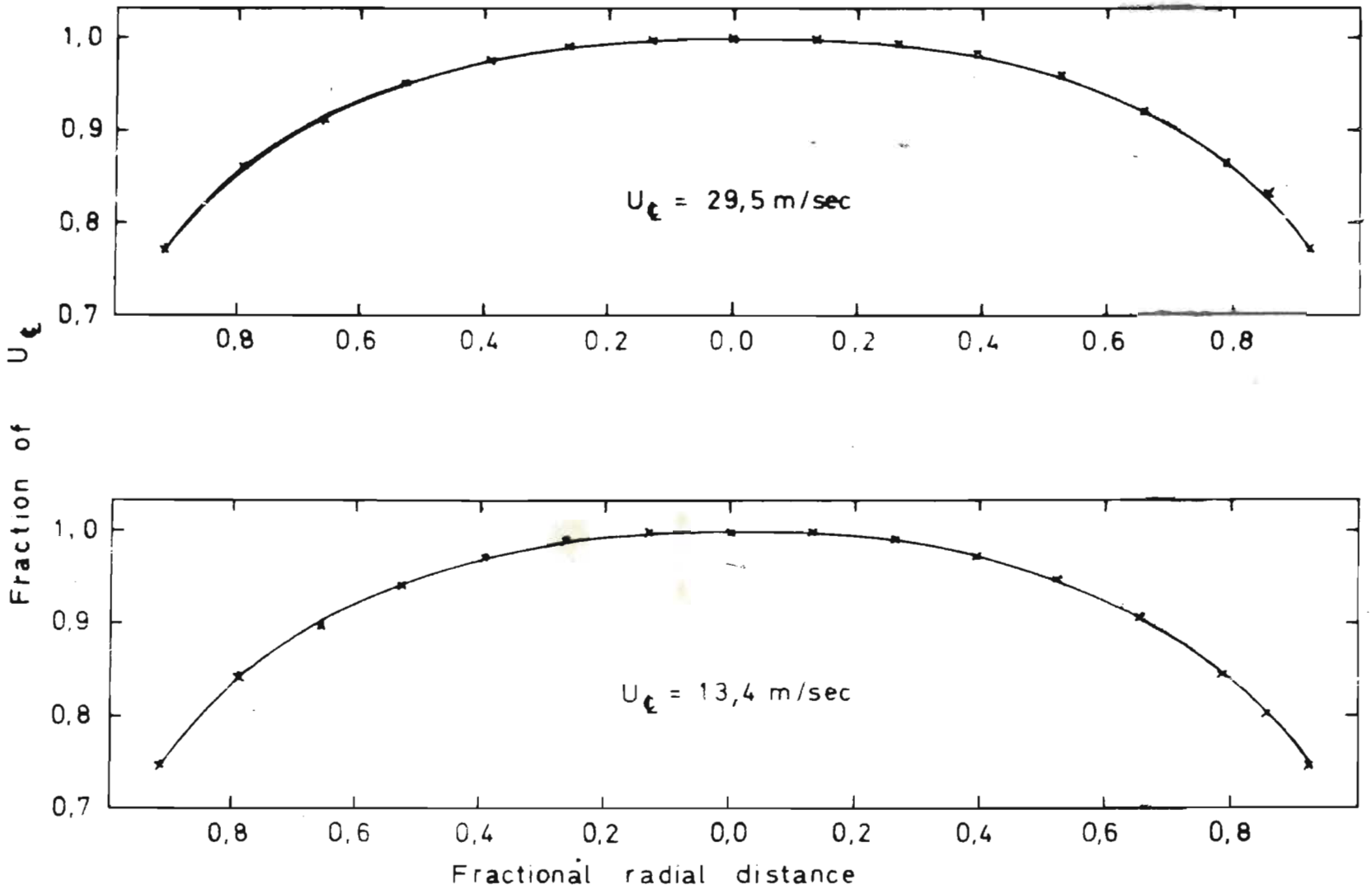

FIG. 2 VELOCITY PROFILES

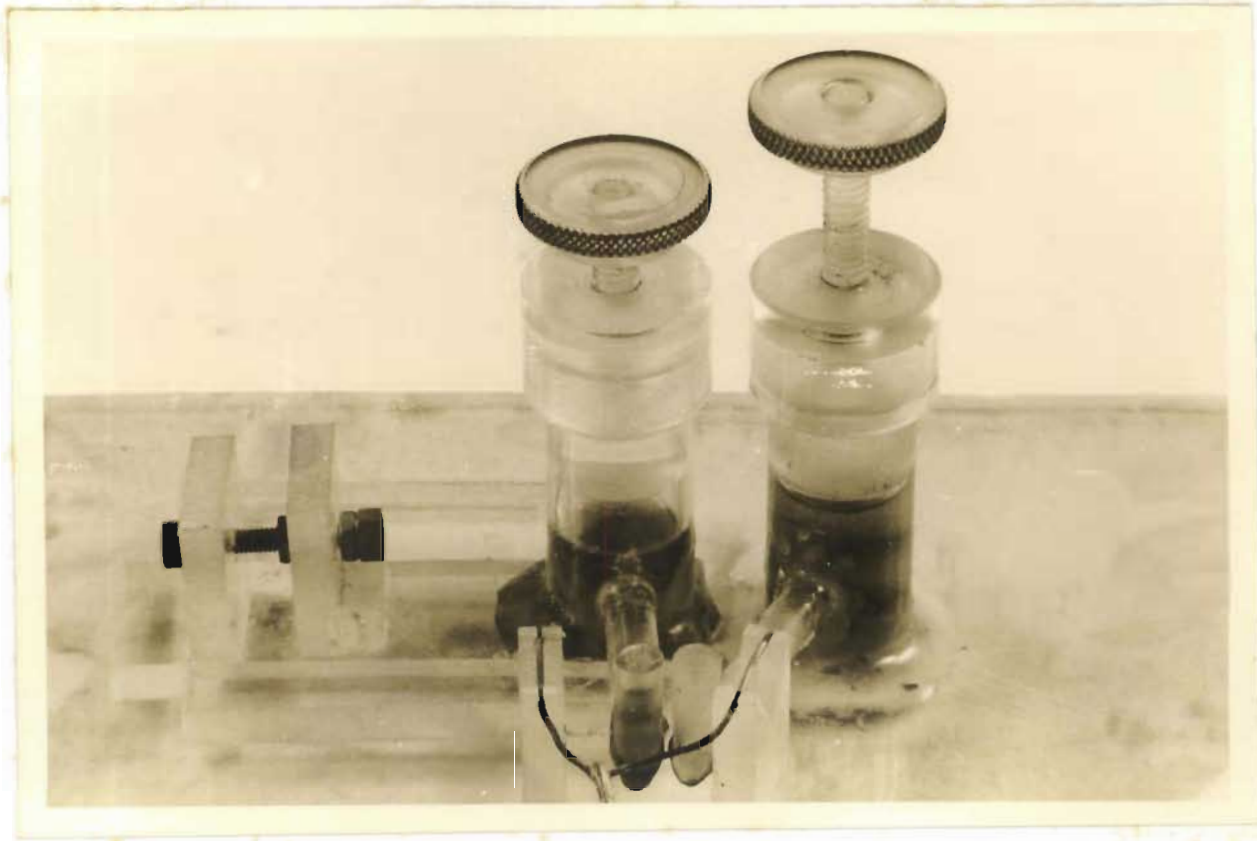

PLATE 3.: The Wire-plating Apparatus.

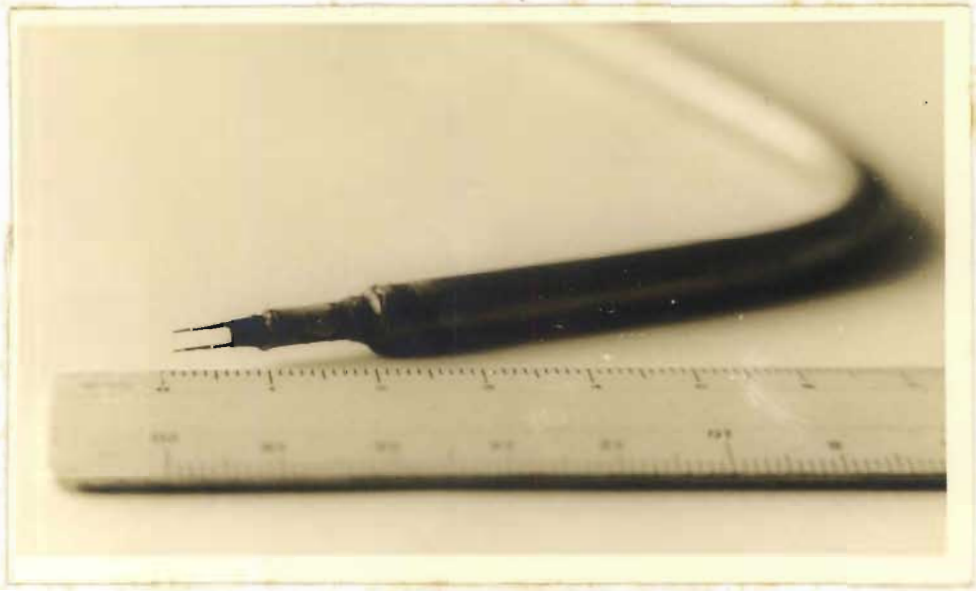

PLATE 4.: The Hot-wire Probe.

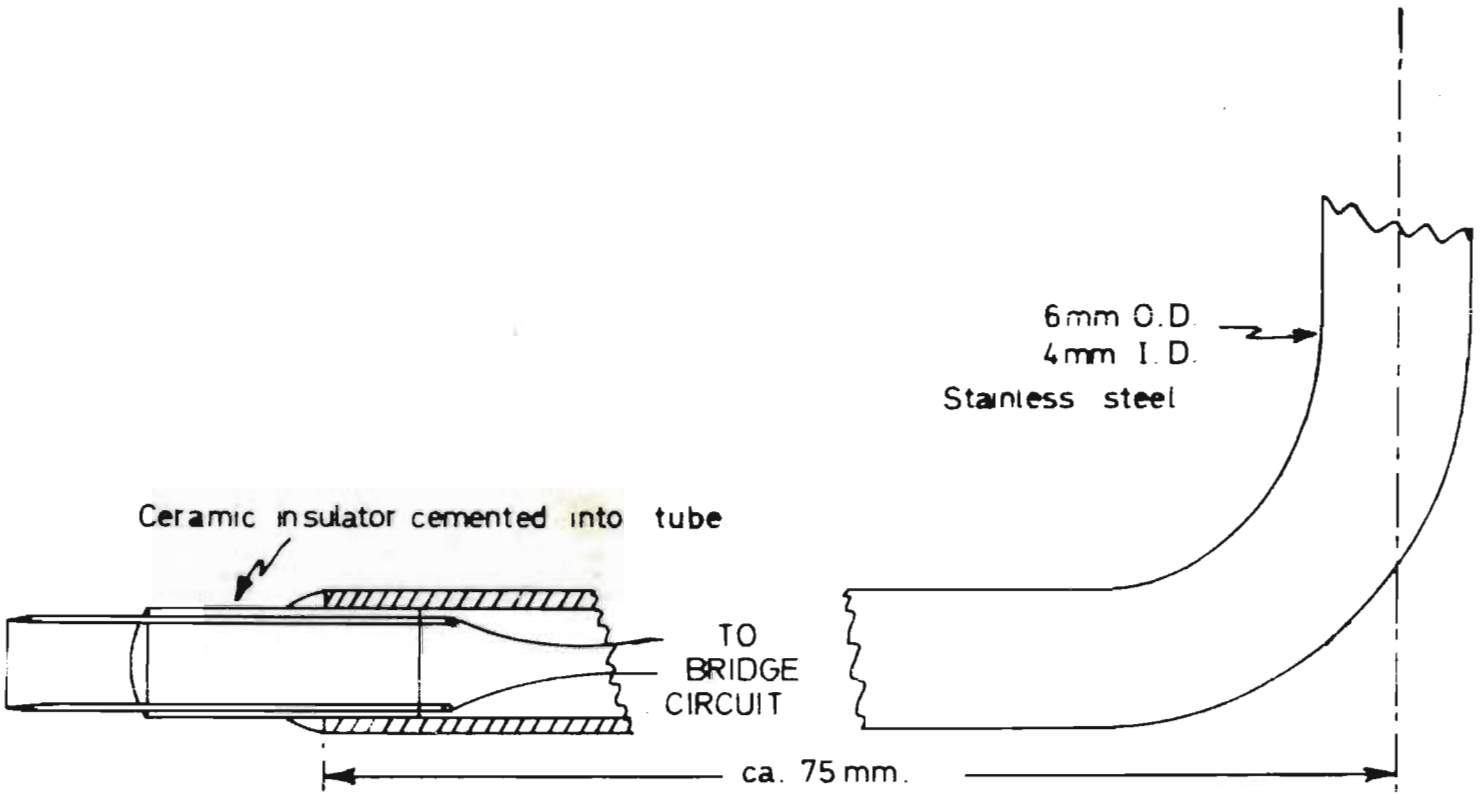

FIG. 3 Hot-wire anemometer probe detail

to the wire by bending the one probe support very slightly inwards before soldering. The probe was mounted 8.4 m., or 55 pipe diameters, from the inlet end of the pipe.

The Flow Corporation constant-temperature anemometer instrument used had a flat frequency response from DC to 100 000 Hz. The hot-wire probe forms one arm of a Wheatstone bridge circuit and a feedback amplifier varies the voltage applied to the bridge to maintain balance. The signal from this instrument was a fluctuating voltage measured across a standard resistor in series with the hot-wire probe: this signal was proportional to the fluctuating current I flowing through the probe. This fluctuating voltage was used to "gate" a 9.5 MHz. sinewave signal which fed through a shaping circuit to a bank of 8 binary counters, which at the smallest sample time was sampled every 100 μsecs. and the digital value from 0 to 255 was recorded on a computer drum recorder adapted from an ICT Model 1202 digital computer. A schematic representation of the sampling procedure is shown in Fig. 4. The instantaneous voltage at any instant determines the slope of the ramp function AB which controls the "gate" to the 9.5 MHz. signal. The length of time over which the signal was actually sampled thus varied from 12.5 μsecs. to 40 μsecs. With the additional time for the transfer of this signal to the drum recorder, this technique allowed the sampling of the fluctuating velocity in the pipe every $(2^{n+1} + 1)\cdot 20$ μsecs. i.e. every 100,180,340.... μsecs., and the recording of this digital value, with appropriate amplification, in the range 0 to 255. The maximum number of tracks available on the

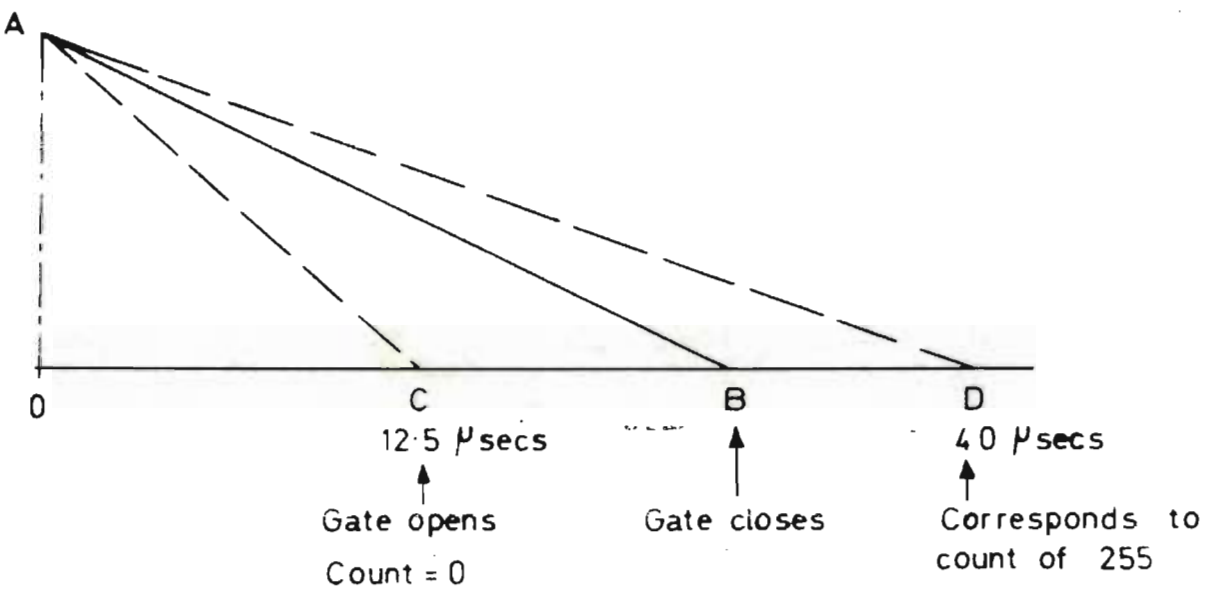

FIG. 4 Schematic digital sampling technique

computer drum was 30, each of which had a capacity of 1024 words, giving total time samples of the turbulent velocity fluctuations depending on the time interval chosen. After recording, the digital values on the drum were punched onto computer cards in a pseudo-binary form of one value per column which could be read into the IBM 1130 computer for direct evaluation of the relevant statistical parameters. The equipment is shown schematically in Fig. 5.

The DC amplifier used to subtract the voltage offset from zero and amplify the voltage fluctuations from the hot-wire anemometer, was designed and built in the Electronics Department of the University of Natal:its measured frequency response curve is shown in Fig. 6.

The correspondence between the digital values on the computer cards and the fluctuating voltage from the hot-wire anemometer was established directly with a square-wave calibration signal of known peak-to-peak voltage fed directly to the amplifier. A typical calibration curve is shown in Fig. 7 which shows a linear relationship between voltage and count recorded.

The mean flow on the axis of the pipe was determined with the Pitot tube and this was used as a calibration with the voltage read from the DC meter on the hot-wire anemometer instrument. The assumption that the meter reading was close to the voltage corresponding to the calibration velocity was not significant as the instantaneous velocity calculated was determined as a ratio of two terms such as equation (2.14)

$$U = U_o\left[\frac{I^2}{I_o^2} - 1\right]^2 \qquad \text{.....(2.14)}$$

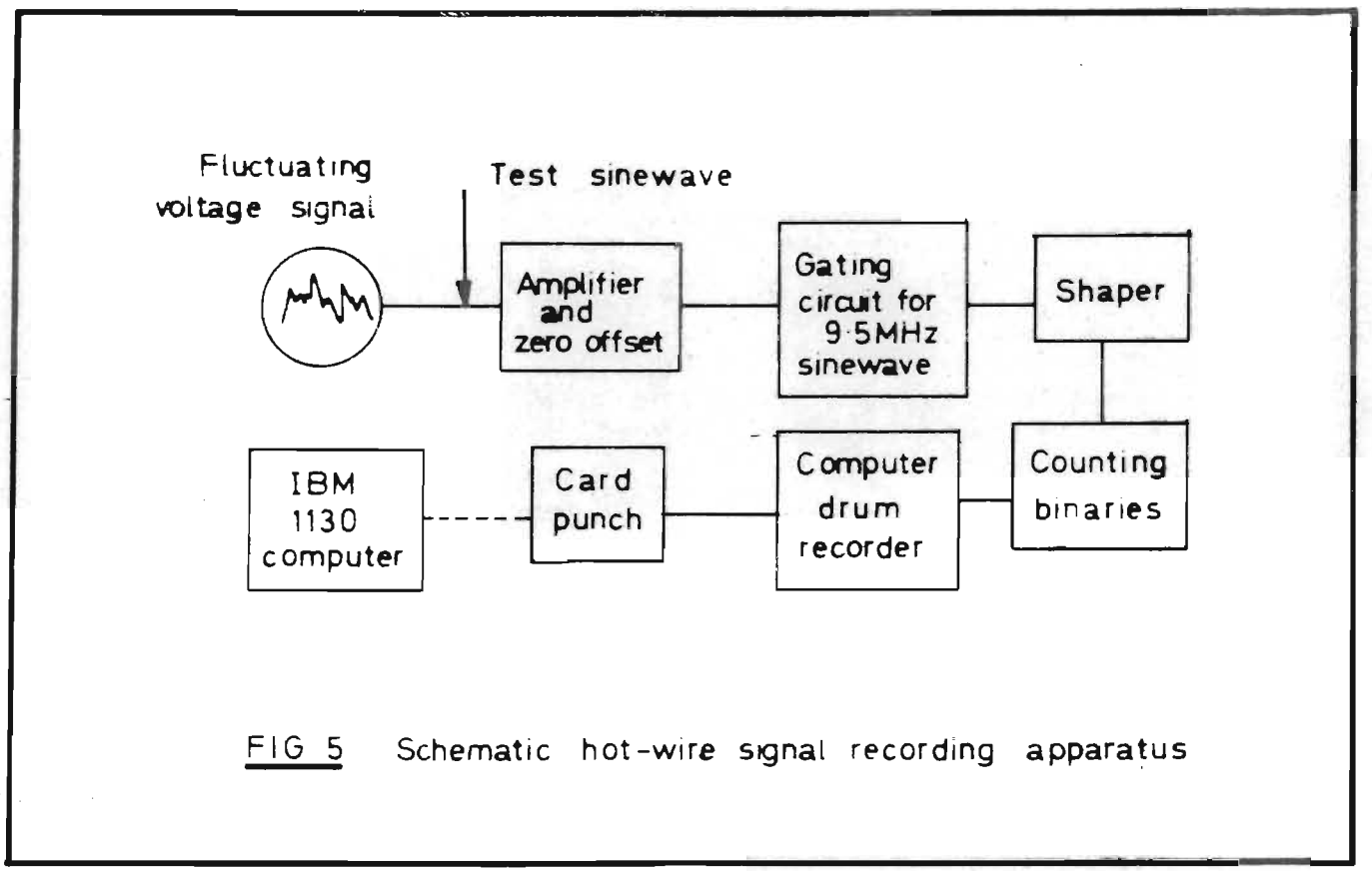

FIG 5 Schematic hot-wire signal recording apparatus

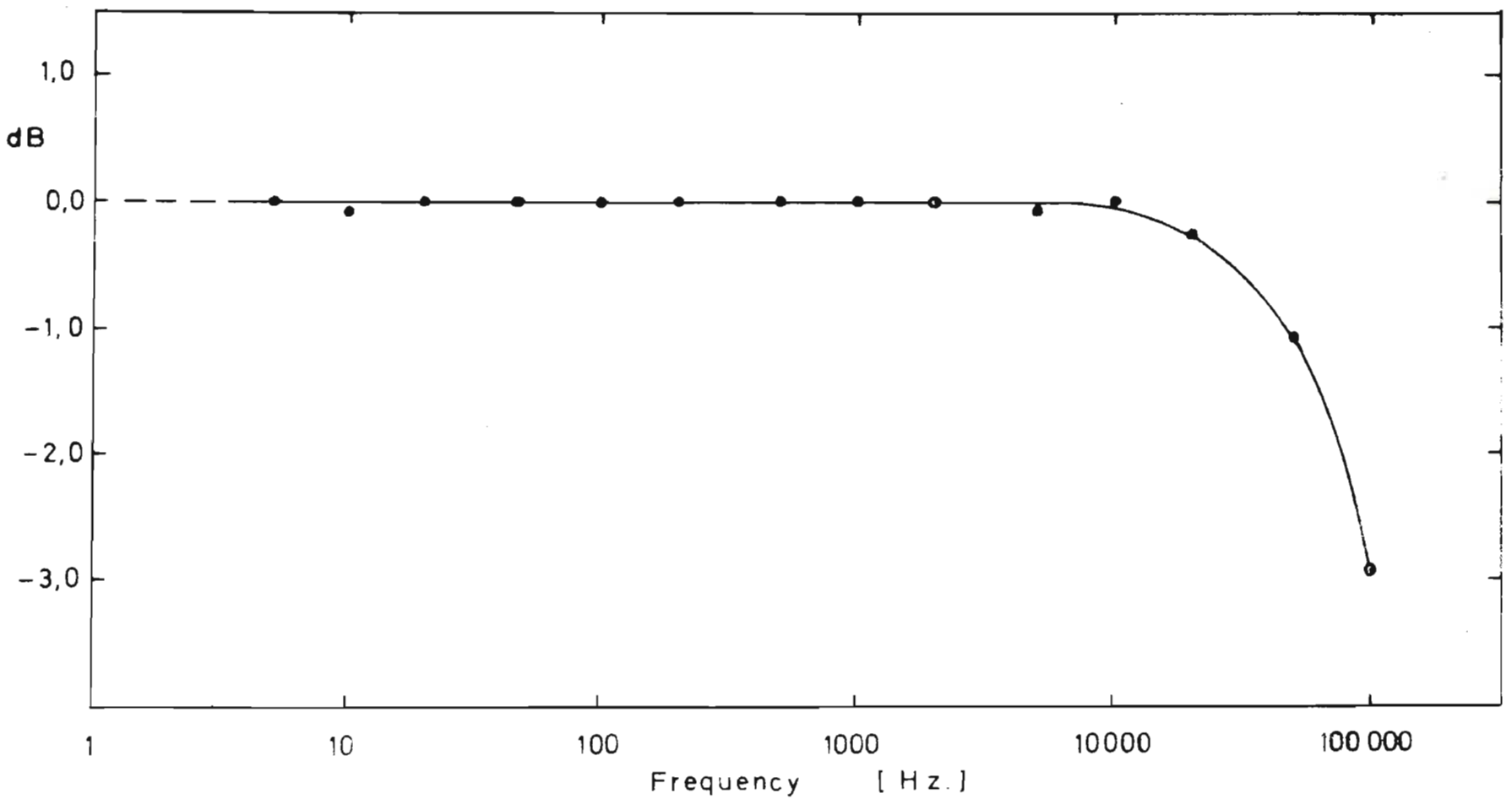

FIG. 6 FREQUENCY RESPONSE OF HOT-WIRE AMPLIFIER

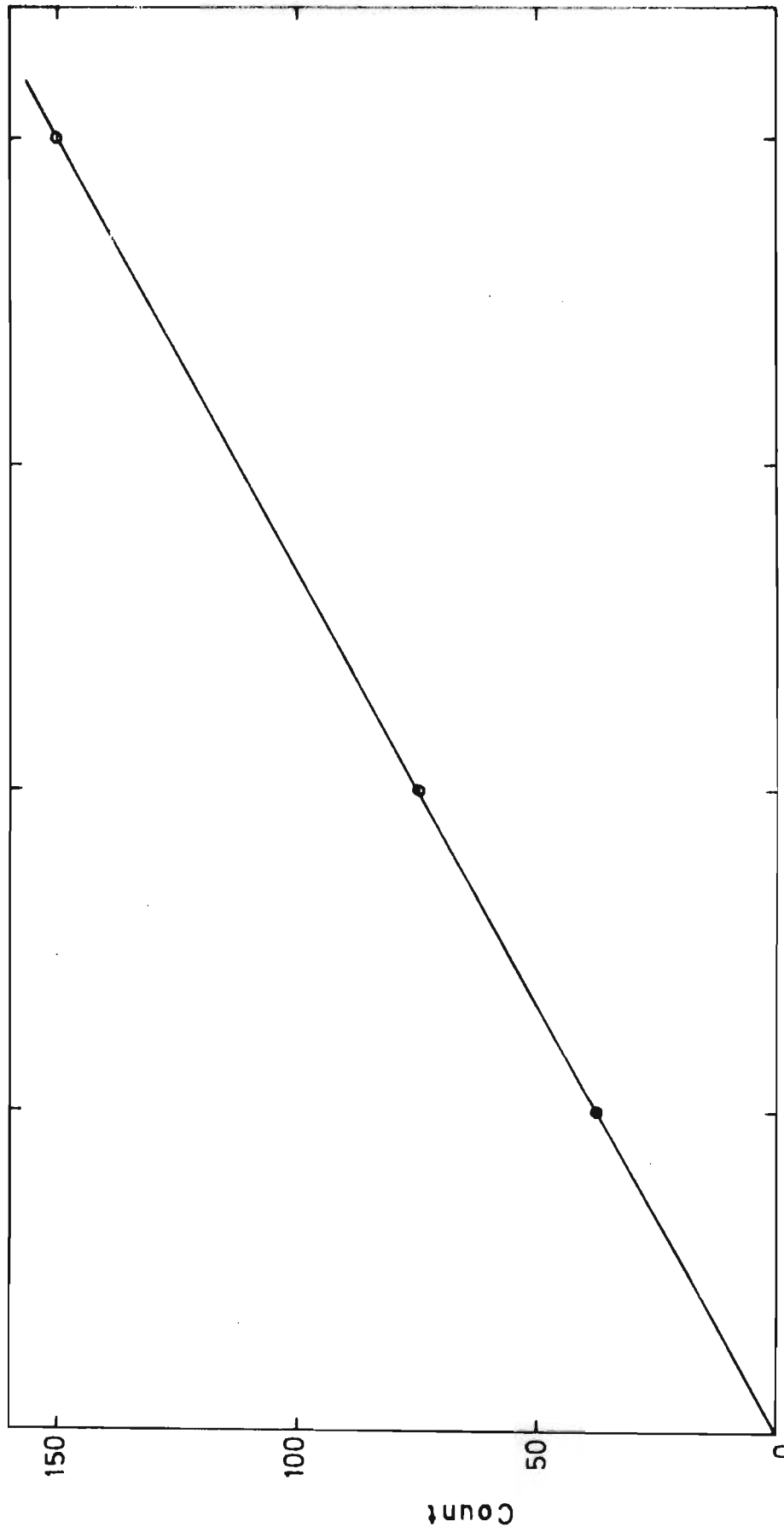

FIG. 7 CALIBRATION OF DRUM READINGS

and U_o cancels. The calibration voltage I read from the long time-constant meter corresponds to the voltage at the center of gravity of the non-Gaussian distribution of the number of occurrences with voltage as shown in Fig. 8, and this could be easily calculated on the computer. The small correction term to the voltage I estimated from Fig. 8 as about 0.0005 Volts may be used in an expression such as equation (2.14) to show that with the typical values of $I = 0.48$ V, $I_o = 0.30$ V, the error in ignoring the small correction voltage in calculating the instantaneous velocity is at most of the order of 0.03%. This was also shown by the fact that the constant mean velocity subtracted from the calculated velocities before the evaluation of the autocorrelation function differed from the calibration velocity by at most 0.05%.

As a check for drift and accuracy of the system after the hot-wire bridge circuit, a 500 Hz. sinewave signal was applied to the amplifier and recorded at 180 μsecs. sample interval. An autocorrelation on this data produced a steady cosine wave. To check on anemometer drift and wire contamination during the run, the steady offset voltage at zero velocity was measured before and after each recording, and any case showing a difference of greater than 0.01 V (in approx. 0.30 V) was discarded.

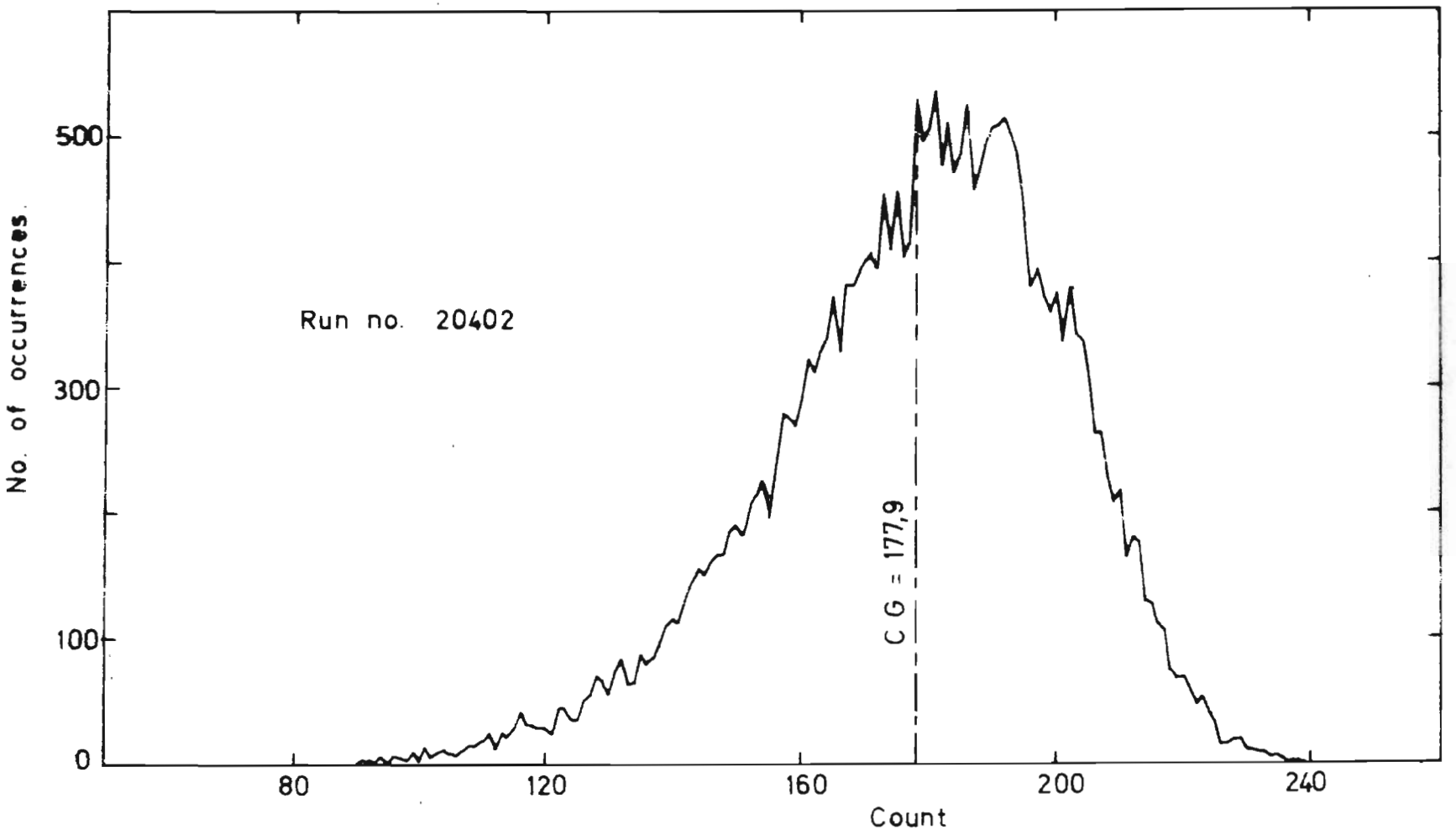

FIG. 8 COUNT DISTRIBUTION

3.3 The Dispersion Measurements.

3.3.1 The Tracer Material.

The types of tracer used in studying turbulent dispersion have varied from heat, carbon dioxide or helium to oil fog or glass beads (17,18,14,51). Most of the detection apparatus was slow-responding and bulky, both of which are undesired properties in the present case. Radioactive gas tracers possess attractive properties but have not been suitable for the usual continuous emission from the source used in studying the radial dispersion. The present investigation, with the injection of pulses of tracer material, is much more suitable for the application of this type of tracer. Krypton-85, a gas which in 99.4% of the disintegrations emits β-particles with a spectrum of energy up to 0.7 Mev and some γ-rays, is particularly suitable as a tracer material: besides being chemically inert and hence not absorbed by the human body in possible leakages during handling or after exhaust to the atmosphere, it has a half-life of 9.4 years, making it easily transportable with a high specific activity. i.e. it is not necessary to inject a large volume of tracer because most of it has already decayed, leaving only a small fraction still active.

The main disadvantage of Krypton-85 as a tracer is common to all radioisotopes: the random nature of the decay produces a fluctuating countrate which, at low concentrations, may obscure the shape of the pulse. It has been shown (52) that the instantaneously observed countrate N' is given in terms of the true countrate N by

$$N' = N \pm K\sqrt{N}$$

where K is a constant. A high countrate will thus decrease the fluctuating component relative to the signal, but this is limited by the amount of radioisotope allowed to be discharged into the atmosphere.

3.3.2 The Injection Apparatus.

It was found that the most suitable injection apparatus was a Beckman gas chromatograph sample valve. Tests with a system of solenoid valves with a time overlap in their operation, and with a rotating drum with a longitudinal slot in the circumference, showed that the gas sample valve provided the most reproducible pulse shape with a short duration which satisfied the criterion on the presence of enough high frequency components to excite the system over the whole spectrum as discussed previously (44,56).

The Krypton-85 was transferred from the 1-curie, 20 cc ampoule to the apparatus shown in Plate 5 from where it could be loaded into the sample valve. The internal passages of this valve were reduced to give a 1 mm. dia. channel for the gas and the valve was mounted immediately adjacent to the pipe. The Krypton was drawn into the approx. 0.2 cc. sample tube and pressurized through the Krypton storage vessel to the same pressure as the purging stream of metered air flowing through the second channel in the valve and giving isokinetic injection on the axis of the pipe in the direction of mean flow. The injection pressure required, about 10 to 15 mm. Hg, was not high

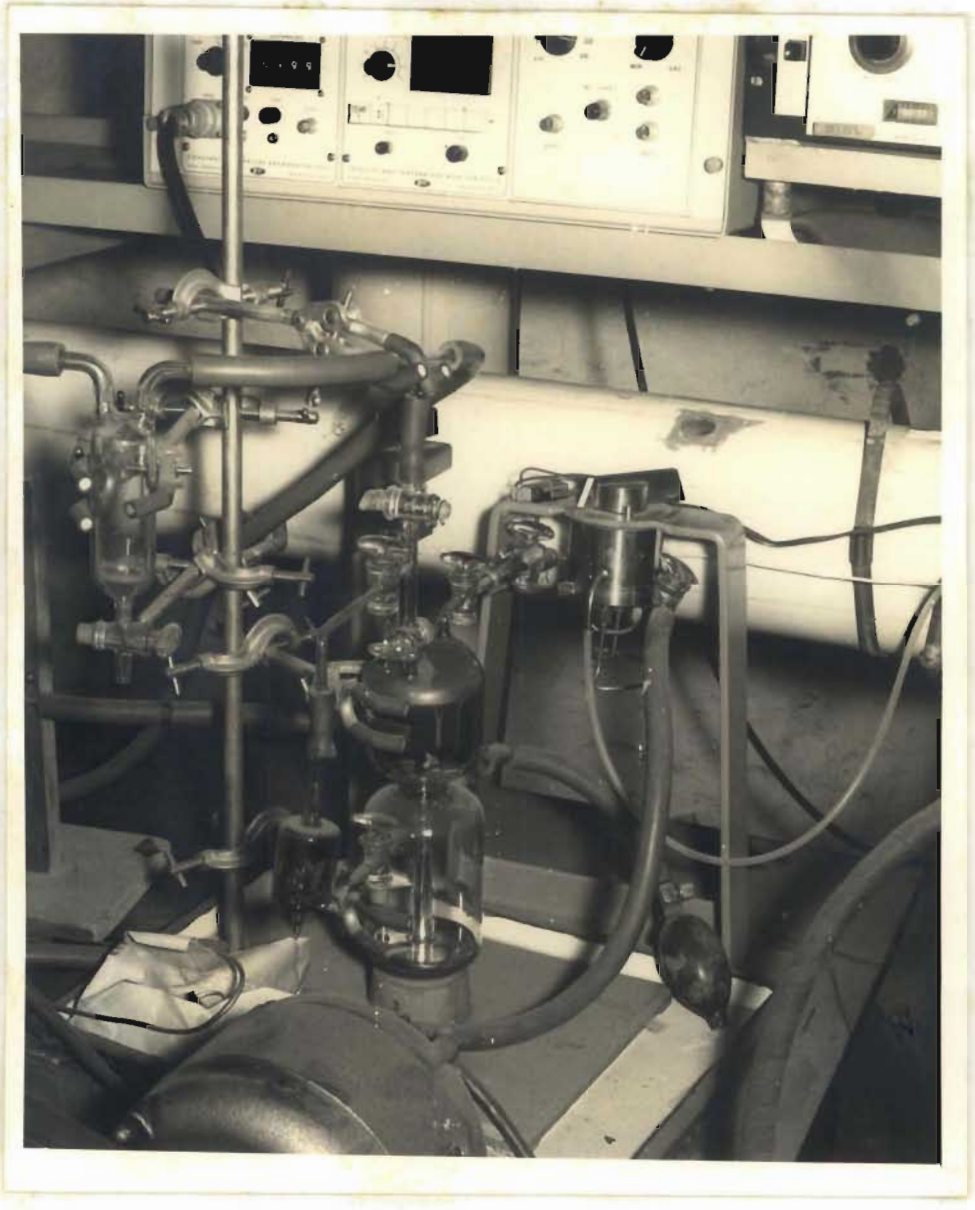

PLATE 5: Injection Apparatus.

enough to introduce serious errors in the metering of the air, but a small correction was applied for the change in density. Experiments were also performed with the injection velocity 20% higher and 20% lower than the calculated value with no detectable change in the results.

The L-shaped injection tube, inserted into the airstream at a point 47 diameters from the entrance, was thin-walled 2.5 mm O.D., 2 mm I.D. stainless steel hypodermic tubing. This "cylinder" disturbs the local flow patterns and the distance downstream at which the effect is negligible was estimated by the method used by Becker et al (18) to be approximately 15 cm. for the present investigation.

3.3.3 The Detection Apparatus.

The radiation detector most suitable for the measurement of comparatively weak β-particle emitters where it is desired to obtain a near-point measurement, is the surface-barrier semiconductor radiation detector. The principle of operation of this type of detector is basically the same as the ionization chamber: an electric field is established across a low-conductivity medium and a radioactive decay product entering the medium produces a wake of charged particles from its collisions with the medium. These charged particles, attracted to the boundaries by the applied potential, produce a pulse of current which may be amplified. The medium usually used is high-purity n-type silicon with a thin conducting gold film evaporated onto the front face and a film of aluminium

covered with silver on the rear face. This establishes the p-n junction necessary for the operation of the counter which has been previously described. (44,53).

These detectors have the advantage of being sensitive mainly to α- and β-particles, being practically completely insensitive to normal background cosmic γ-radiation which is often a problem in the use of scintillation or Geiger-Müller radiation detectors. Additional advantages of the surface-barrier detector are the small amount of shielding of the detector necessary to produce highly-directional properties,due to the short range of the β-particles in any fairly dense medium, and the high counting efficiency of up to 80% for β-particles. The very short time of about 25 millisecs. for the pulses of Krypton injected to pass the detector station, required a high maximum possible countrate for the detectors: the surface-barrier counter attains values of 10^6 counts/sec., the recovery after a pulse being more rapid than a G.M. tube which has a certain dead-time after a pulse during which any radiation penetrating the tube is not detected, although this is usually treated by introducing an artificial paralysis time longer than the dead-time and applying a correction to the count-rate.

The disadvantages of this type of detector are the high sensitivity to temperature variation which makes calibration difficult, and the small signal which requires very sensitive preamplifiers and amplifiers with a fast risetime. The sensitivity to light was not of importance in this investigation as the pipe was practically opaque.

The method of construction of the type of detector used in this investigation has been previously reported (44) and the procedure will only be summarized here.

The discs of high-purity n-type silicon 6 mm. and 15 mm. diameter and about 1 mm. thick, were polished on a sheet of glass with water and very fine aluminium oxide powder to remove visible imperfections. The discs were then etched in a nitric acid/hydrofluoric acid/acetic acid etch solution to produce a mirror finish, following which the rear contact of aluminium and then silver was evaporated onto the disc under very low pressure of about $5 \cdot 10^{-5}$ mm. Hg, the silver preventing oxidation of the aluminium. After allowing a few days for the natural oxidation to form the p-type silicon on the front face, the disc was cemented on its brass shield and the front contact of gold was evaporated on under high vacuum. The rear contact was made by cementing a small brass bolt to the silver contact with silver conducting-paste and covering the rear of the detector with Araldite, an epoxy-resin type cement. A thin film of Mylol was cemented over the sensitive face to prevent "pockets" of tracer forming in this area.

The downstream detector was of larger diameter than the upstream detector to compensate for the increasing dilution of the tracer with distance from the source. The sensitive areas of the two detectors were 4 mm. and 11 mm. diameter respectively, and the overall diameters were 8 mm. and 22 mm. resp. The error introduced by the space effect of the larger detector would be small considering the

linear dimensions of the pulse of tracer.

The small detector was mounted as shown in Fig. 9 and Plate 6 on the end of a 3 mm. O.D. hypodermic tube while the larger detector was mounted on an aerofoil section, and these were fastened to the wall of the pipe so that the faces of the detectors were on the axis of the pipe with the mean flow parallel to the face. The detector was connected to the RIDL charge-sensitive preamplifier by a low-capacitance coaxial cable kept as short as possible to prevent loss of the small signal by capacitance in the cable. The main amplification was performed on an RIDL amplifier which had a noise-level control for raising the threshold voltage to enable the exclusion of the thermal noise produced in the detector: this had to be regularly checked during each experiment, as a small variation in the temperature would cause the noise-level to change. This effect was, however, clearly visible as a rise in the background count which was adjusted to be less than 0.2 counts/sec. before each recording.

3.3.4 The Pulse-recording Apparatus.

A photographic technique was used to obtain the exact time-distribution of the amplified pulses from the surface-barrier detectors. A schematic diagram of the recording system is shown in Fig. 10, and is also shown in Plate 7. The signals from each detector channel were fed with opposite polarity to the two input channels of a single-beam oscilloscope where, after algebraic addition, the resultant signal caused vertical displacement on the

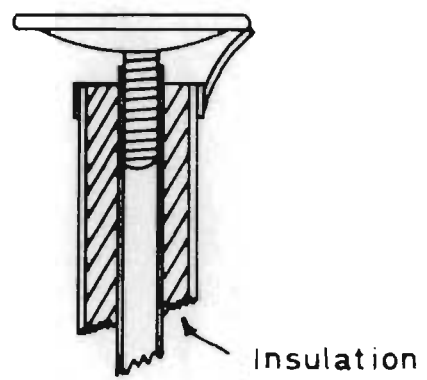

Inlet detector

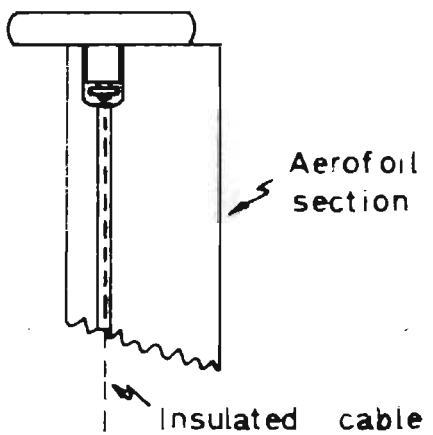

Outlet detector

FIG. 9

PLATE 6: The Surface-barrier Detector.

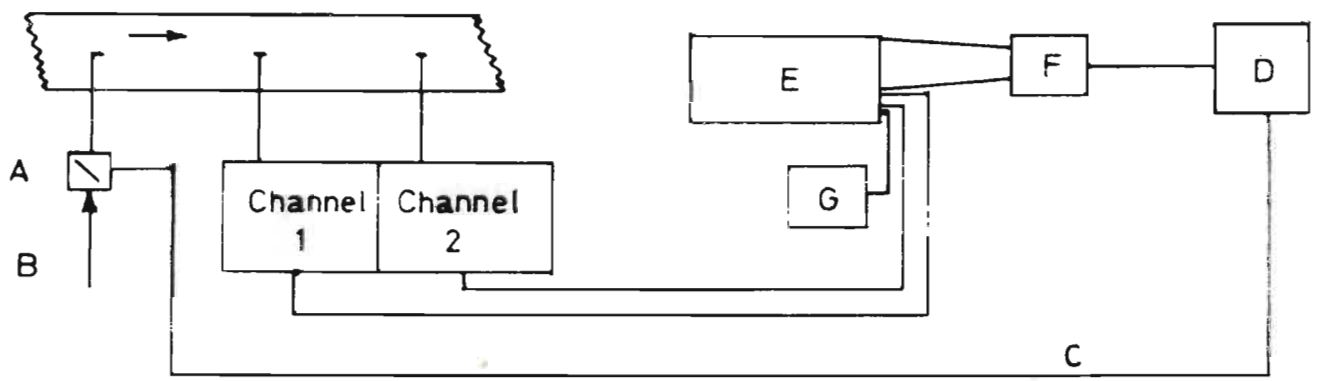

A G.C. Valve
B Purge air
C Camera trigger
D Camera control unit
E Oscilloscope
F High-speed streak camera
G Sawtooth generator

FIG. 10 - SCHEMATIC PULSE-RECORDING APPARATUS

PLATE 7

The Pulse-recording Apparatus.

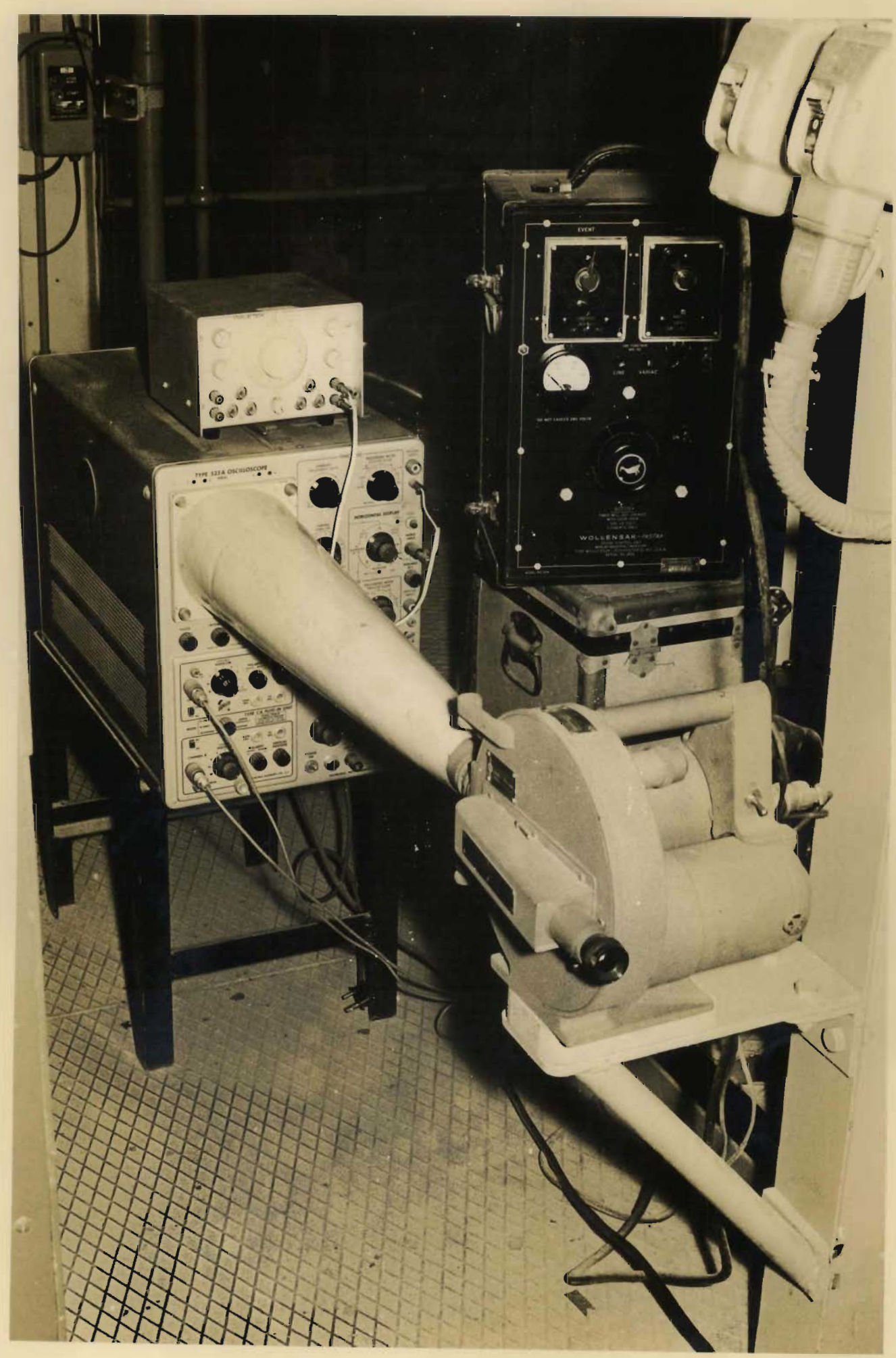
EVENT
WOLLENSAK

screen, the first station detector causing upwards deflection and the second station deflecting downwards. A 5 kHz. sawtooth signal was applied to the horizontal deflection plates of the oscilloscope as a carrier wave. The oscilloscope screen was photographed with a 16 mm. high-speed streak camera which was triggered by a micro-switch operated by the gas sample injection valve.

On development of the film, the exact distribution of the pulses in time could be determined by visually counting on a film editor the number of pulses per time interval determined by the carrier-wave frequency. From these values, the shape of the tracer pulse at each station could be reconstructed.

An example of the pulses on the film is shown in Plate 8.

This method, although extremely laborious, provided a reliable and permanent digital record of the pulse behavior.

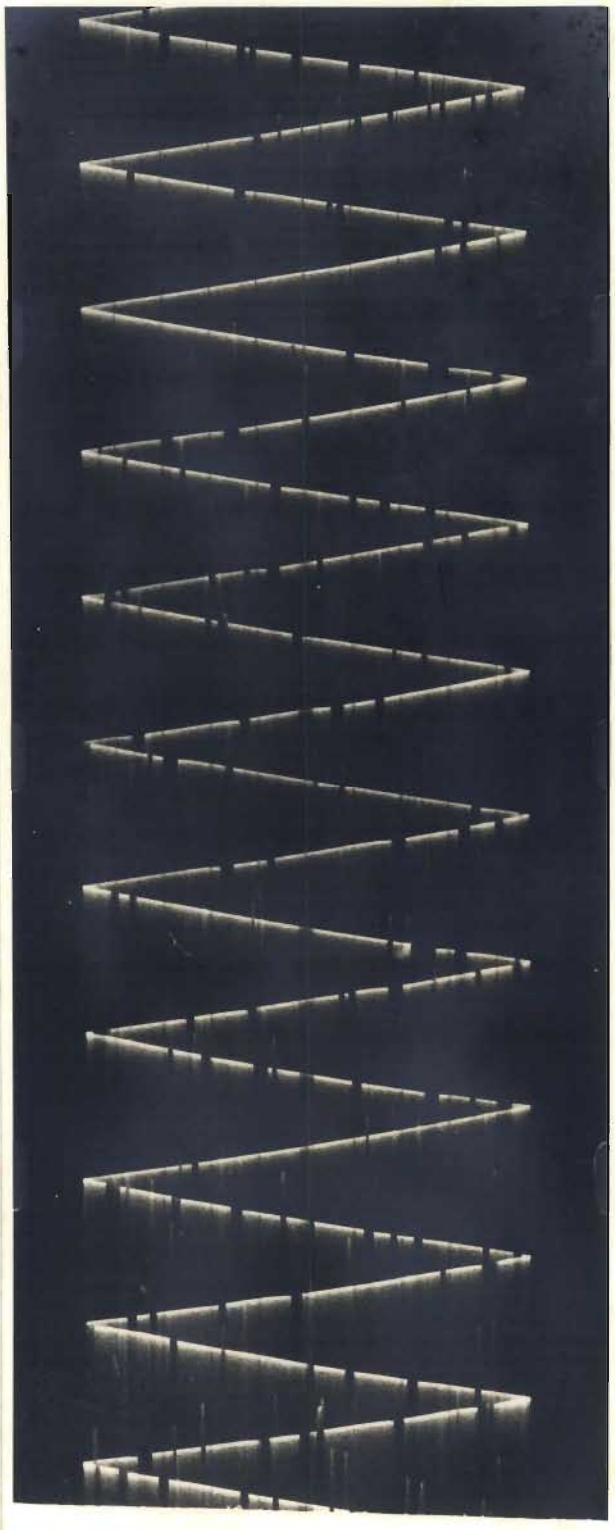

PLATE 8: Surface-barrier Detector Pulses Recorded on Film.

CHAPTER 4.

RESULTS.

4.1 Hot-wire Anemometer Results.

4.1.1 The Velocity Fluctuation Distribution.

The distribution of the longitudinal velocity fluctuations about the mean velocity were calculated directly on the computer with the program EVELD, included in the Appendix, after conversion of the pseudo-binary data to velocities. Examples of the results of this calculation are shown in Figs. 11 and 12 for the mean velocities of 13.4 m/sec. and 29.5 m/sec. resp., together with the Gaussian distribution having the same standard deviation. The skewness and flatness factors, $\overline{u^3} / \left(\overline{u^2}\right)^{3/2}$ and $\overline{u^4} / \left(\overline{u^2}\right)^2$ resp., are summarized in Table 4.1 and may be compared with the values of 0 and 3.0 resp. for the Gaussian distribution.

TABLE 4.1

RUN NO.	MEAN VEL. (m/sec)	SAMPLE TIME (μsecs)	SKEWNESS	FLATNESS
16040	13.4	180	-0.586	3.566
20401	13.4	100	-0.408	3.458
20402	13.4	340	-0.447	3.172
22401	13.4	180	-0.523	3.089
22402	13.4	100	-0.457	3.263
5080	13.4	180	-0.452	3.348
24401	29.5	100	-0.419	3.172
24402	29.5	180	-0.437	3.193
27801	29.5	100	-0.487	3.432
27802	29.5	100	-0.314	2.954
27803	29.5	100	-0.490	3.250

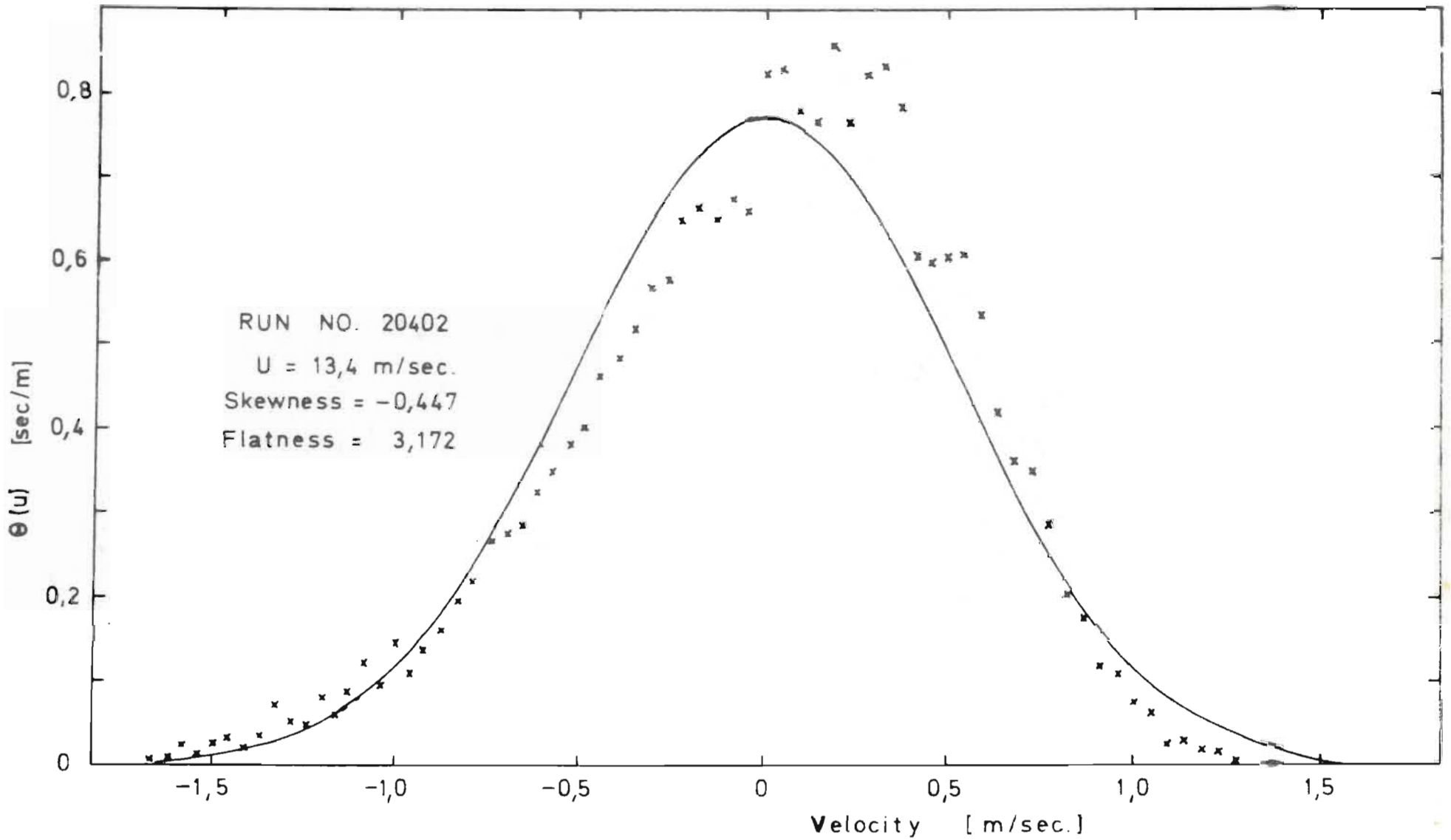

FIG. 11 VELOCITY PROBABILITY DENSITY FUNCTION

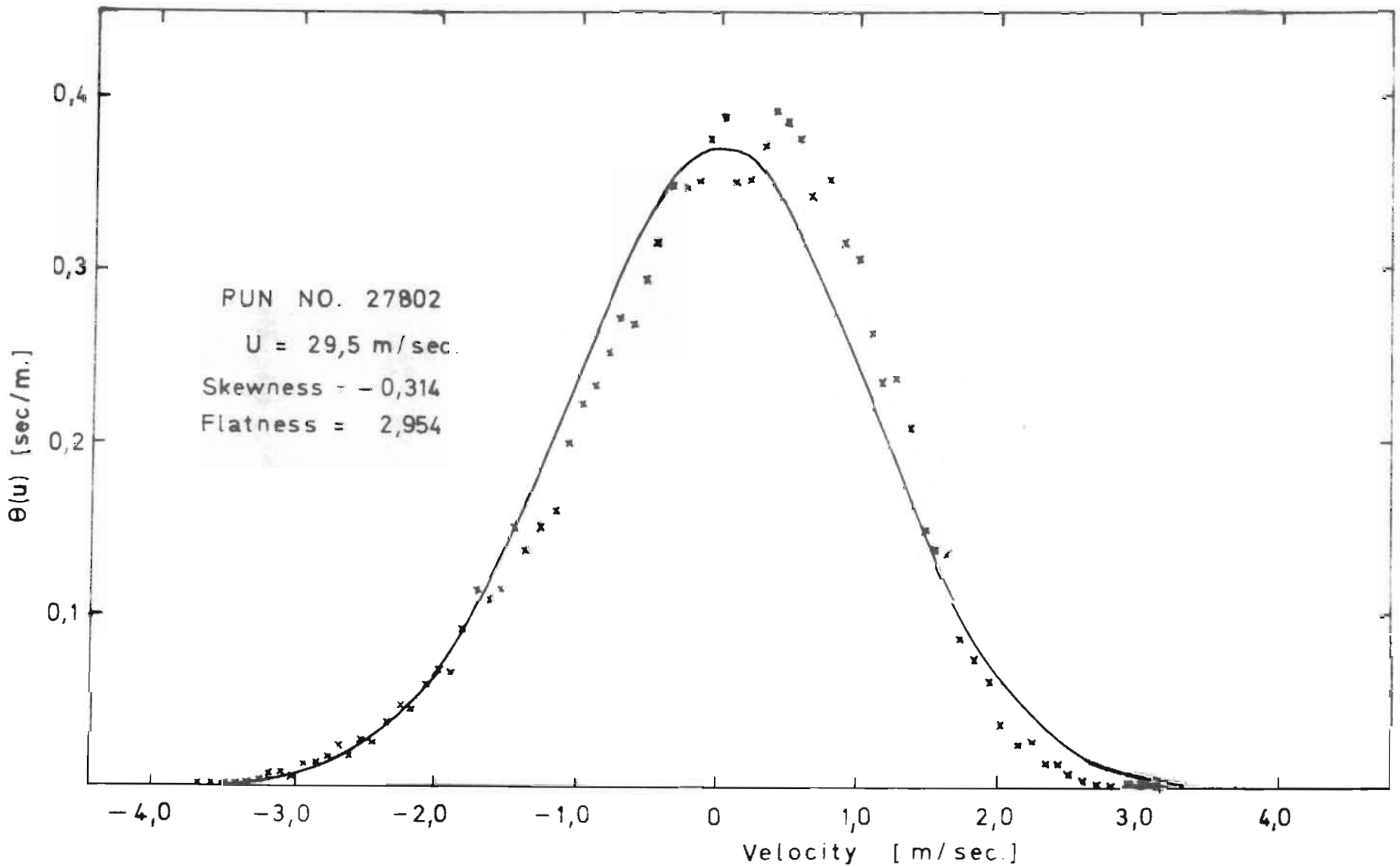

FIG. 12 VELOCITY PROBABILITY DENSITY FUNCTION

It is obvious that there is a sustained deviation from the Gaussian distribution with small positive deviations from the mean being more likely than small negative deviations. The nearly-constant value of the skewness at about -0.45 is surprising, but it will be shown in Section 4.4.5 that there does not appear to be a systematic error in the data treatment which could cause this, other than that discussed in Section 3.2, and it must be considered a real effect. Baldwin (17) has published data on skewness factors which show an increasing deviation from zero at lower velocities.

As Batchelor has pointed out (15), a flatness factor greater than 3.0 indicates a curve with a higher peak and wider skirts than the Gaussian curve with the same standard deviation i.e. very small and very large values of the random variable are more likely than for the Gaussian case. Baldwin (17) has also observed that a flatness factor greater than 3.0 may indicate bursts of high amplitude turbulence.

4.1.2 The Velocity Autocorrelation Function.

The autocorrelation function on the fluctuating longitudinal velocity at a fixed point was evaluated on about 30 000 data points on the computer directly as

$$R_E(t) = \frac{\overline{u(0)u(t)}}{\overline{u^2}}$$

The results are shown in Figs. 13 to 16. It is immediately apparent that there are low frequency

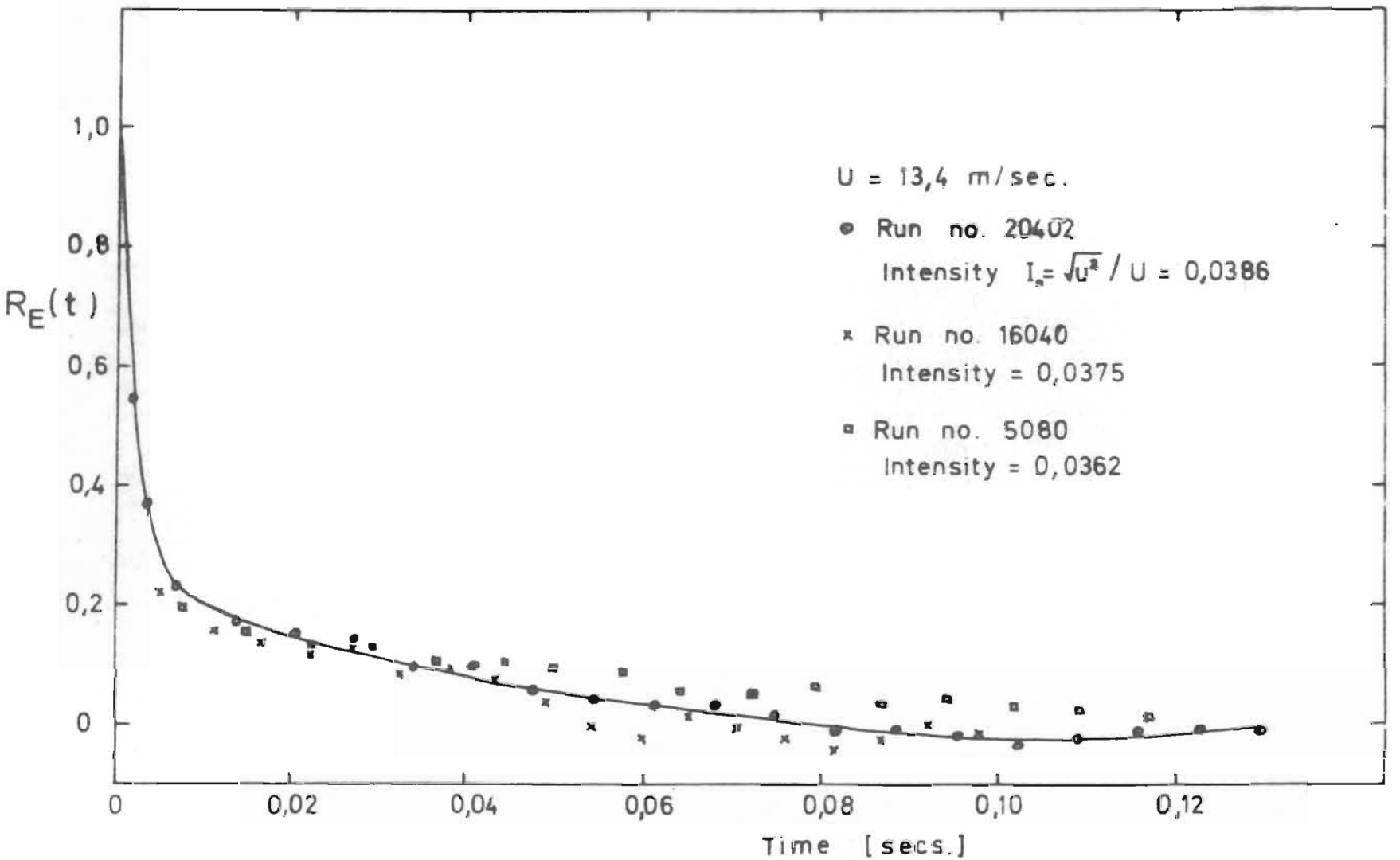

FIG 13 APPARENT EULERIAN AUTOCORRELATION

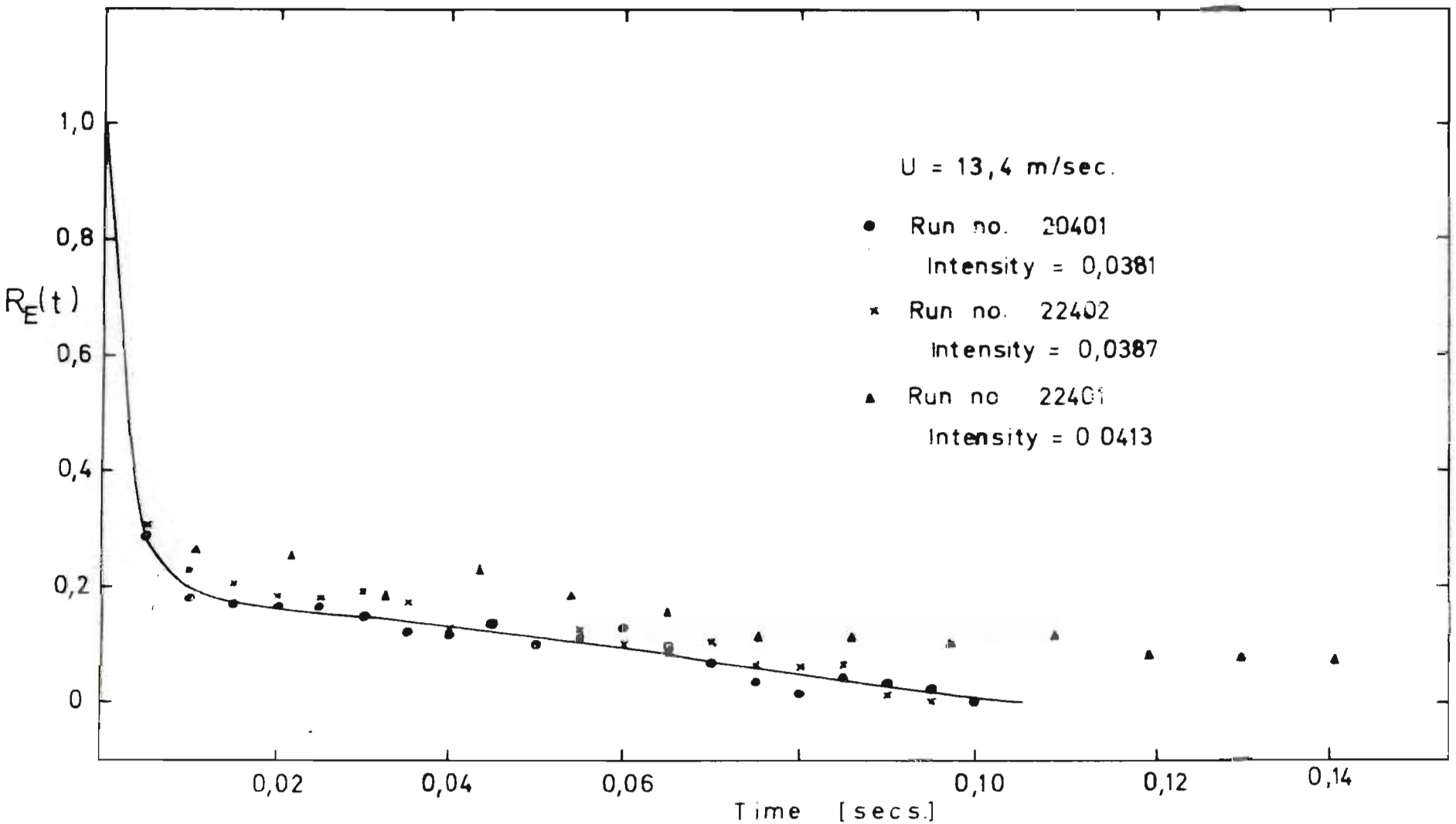

FIG. 14 APPARENT EULERIAN AUTOCORRELATION

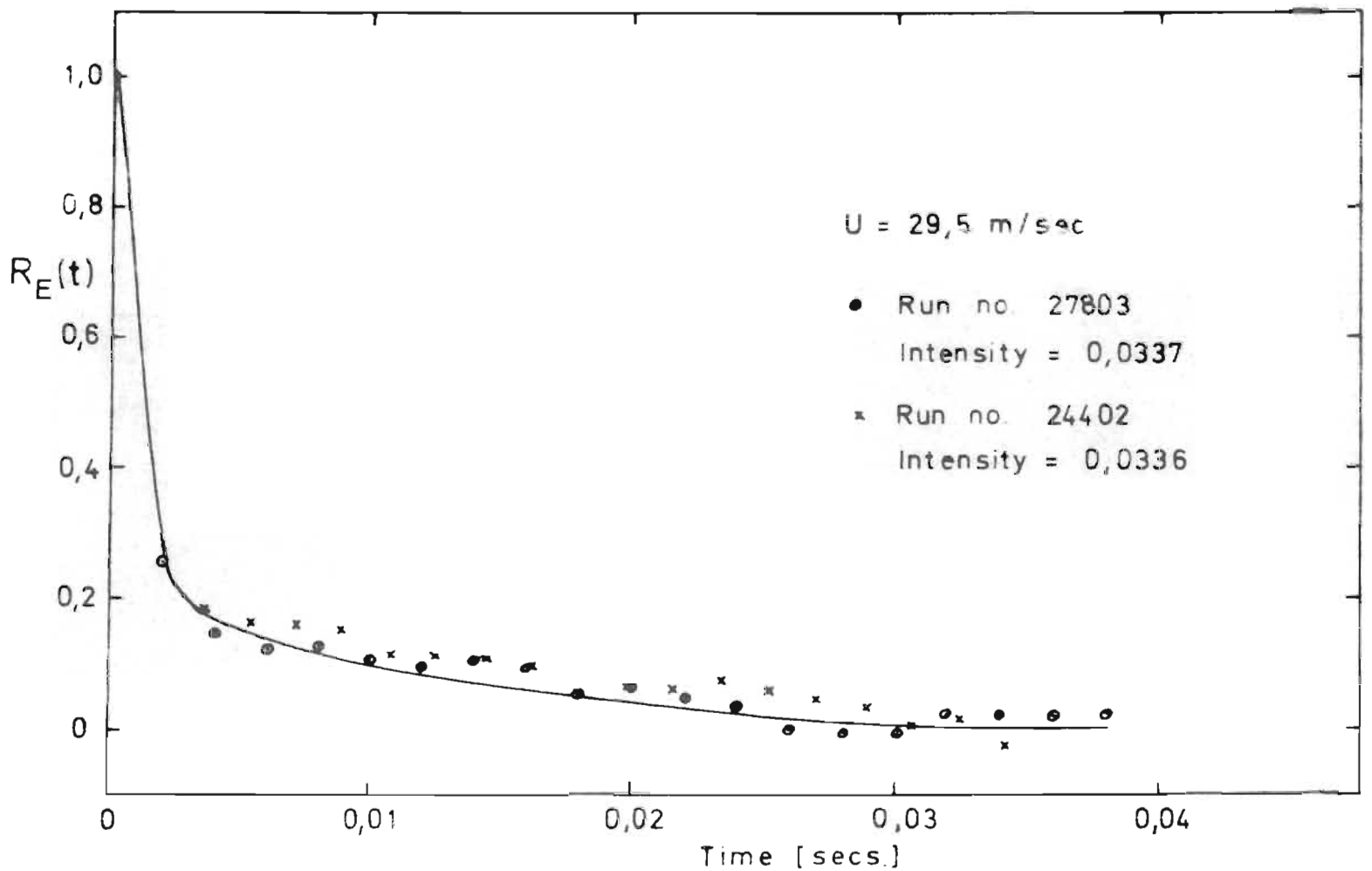

FIG. 15 APPARENT EULERIAN AUTOCORRELATION

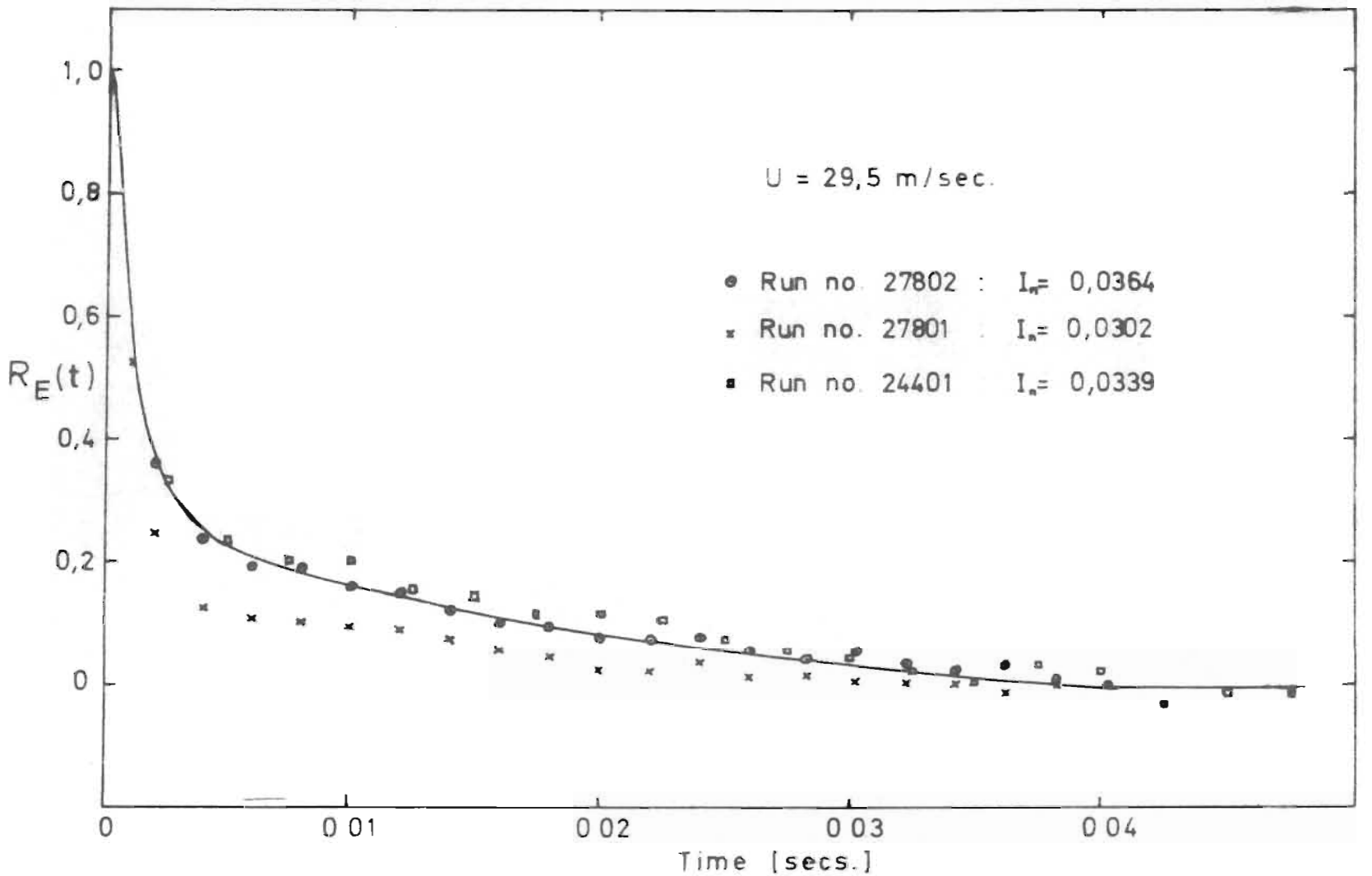

FIG 16 APPARENT EULERIAN AUTOCORRELATION

components present which cause the gradual approach to zero measured in all cases, together with a high value for the turbulence intensity. As there appears to be a fairly sharp distinction between the high and low frequency components, it was initially suspected that the low frequency fluctuations were not a logical part of the general turbulence field in the pipe and could conceivably be introduced by peculiarities of the apparatus. Considerable effort was thus devoted to the tracing of the possible cause of these components.

It is seen from a comparison of the auto-correlations at the two mean velocities considered that the slow fluctuations are not of a constant frequency. The correct reproduction of a cosine wave in the autocorrelation from the recording of a sinewave signal also indicates that no "noise" was being recorded superimposed on the signal. The hot-wire probe was rigidly constructed and it did not appear possible for vibrations to be set up in the probe itself. Particular care had also been taken in mounting the pipe to insulate it from any source of mechanical vibration.

The apparatus did not originally incorporate an anti-surge vessel between the pipe and the fan, the pipe being coupled directly to a single-shroud centrifugal fan with a flexible coupling, the throttle being placed before the fan: when the presence of low frequency fluctuations became apparent, the large volume vessel was installed with a higher capacity double-shroud centrifugal fan allowing greater throttling to smooth any possible surging

introduced by the fan. The time constant of this vessel based on the volumetric throughput and the volume of the vessel was about 22 secs. and 10 secs. resp. for the two velocities studied, and should thus be adequate in removing velocity fluctuations with a frequency higher than that corresponding to these values. This installation produced a slight lowering of ca. 5% of the mean variance of the velocity fluctuations but had little measurable effect on the low frequency components in the velocity autocorrelation function. The opening of the filter box on the inlet end of the pipe also produced no measurable effect on this function.

It was thus decided that the low frequency components of the velocity fluctuations in the longitudinal direction were an ineradicable part of the turbulence field in the central core of the pipe. It is possible that such low frequency components have been present to a greater or lesser degree in previous workers' apparatus, but have not been measured due to the low sensitivity of conventional recording techniques to frequencies below about 20 Hz. The importance of the frequencies below about 15 Hz. on the Eulerian integral scales has been shown by Patterson and Zakin (29) in liquids in 1-in. and 2-in. diameter pipes. It might be speculated that the slow longitudinal eddies are a function of the pipe geometry, becoming more noticeable in smaller pipes. It would have been interesting to study the velocity fluctuations in a 20 cm. or 25 cm. diameter pipe, but the limited capacity of the available fan did not justify the construction of

larger apparatus.

The fluctuation in the autocorrelation functions obtained under ostensibly identical conditions, indicates that the total time of recording of the signal, which varied from approximately 3 secs. to 10 secs. depending on the sample-time interval, was inadequate to define the low frequency components unequivocally; a larger capacity digital recording system was however not available. As noted in Section 1.3, Frenkiel and Klebanoff (31) found that in their work behind grids, also with a digital sampling technique, a recording time of 12.5 secs. was not sufficient to establish a constant autocorrelation function.

4.2 The Tracer Dispersion Results.

The dispersion of the radioactive tracer material was measured between two stations with varying distance between them, to obtain values of the mixing coefficient and mean velocity as a function of the separation distance. The first detector was situated 15 cm. from the injection point in the majority of runs: tests with greater separation from the injection point showed no significantly different results. The pulses recorded on the film were visually counted and summed over 5 unit time intervals of 0.0002 secs. to give the number of counts per millisecond as a function of time. This resulted in a series of digital values randomly distributed about the smooth concentration curve. This smooth curve was estimated by filtering the data with the quadratic dynamic programming filter which has been used previously for smoothing radioactive decay "noise" (54).

The filter strength was adjusted until a good fit appeared to be obtained on the digital values. A statistical criterion on the quality of fit would have been meaningless as a filter strength of zero causes the filtered curve to pass through every data point. These filtered curves were then used in the regression program: an estimate was first obtained by the method of moments of the two parameters U and E to be used as starting values in the regression, but this was a matter of convenience only and ensured fast convergence. Any reasonable starting values could have been chosen and would have resulted in convergence: the method of moments will thus not be discussed here.

Examples of the inlet and outlet pulses at the two velocities together with the regressed fit obtained are shown in Figs. 17 to 24. The greater dilution of the Krypton at the higher velocity resulted in curves which were not as well-defined as those obtained at the lower velocity. The majority of the dispersion measurements were thus made at the lower velocity although a series of measurements was made at the higher mean velocity for large separation of the two detection stations to obtain an estimate of the asymptotic value of the mixing coefficient. A more concentrated sample of Krypton than that available in these experiments would probably allow more accurate measurements at higher velocities.

The values of U and E obtained from the regression are presented in Tables 4.2.1 and 4.2.2, together with the Peclet number calculated on these values. It is seen that there is a wide spread in the values of the mixing

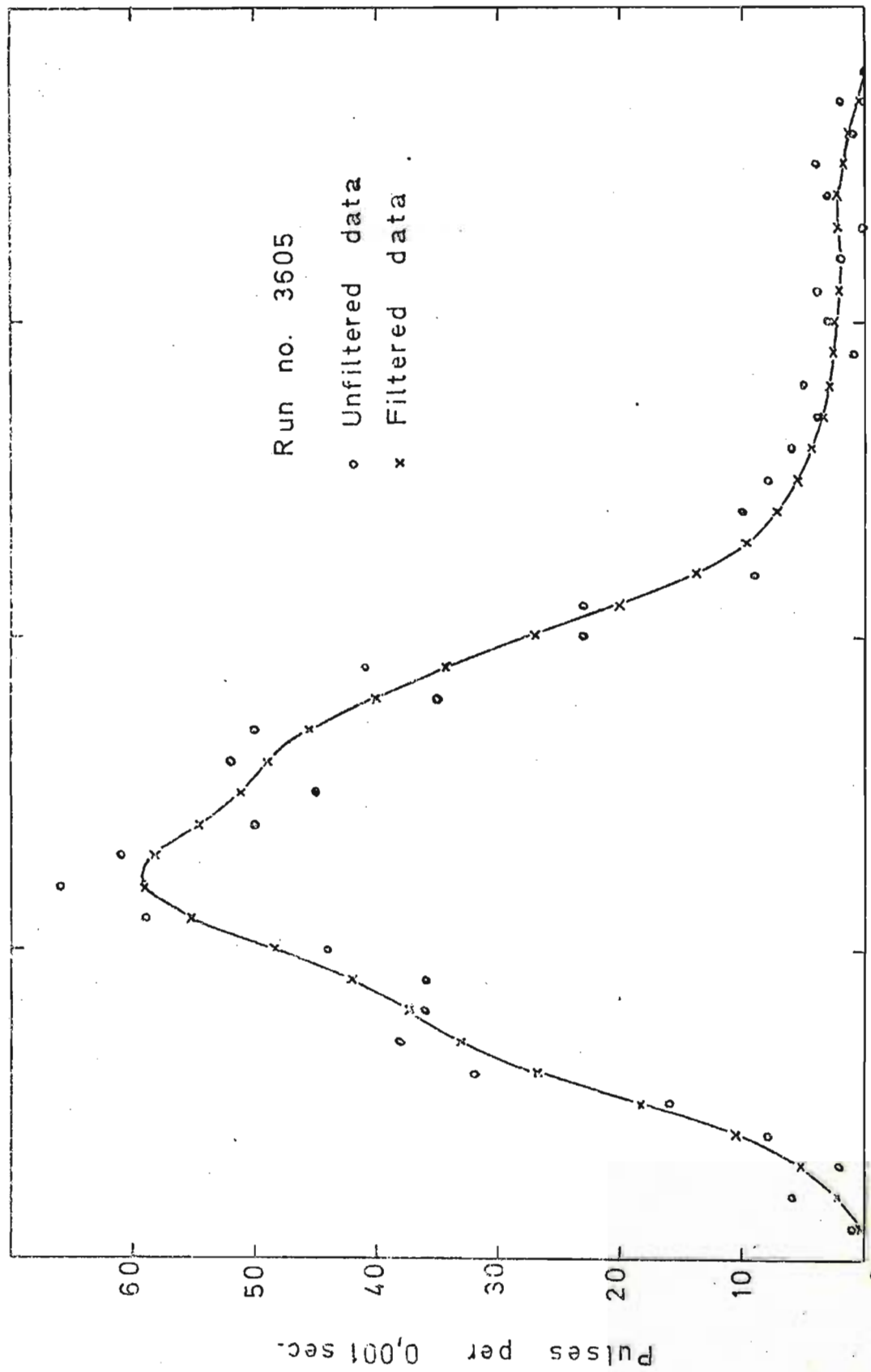

FIG. 17 INLET PULSE

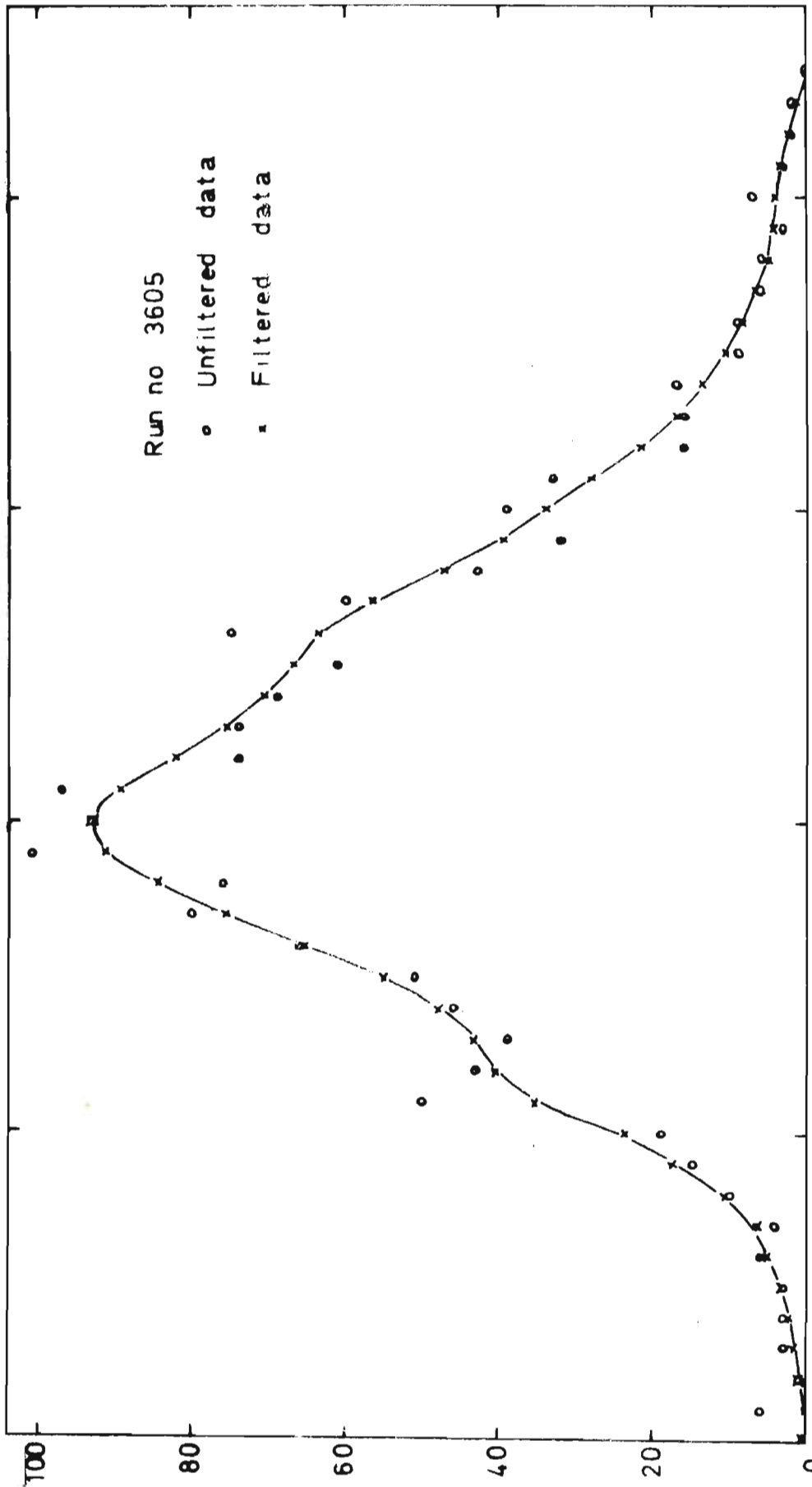

FIG 18 OUTLET PULSE

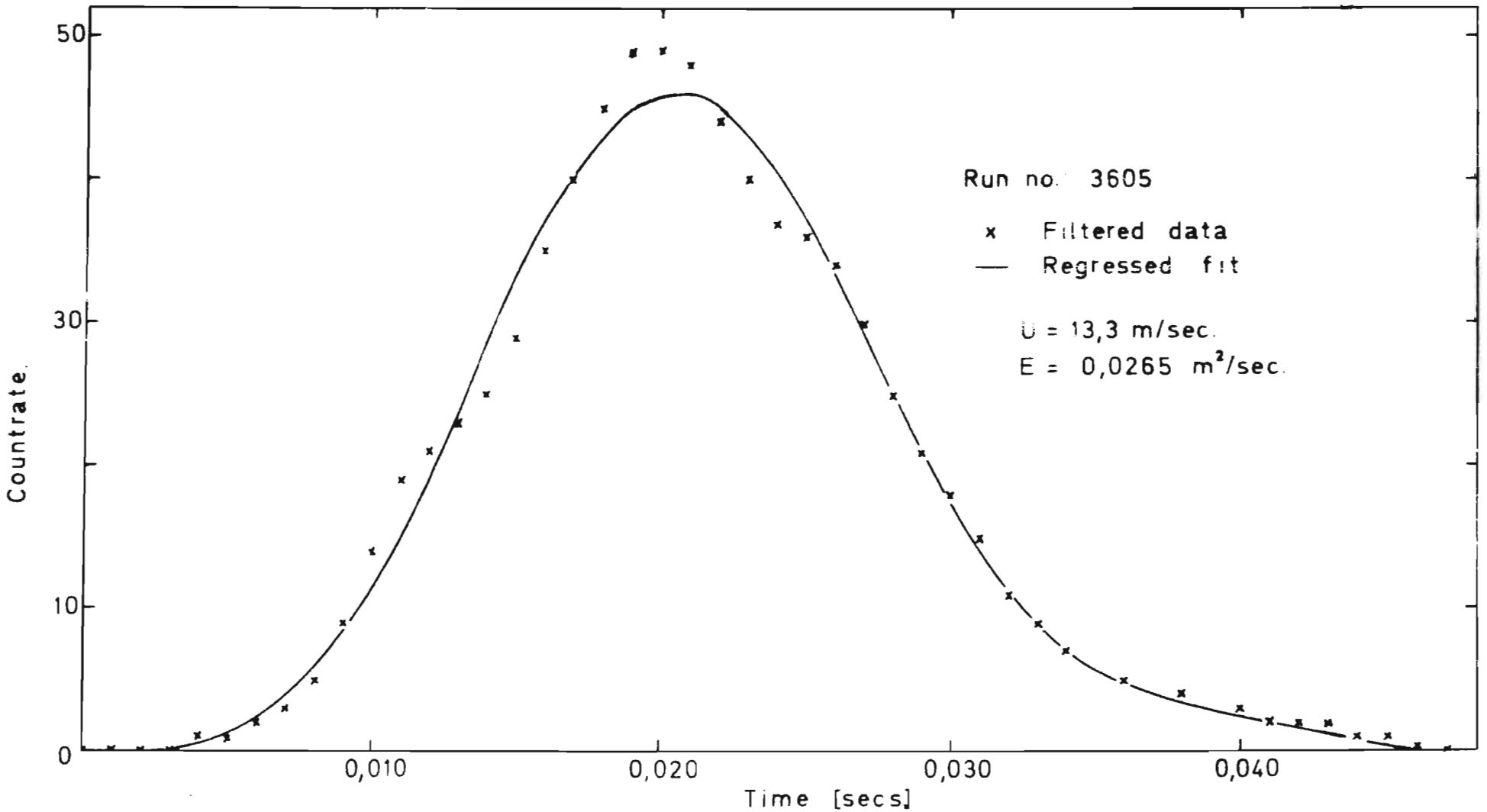

FIG 19 OUTLET PULSE REGRESSED FIT

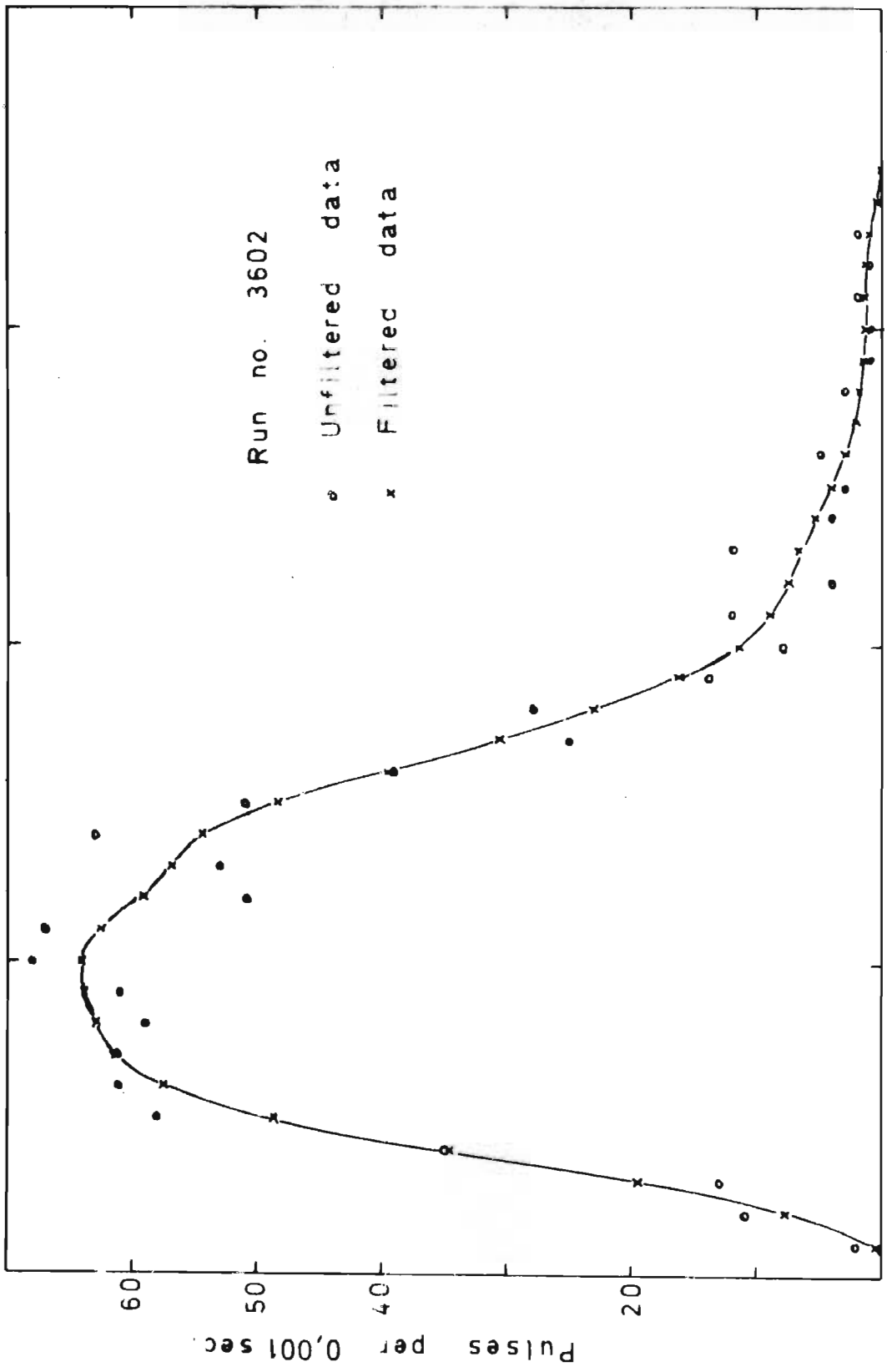

FIG 20 INLET PULSE

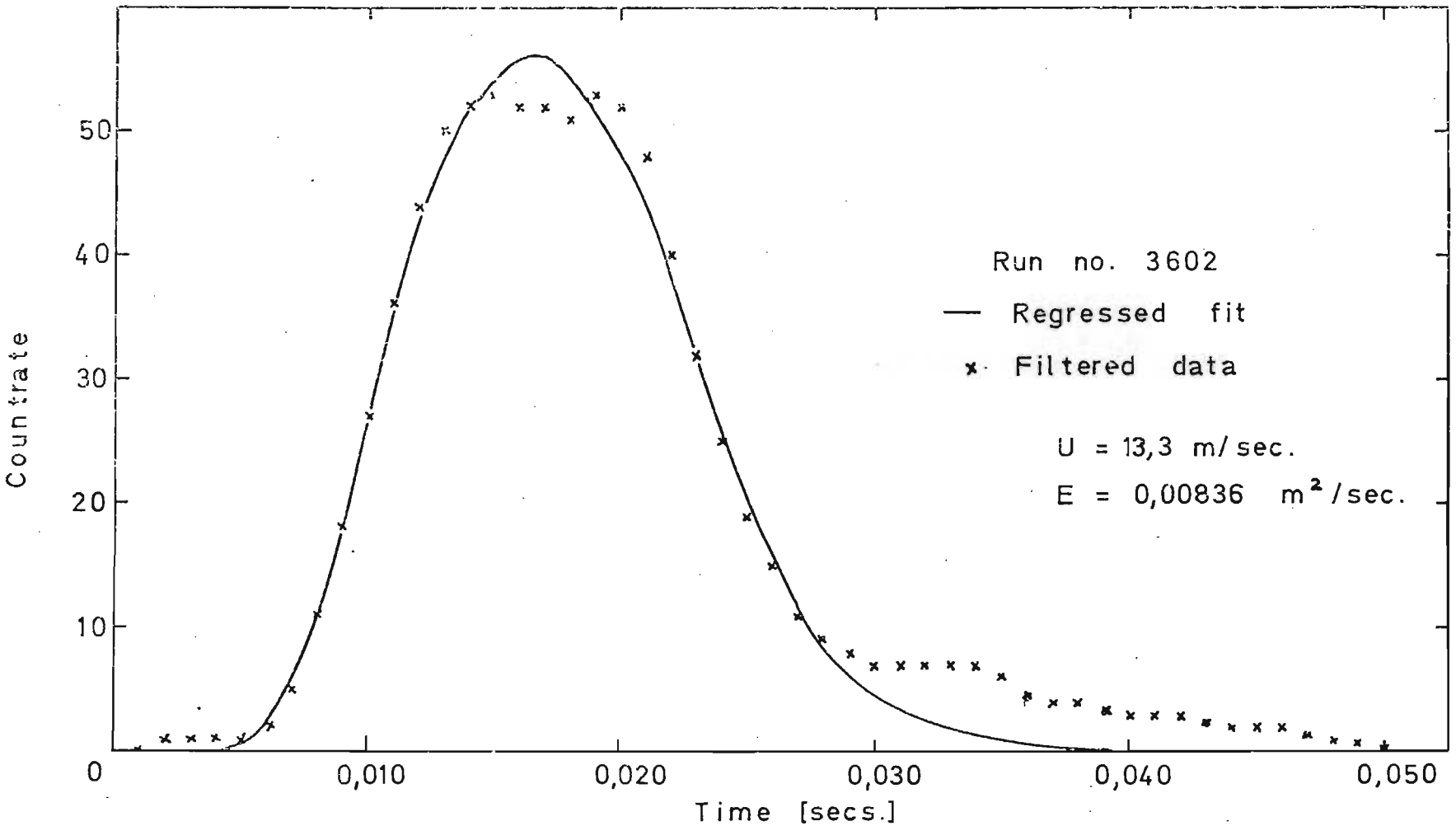

FIG. 21 OUTLET PULSE REGRESSED FIT

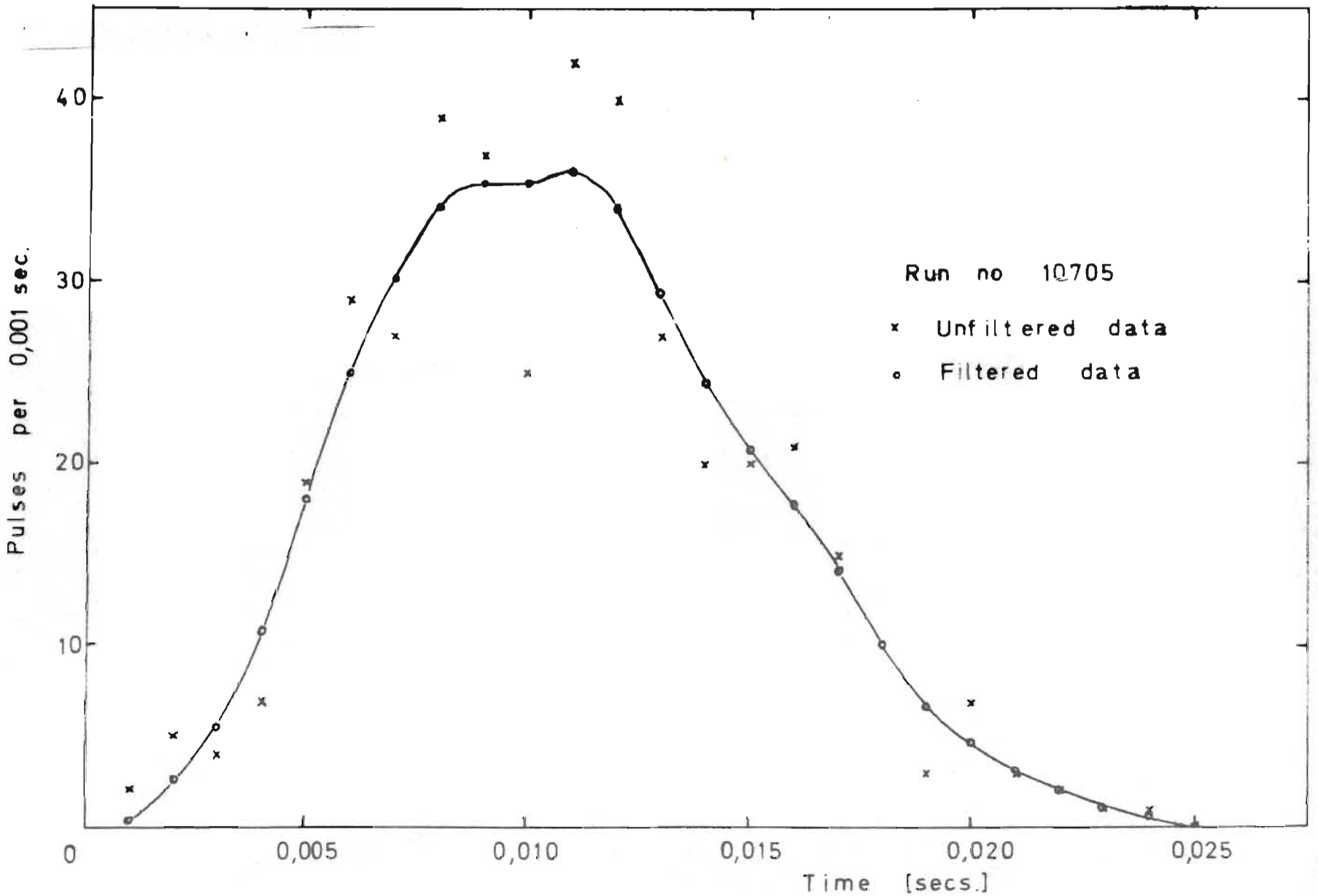

FIG 22 INLET PULSE

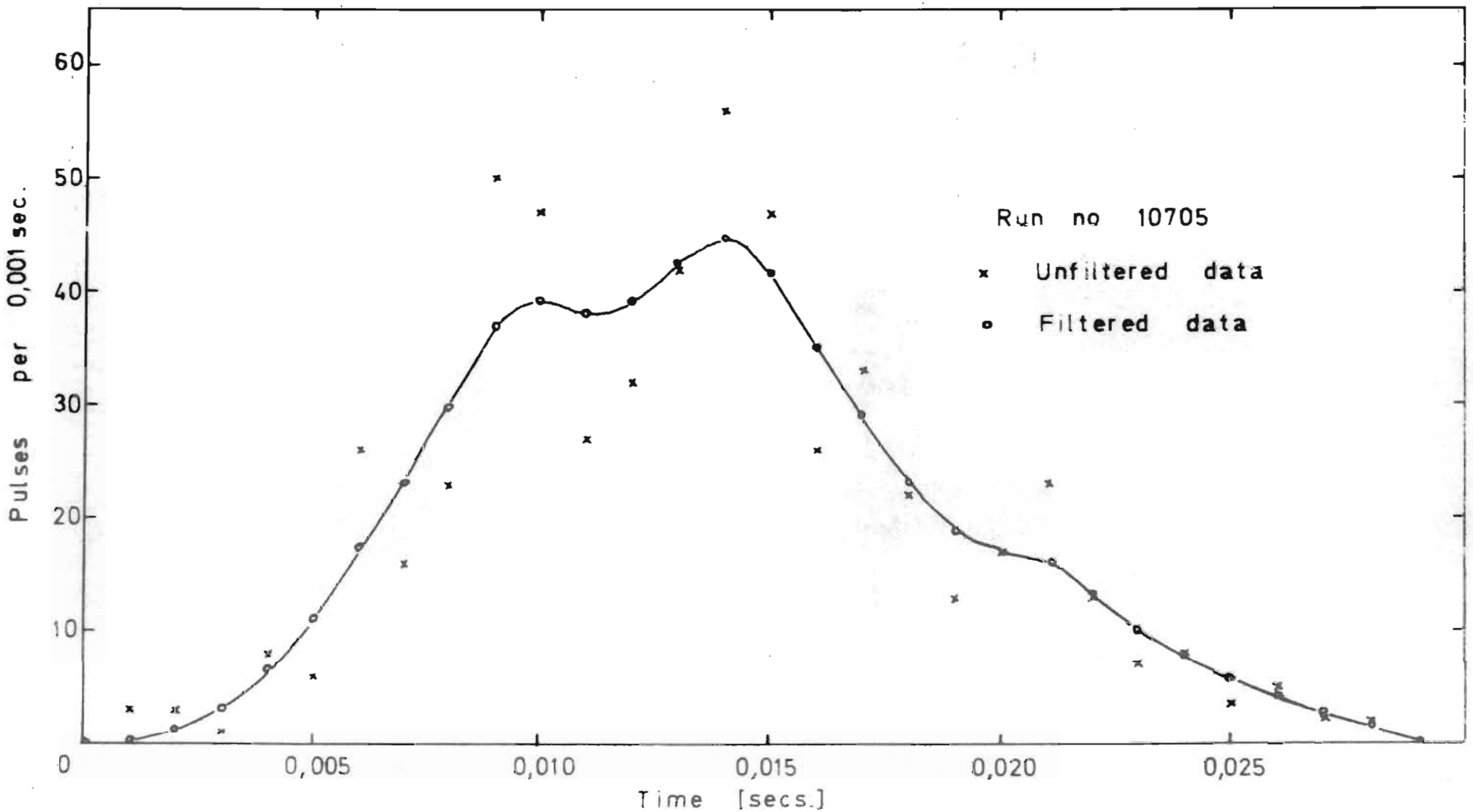

FIG 23 OUTLET PULSE

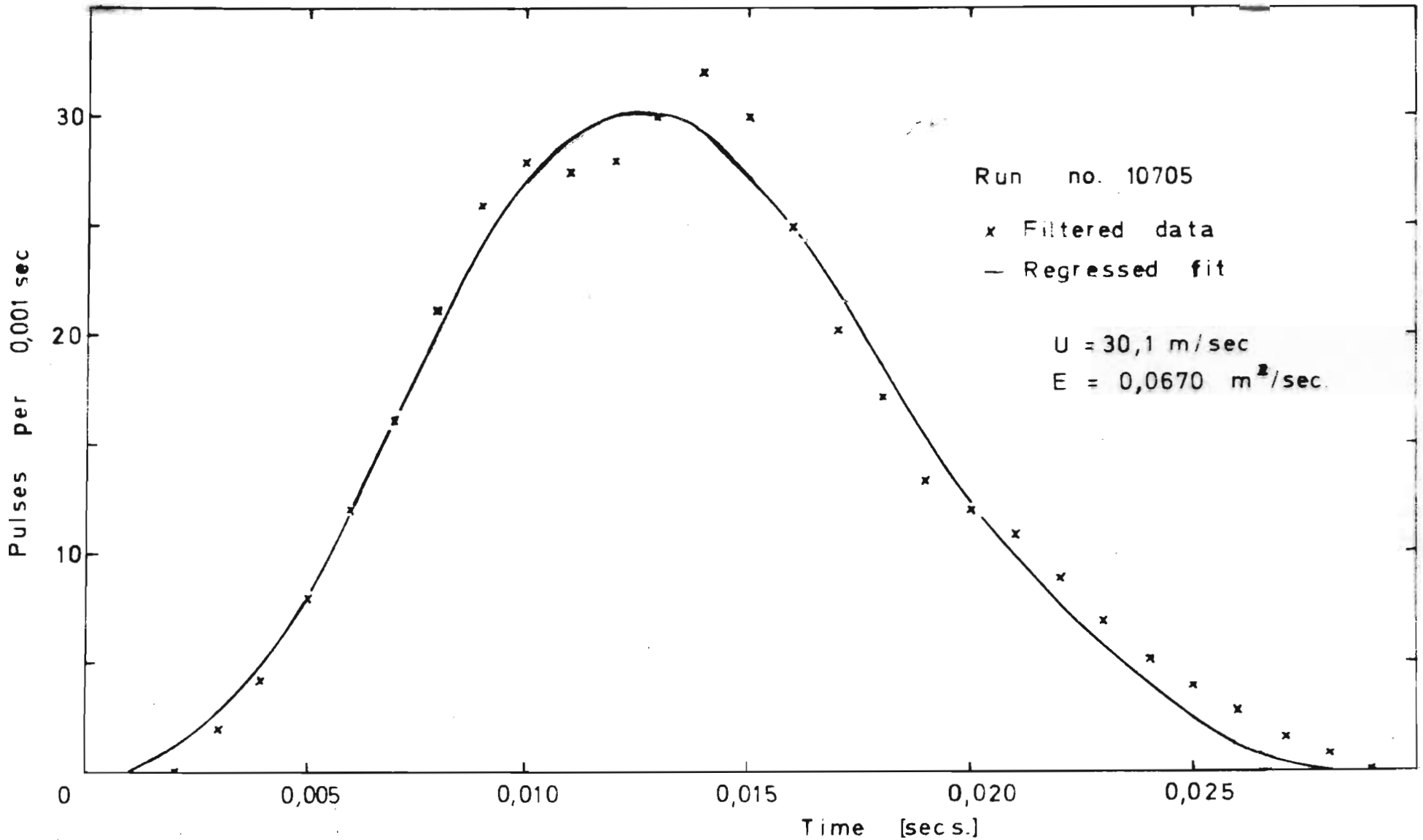

FIG. 24 OUTLET PULSE REGRESSED FIT

TABLE 4.2.1

REGRESSED VALUES OF U AND E FROM DISPERSION DATA.

Probe Separation(m)	Run No.	U(m/sec)	E(m^2/sec)	Peclet No.
0.457	11693	13.95	0.0126	169
	11694	13.30	0.0148	137
	11593	13.62	0.0113	184
	11494	12.90	0.0096	205
	11493	13.00	0.0151	131
	11692(X)	12.65	0.0062	311
	11594(X)	13.47	0.00186	1105
	11492(X)	12.50	0.00195	978
0.610	19303	13.93	0.0191	111.2
	19302	13.03	0.0155	128
	19301	13.02	0.0122	163
	25302	13.17	0.00465	432
	25304	12.42	0.0201	94.1
	25307	14.10	0.00957	225
	18303(X)	11.54	0.00438	402
	25301(X)	13,23	0.0935	21.6
0.762	27503	14.10	0.0183	117.4
	22502	13.62	0.0142	146
	3604	13.03	0.0289	68.7
	3605	13.28	0.0265	76.5
	3606	12.97	0.0223	88.7
	3607	13.37	0.0149	136.8
	3608	13.78	0.0250	84.0
	3609	13.03	0.0209	95.2
	3611	13.89	0.0102	207
	3601(X)	13.30	0.00781	260
	3602(X)	13.32	0.00837	242
	3603(X)	13.77	0.00697	301
	3610(X)	12.57	0.00772	248
	28501(X)	12.32	0.0307	61.2
	28503(X)	13.00	0.0391	50.7
	27502(X)	12.63	0.0306	62.9
	22501(X)	13.58	0.0013	1593
	18504(X)	13.88	0.00158	1340

TABLE 4.2.1 (contd.)

Probe Separation (m)	Run No.	U (m/sec)	E (m^2/sec)	Peclet No.
0.913	11792	12.80	0.0132	147.8
	11793	13.12	0.0221	90.5
	11794	13.04	0.0214	92.9
	11796	12.96	0.0108	183
	11797	13.28	0.0140	154.2
	11798	13.60	0.0139	149.2
	11799	13.10	0.0254	78.6
	11791 (X)	13.04	0.00344	578
	11790 (X)	13.62	0.00715	290
	11795 (X)	13.18	0.0427	47.0
1.37	11301	13.63	0.0284	73.2
	10301	14.20	0.0192	112.7
	5301	14.03	0.0255	84.0
	5302	13.92	0.0149	142.4
	10303 (X)	13.52	0.0408	50.5
	10306 (X)	13.78	0.0730	28.8
	9304 (X)	12.82	0.00279	700
1.675	29602	13.23	0.0183	110.2
	29603	13.43	0.0132	155.0
	29604	13.28	0.0160	126.5
	29608	13.02	0.0198	100.0
	29609	12.97	0.0234	84.5
	29610	13.32	0.0280	72.5
	29611	12.85	0.0172	114.0
	29601 (X)	13.52	0.00446	452
	29605 (X)	13.37	0.00688	296
	29606 (X)	13.40	0.00223	917

TABLE 4.2.2.

REGRESSED VALUES OF U AND E FROM DISPERSION DATA.

Probe Separation = 1.675 m.

Run No.	U(m/sec)	E(m^2/sec)	Peclet No.
10702	28.6	0.0811	53.8
10703	29.2	0.1813	24.3
10704	28.6	0.0302	144.3
10705	30.1	0.0670	68.5
10706	30.0	0.0762	60.0
10707	29.8	0.1022	44.5
10709	30.1	0.0672	68.3
10712	29.0	0.0250	177.0
10701(X)	28.7	0.0154	284.0
10713(X)	30.1	0.1817	25.2

TABLE 4.2.3

U AND E FROM REGRESSION ON IMPULSE RESPONSE.

Probe Separation(m)	U(m/sec)	E(m^2/sec)	Peclet No.
0.457	13.35	0.0154	132
0.610	13.30	0.0187	108
0.762	13.42	0.0220	83.0
0.913	13.13	0.0186	108
1.370	13.96	0.0228	93.4
1.675	13.18	0.0216	93.0
1.675	29.30	0.0787	56.7

coefficient obtained. There is little doubt that this is due to the random nature of the slow fluctuations found in the hot-wire anemometer measurements which make it practically impossible to obtain reproducible dispersion measurements in a longitudinal direction from pulse measurements over distances short enough not to be much affected by the velocity profile in the pipe. It was, however, decided to try to obtain a measure of the mean effect of the dispersion produced by these large eddies by averaging the impulse responses of those results which had apparently been affected by these eddies. Figs. 25 and 26 show examples of the impulse responses on which these calculations were performed. Cases such as curve 1 in Fig. 25 were excluded from consideration, as were all those cases in Tables 4.2.1 and 4.2.2 where the run number is followed by a cross, usually due to a value of U or E significantly deviating from the average behavior. It would be desirable to have a large number of samples so that the large deviations would, on average, contribute little to the mean, but as the number of samples was limited, the above treatment was applied. This method of data handling may be compared with the method of determining the rate of dispersion of a tracer material by the single-release method in which one particle is released at a time, the position being plotted at subsequent time intervals and an average displacement about the mean being obtained over many individual particle releases.

A least squares regression was performed on the average impulse response for each value of the probe

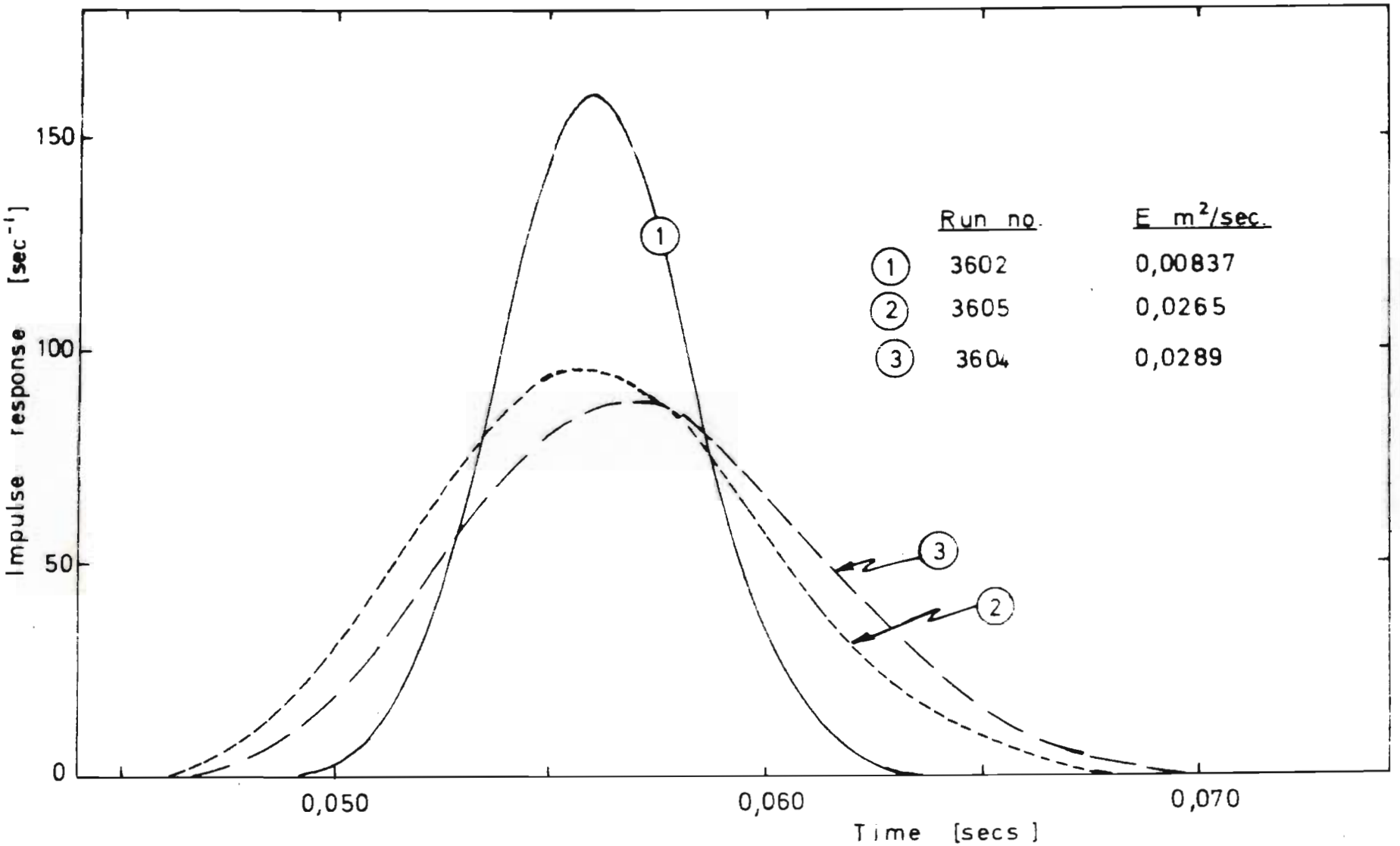

FIG 25 IMPULSE RESPONSES

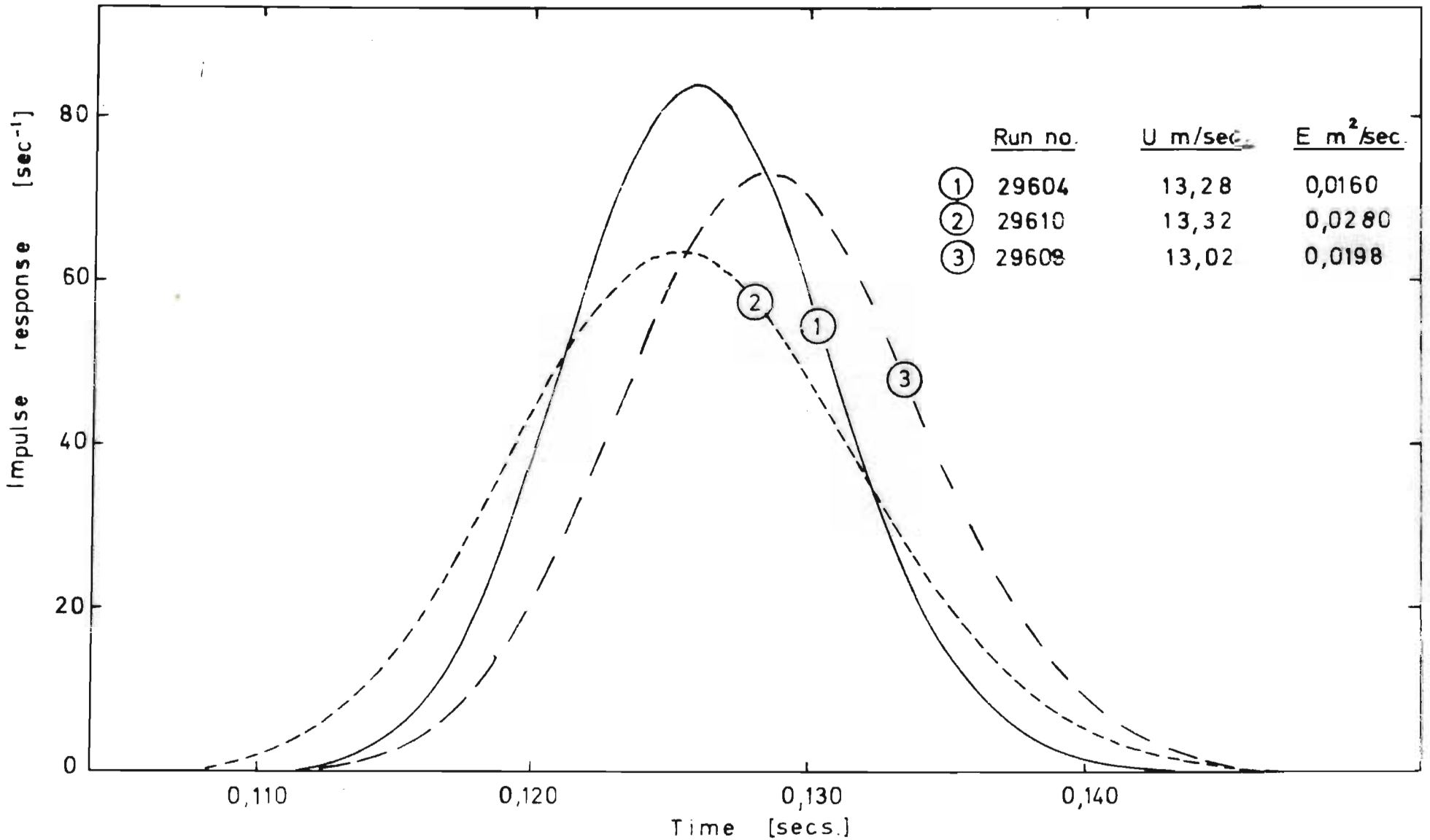

FIG. 26 IMPULSE RESPONSES

separation to obtain values of U and E in fitting the axial mixing impulse response function to this curve. The results of this procedure are shown in Figs. 27 to 30 and Table 4.2.3. The quality of the mean impulse response obtained is perhaps surprising, considering the fairly wide scatter of the individual data and the relatively small number of samples. It appears that the mean mixing coefficient obtained from this procedure and plotted in Fig. 30 has reached an asymptotic value for the large probe separations. A small correction is still necessary for the non time-linear behavior of the displacement variance curve: using the mean mixing coefficients and velocities obtained for each value of the probe separation ΔX, the displacement variance was calculated from the expression $\overline{\Delta X^2} = 2E \cdot \Delta t$ where $\Delta t = \Delta X/U$. Provided that the time taken for the pulse to pass the measurement stations is small compared with the time of flight, and it is kept in mind that the mixing coefficient obtained is an average value describing the mixing between the two probes, these parameters describe the dispersion quite well and may be plotted as shown in Fig. 31. The straight line fitted to this data with a least squares criterion gives a slope of $E = 0.0251\ m^2/sec.$ and a Peclet no. of 81.4 for the mean velocity of 13.4 m/sec. The average impulse response at a mean velocity of 29.5 m/sec. for large probe separation gave a Peclet no. of 56.7 which, when corrected as above, would yield a value of about 50.

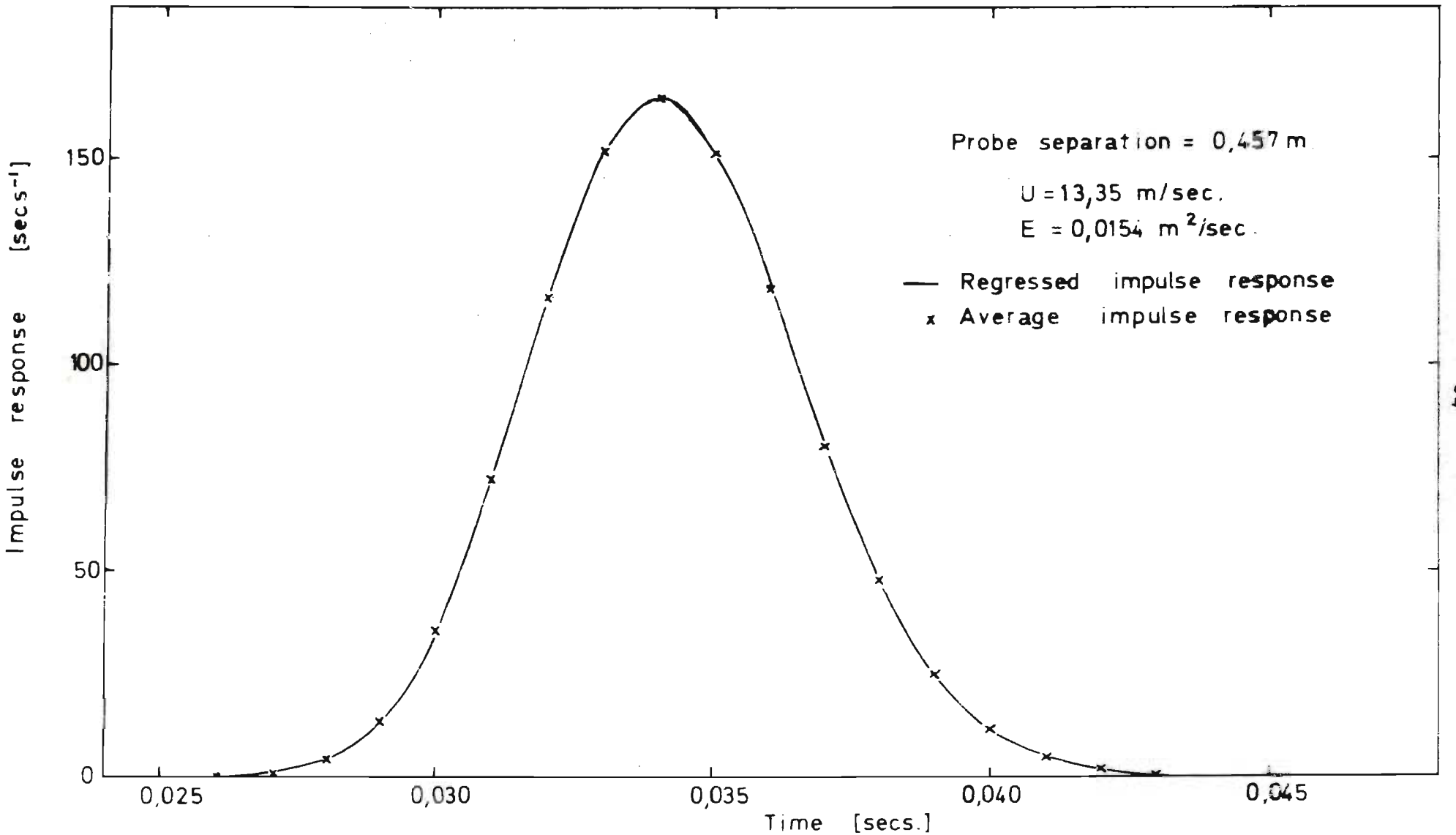

FIG. 27 REGRESSED FIT ON IMPULSE RESPONSE

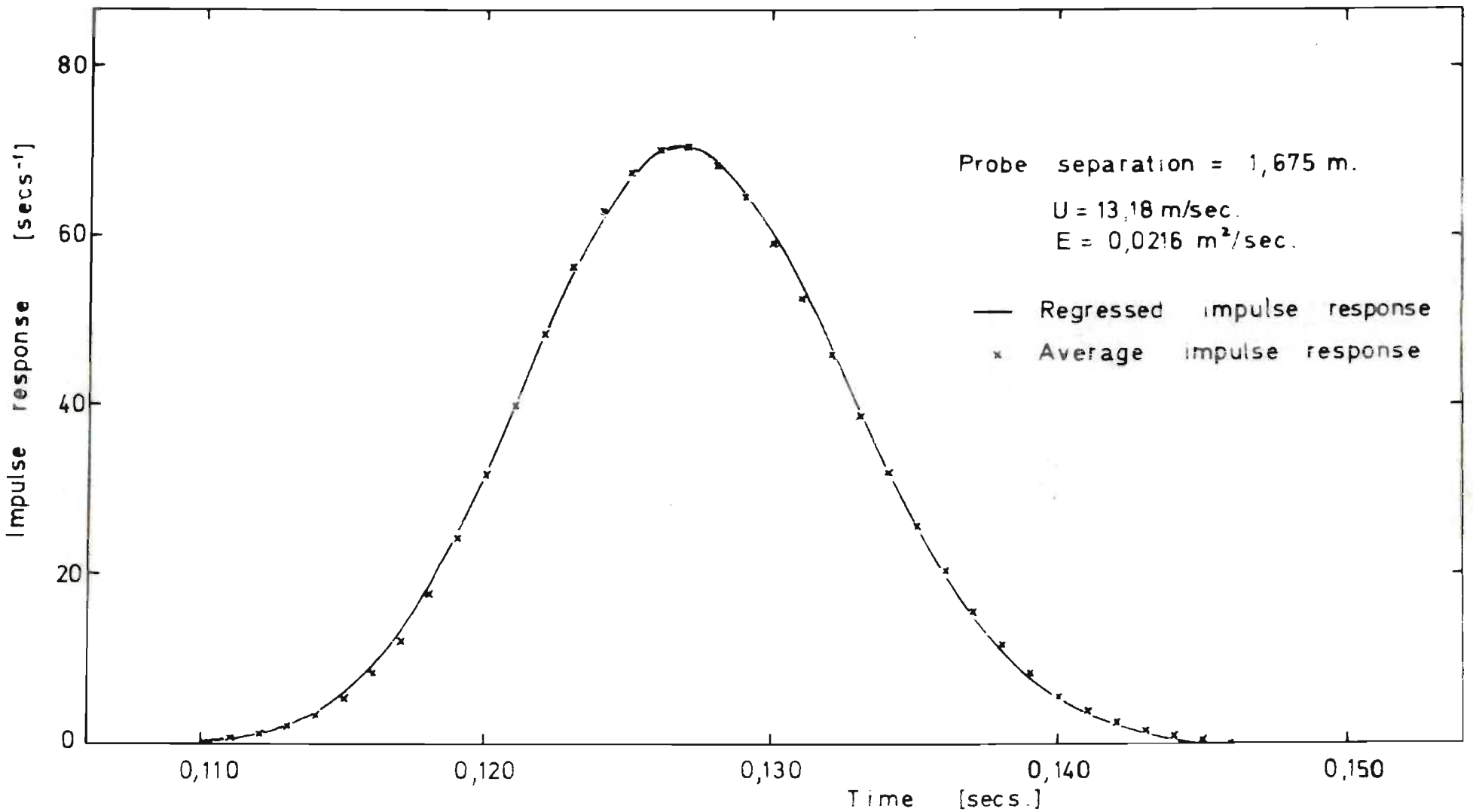

FIG. 28 REGRESSED FIT ON IMPULSE RESPONSE

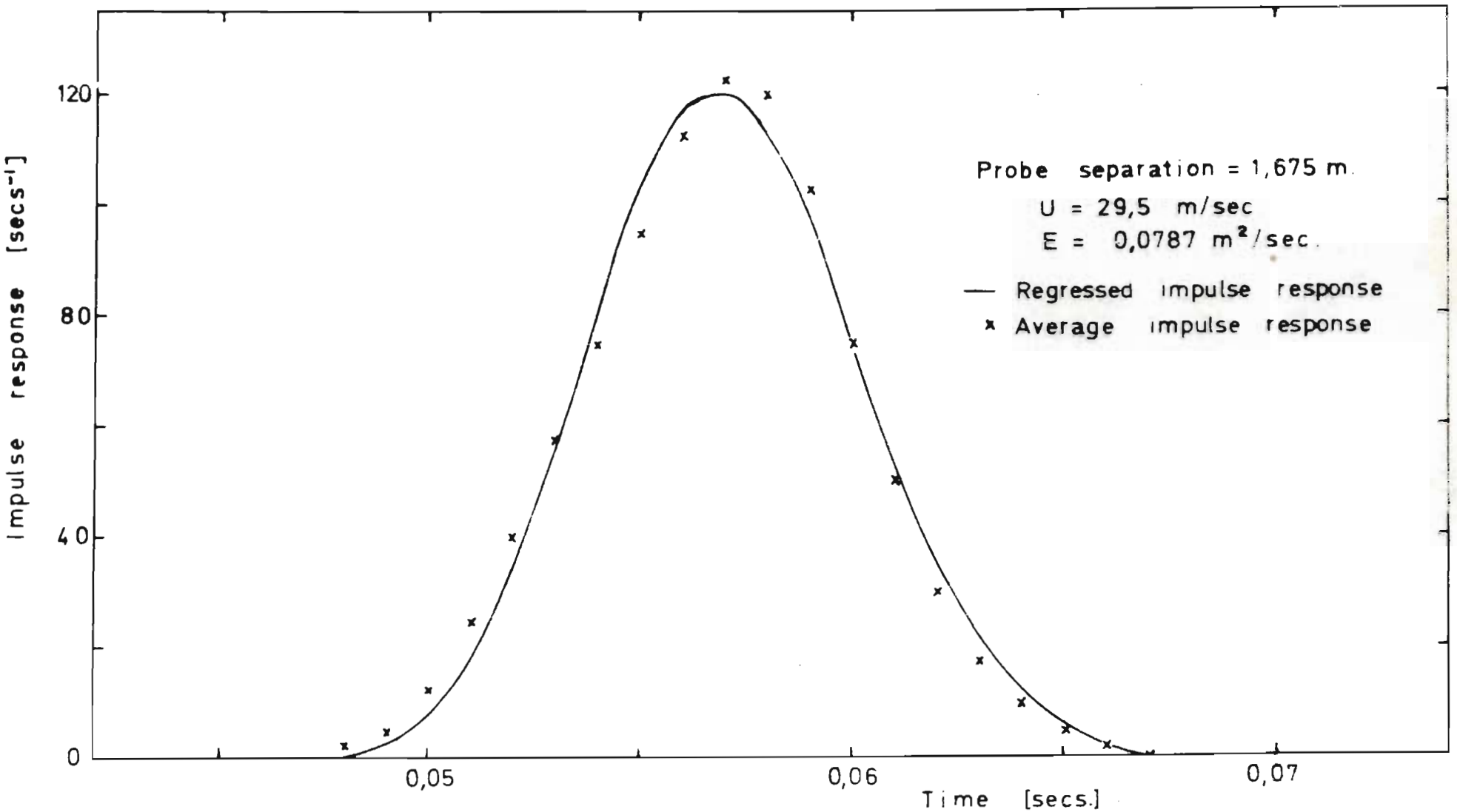

FIG 29 REGRESSED FIT ON IMPULSE RESPONSE

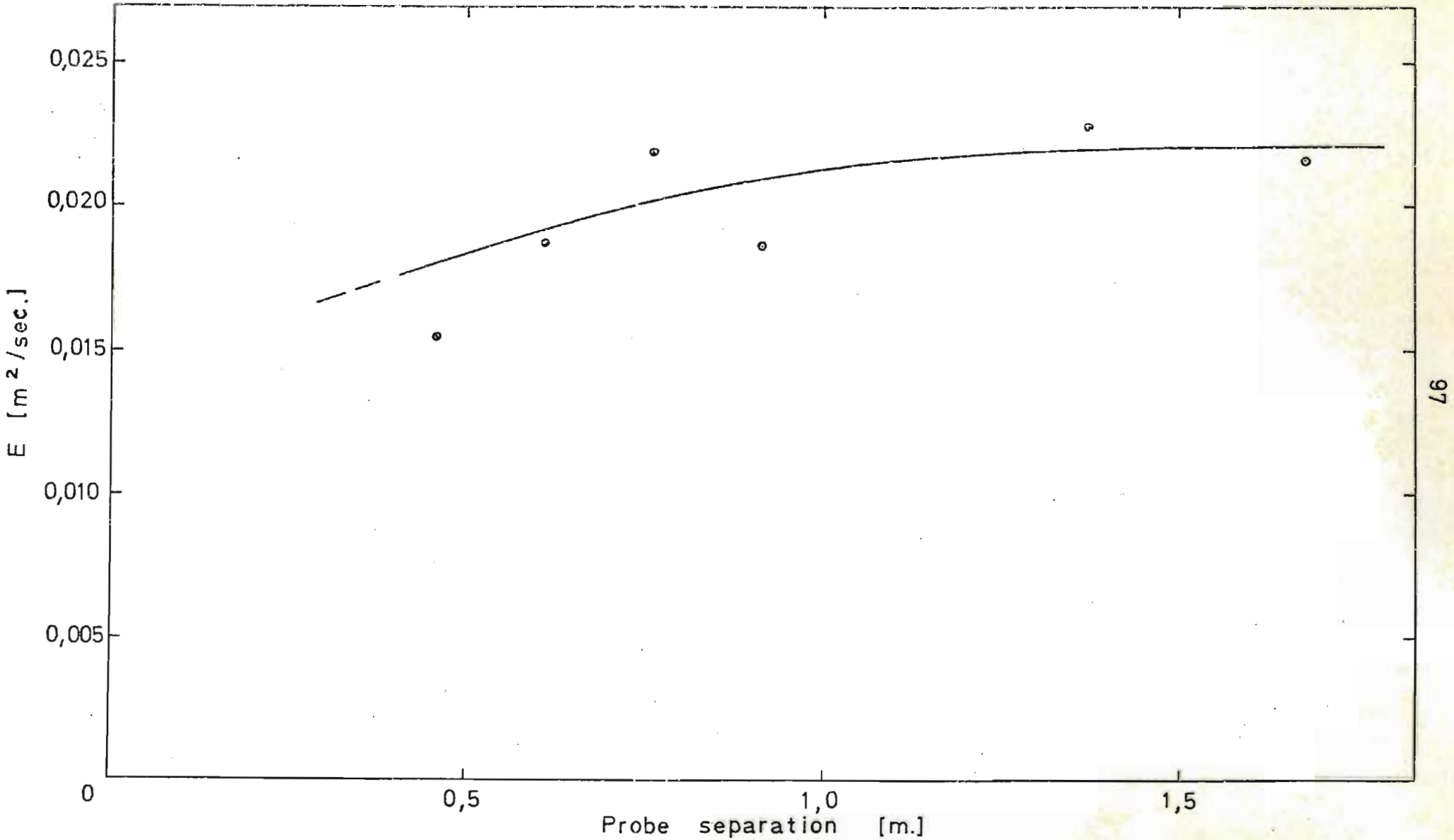

FIG. 30 MIXING COEFFICIENT VARIATION WITH PROBE SEPARATION.

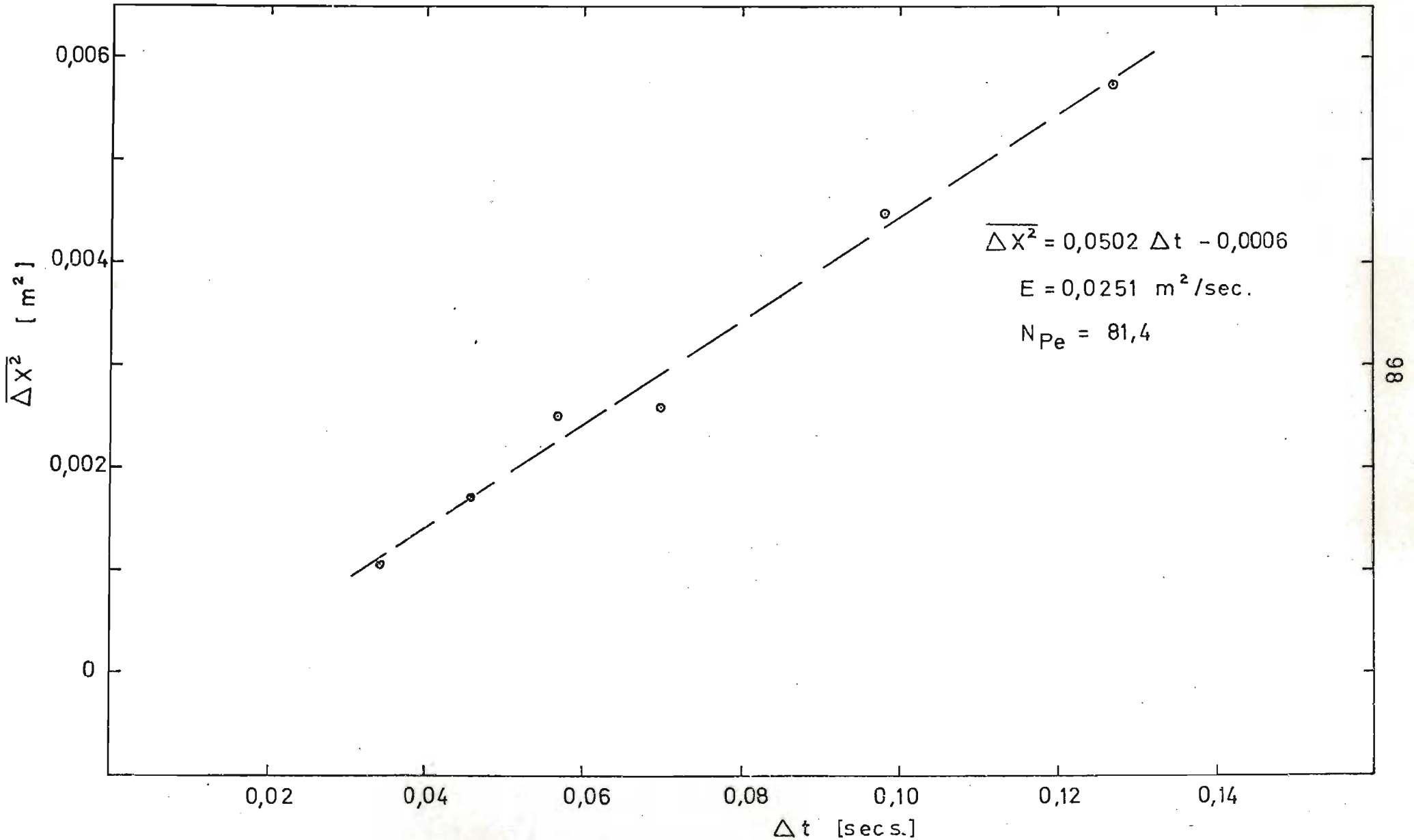

FIG. 31 DISPLACEMENT VARIANCE FROM REGRESSED PARAMETERS.

4.3 Use of the Velocity Distribution to Predict Dispersion: Philip's Theory.

The Lagrangian autocorrelation function proposed by Philip was calculated by an iterative procedure with the program EITER. Although the turbulence field in the present case was known to be far from the ideal case for which this model was derived, the method was applied to the longitudinal Eulerian autocorrelation function to predict a Lagrangian autocorrelation function and hence a turbulent axial mixing coefficient E, which was used to evaluate a Peclet no. Ud/E . The values are summarized in Table 4.3 together with the experimental Peclet number from the dispersion measurements.

TABLE 4.3

Unfiltered Hot-wire Anemometer Data.

Run No.	Velocity (m/sec)	Intensity	Peclet No. N_{Pe}	Experimental N_{Pe}
20402	13.4	0.0386	65.7	
20401	13.4	0.0381	50.4	
22401	13.4	0.0413	25.5	81.4
16040	13.4	0.0375	85.0	
22402	13.4	0.0387	44.0	
5080	13.4	0.0362	53.7	
24401	29.5	0.0339	56.1	
24402	29.5	0.0336	83.2	
27801	29.5	0.0302	126.5	~ 50
27802	29.5	0.0364	60.9	
27803	29.5	0.0338	102.5	

4.4 Filtering of Fluctuating Velocity Data.

The presence of the slow velocity fluctuations, which do not appear to be a consistent part of the spectrum of eddies one might expect in pipe flow, results in an autocorrelation function which has an initial sharp fall followed by a slow approach to zero. It might be expected, and various workers have assumed, that the Lagrangian and Eulerian autocorrelation functions would not be of a radically different shape. This has been shown (16,17) to be roughly true for dispersion in a radial direction. It would thus be of interest to remove the low frequency fluctuations from the recorded hot-wire anemometer longitudinal velocity data to obtain an Eulerian autocorrelation without the influence of the disturbing slow fluctuations. The criterion to be applied in this procedure will be discussed in the following sections.

4.4.1 The Quadratic Dynamic Programming Filter QDPF.

The possibility of filtering the fluctuating longitudinal velocity data to remove the low frequency components is an attractive advantage offered by the method of digital recording. The filtering may be performed on the original set of data with various filter strengths to meet the required criterion and give statistical data which may be compared with that determined by previous workers with analog recording techniques. The data, with appropriate filtering, may also be used to approximate the radial fluctuations which, being confined by the pipe walls, will not contain the same low frequency

components.

The two types of digital filter examined were both low-pass filters which were used with high filter strengths to establish a moving baseline which was then subtracted from the instantaneous value of the velocity. The first was the running or shifting mean filter; the second the quadratic dynamic programming filter QDPF (54,55). The latter filter produces a smooth set of data S_i from a noisy set R_i by minimizing the function

$$F = \sum_{i=1}^{M} \left[(R_i - S_i)^2 + E(S_{i-2} - 2S_{i-1} + S_i)^2 \right]$$

where M is the number of points. The second term represents the effect of the second derivative of the curve which is controlled by the filter strength E. The minimization is performed with dynamic programming (55). The band pass of this filter is unknown and a method of trial and error was adopted to determine the filter strength necessary to achieve the desired result.

A comparison is shown in Fig. 32 of the auto-correlation functions determined on the same set of raw data after filtering with the two types of filter to give the same value for the turbulence intensity of 0.0314. As the quadratic dynamic programming filter provided a direct control on the second derivative of the curve, it was felt that this resulted in a better-defined control on the frequencies passed by the filter. This filter was thus considered to be preferable to the running mean filter, although practically there appears to be little difference in their effect.

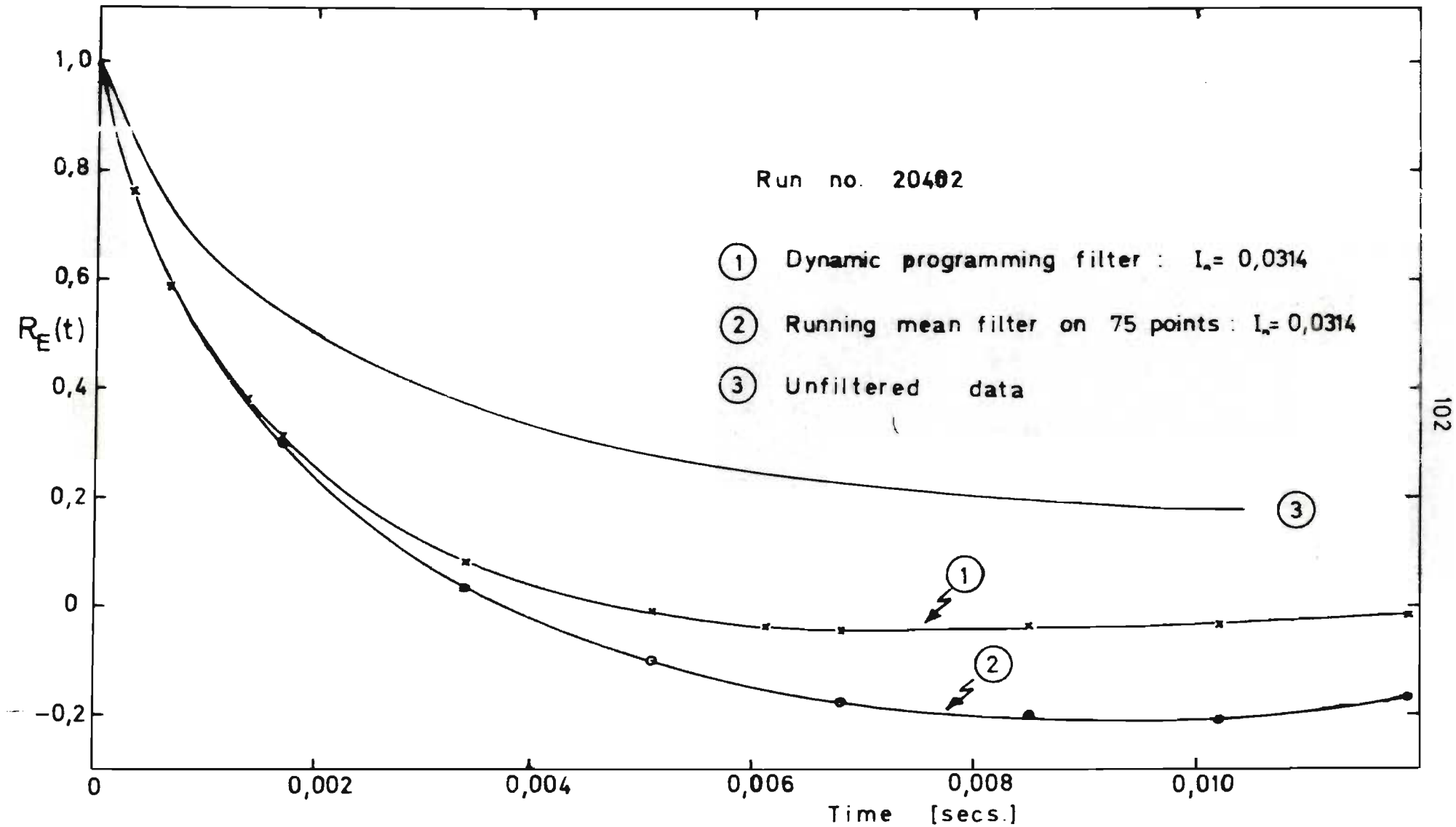

FIG. 32 AUTOCORRELATION ON FILTERED DATA

Fig. 33 shows the base curve obtained by filtering the same data with the dynamic programming filter with a filter strength of 50 000 and it is obvious that quite strong filtering is taking place. Fig. 34 represents the effect on the autocorrelation function of filtering the fluctuating velocity data with QDPF with various filter strengths. The shape of the unfiltered curve in this figure may be noted as it shows clearly the initial quite smooth decrease which is followed by the slower approach to zero.

4.4.2 Dispersion in a Radial Direction.

The Peclet number for the turbulent dispersion of a tracer material in a radial direction under conditions comparable with those of the present investigation, has been measured by many workers as discussed in Chapter 1. The turbulent intensity $(\overline{v^2})^{\frac{1}{2}}/U$ in the radial direction has been established from these measurements (17,18) as being approximately 0.0284. The comparison of a predicted Peclet number with the experimentally observed values in the radial direction was thus an attractive possibility. The hot-wire anemometer data recorded was thus filtered to remove the low frequency components until a turbulence intensity of about 0.0284 was obtained. These Eulerian autocorrelation functions were then used with Philip's method to predict radial Peclet numbers which are presented in Table 4.4.2 together with values showing the sensitivity of the Peclet number to the filtering operation.

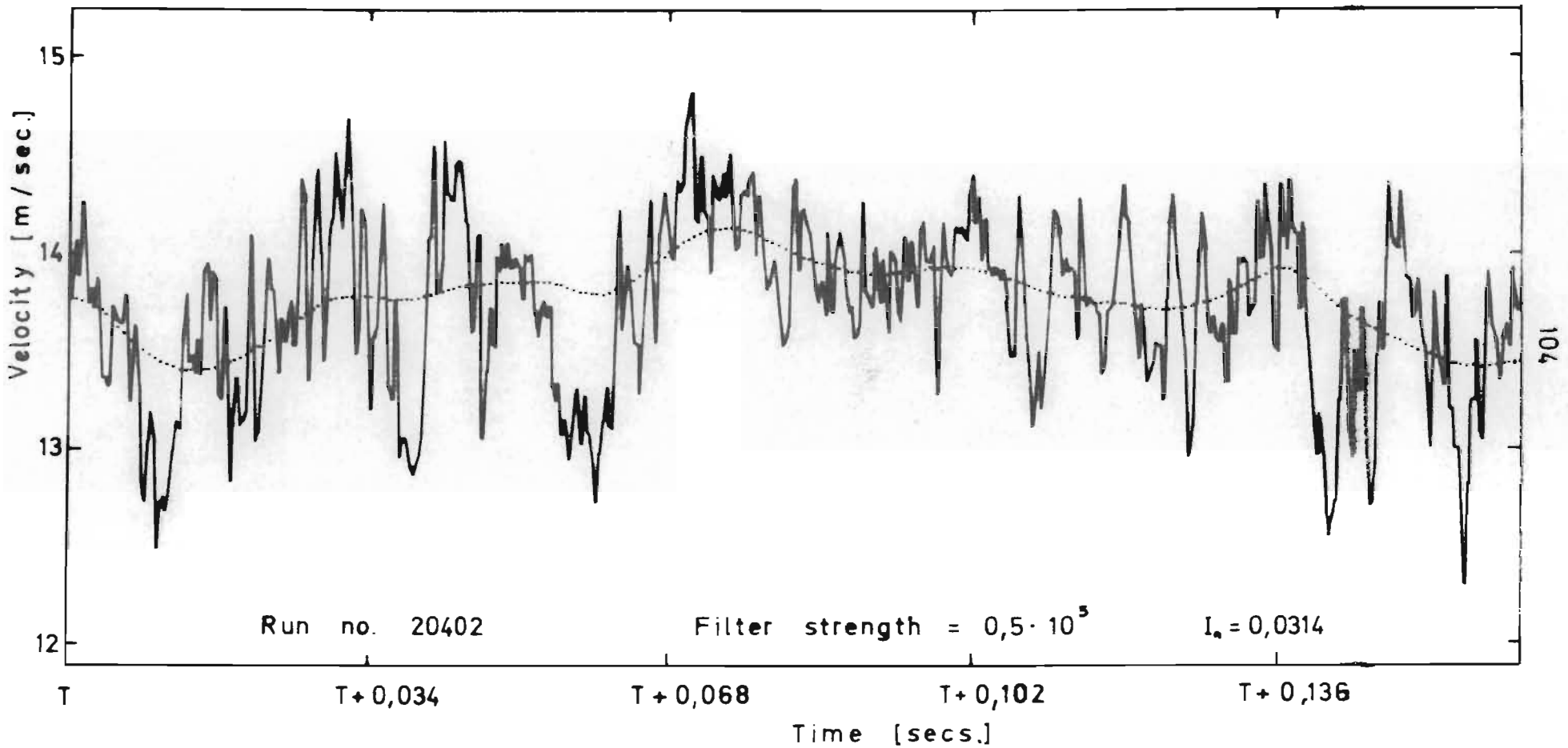

FIG. 33 QUADRATIC DYNAMIC PROGRAMMING FILTER

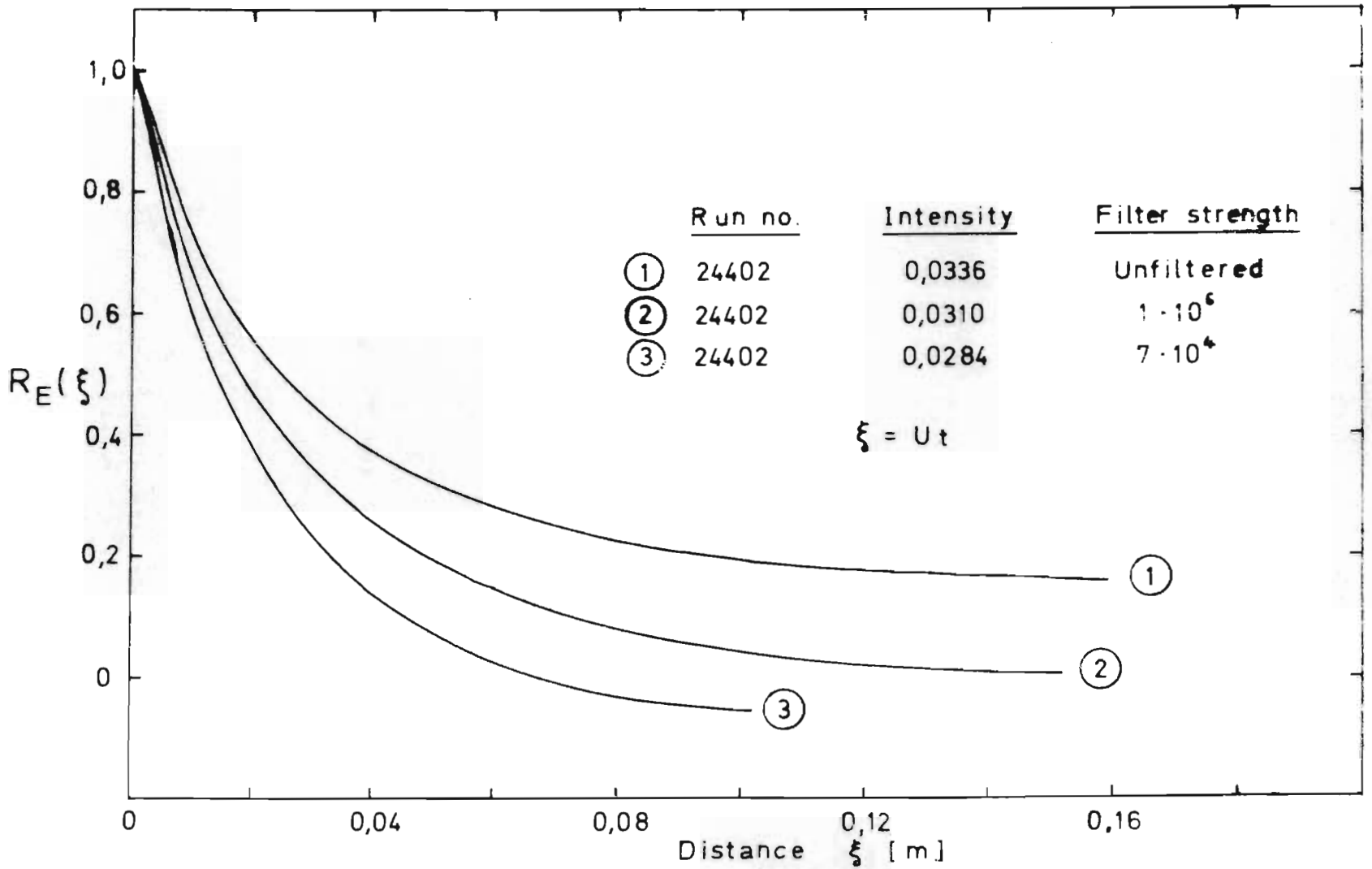

FIG. 34 FILTERED DATA AUTOCORRELATION

TABLE 4.4.2

Run No.	Velocity (m/sec)	Intensity	N_{Pe}	Previous radial N_{Pe} (author)
20402	13.4	0.0285	940	750 (Towle & Sherwood)
22401	13.4	0.0286	822	910 (Baldwin)
16040	13.4	0.0282	928	1200 (Flint et al)
22402	13.4	0.0285	915	630 (Malengé & Gosse)
20401	13.4	0.0283	928	852 (Becker et al)
5080	13.4	0.0284	905	760 (Boothroyd)
24401	29.5	0.0285	470	620 (Groenhof)
24402	29.5	0.0284	609	
27801	29.5	0.0281	738	
27802	29.5	0.0284	617	
27803	29.5	0 0283	630	
Sensitivity:				
27803	29.5	0.0276	697	
27803	29.5	0.0286	595	
27803	29.5	0.0283	630	
20401	13.4	0.0311	665	
20401	13.4	0.0287	886	
20401	13.4	0.0277	1015	
20401	13.4	0.0283	928	

It may be noted that the previously reported radial Peclet numbers, although quite scattered, appeared to show no significant dependence on the mean velocity or Reynolds number at which they were measured.

From the table it is apparent that Philip's method predicts lower Peclet numbers at the higher velocity, although all the values lie in the range previously reported. The agreement among the values at the lower velocity is remarkable considering the method used to obtain the Eulerian data. The Lagrangian autocorrelations predicted

for each of the velocities are shown in Fig.35.

4.4.3 Dispersion Predicted with Baldwin's Data.

The data obtained at a mean centerline velocity of 29.5 m/sec. corresponds to a Reynolds no. of 285 000 and should thus be directly comparable with the data obtained by Baldwin at 72.6 ft/sec. mean centerline velocity in an 8-in. diameter pipe (17). Fig. 36 shows the auto-correlation curve obtained by Baldwin with a conventional analog recording technique on a correlator which had a frequency response flat within ±3 dB from 30 to 4 000 Hz., compared with the autocorrelation curve obtained on the present data filtered to give the same intensity of turbulence as that measured by Baldwin. This comparison is perhaps not strictly justifiable as Baldwin's axial intensity data was measured with a root mean square meter having a flat response ±3 dB from 5 to 500 000 Hz., and would have included the effect of lower frequencies,if present,than were recorded or correlated. The difference between the two curves is, however, not very large although there is a marked difference in the amplitude at small time lag. The Eulerian integral scales are, however, approximately equal.

Philip's method of prediction of the Lagrangian autocorrelation function was thus applied to Baldwin's longitudinal Eulerian data obtained at four mean velocities, the autocorrelation data being read directly from the reported curves. The resulting Peclet numbers as a function of mean velocity are presented in Table 4.4.3.

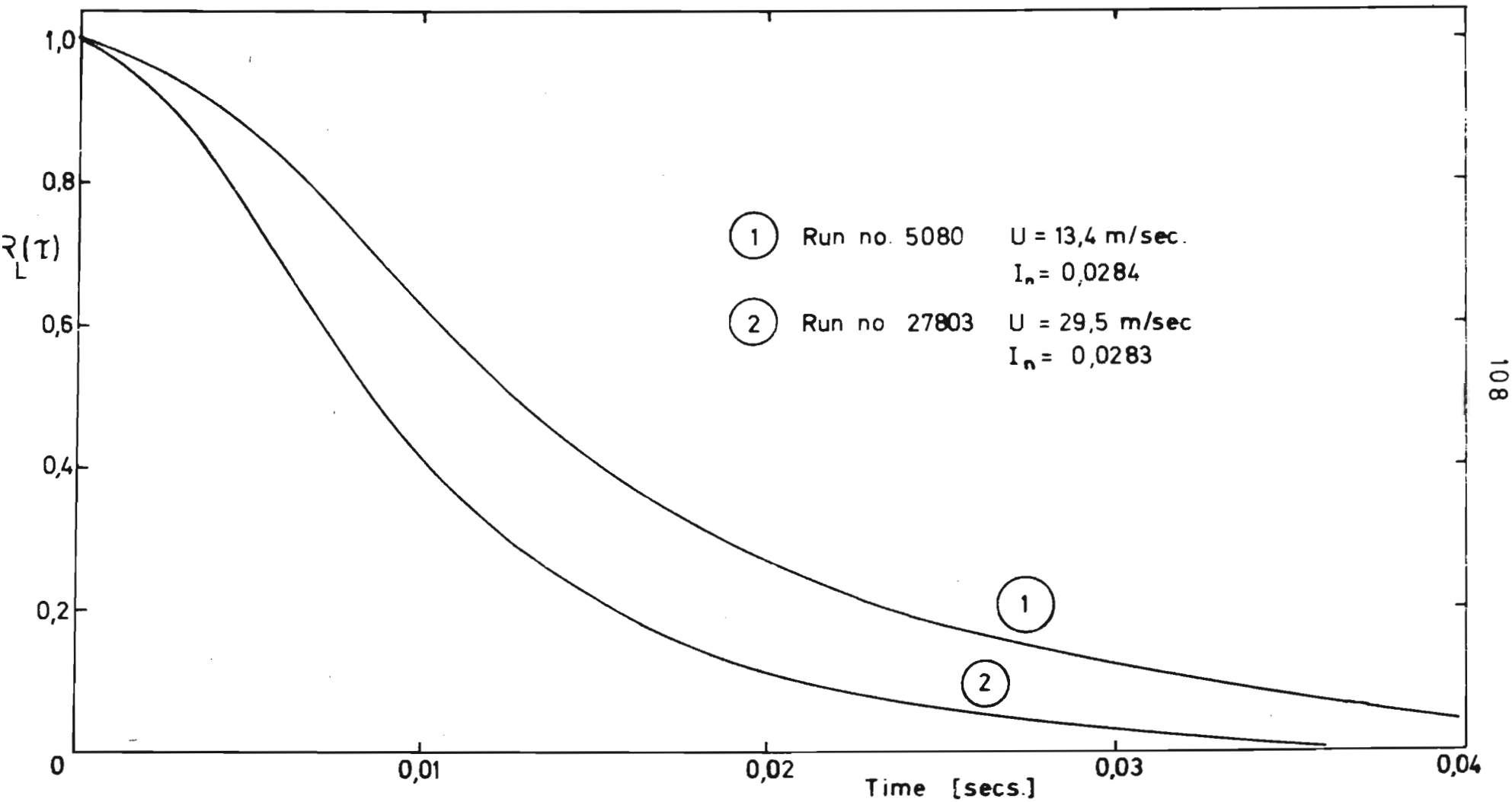

FIG. 35 PREDICTED LAGRANGIAN AUTOCORRELATION.

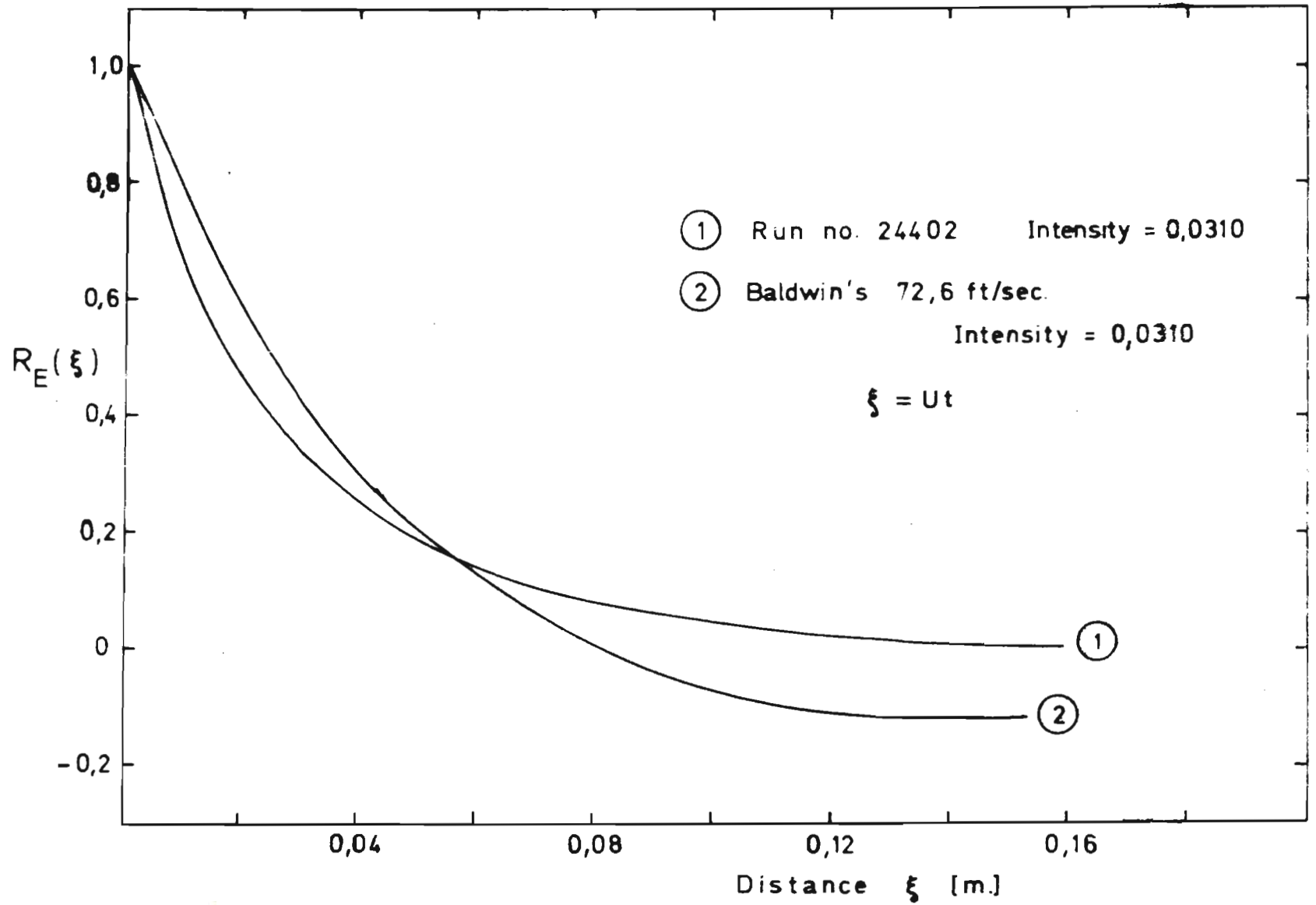

FIG. 36 APPARENT EULERIAN AUTOCORRELATION

TABLE 4.4.3

Philip's Theory with Baldwin's Data.

Mean Velocity (ft/sec.)	Peclet No.
72.6	484
106	397
135	326
160	258

It is seen that the predicted value shows a steady decrease with increasing mean velocity. On the basis of the results in Table 4.4.2 it would appear that this result is to be expected and that Philip's method of prediction is more accurate at low velocities. The results presented in the following section might suggest, however, that the possible presence of low frequencies which were sharply attenuated in Baldwin's processing technique could account for a decrease in Peclet number with increasing velocity when low frequency components are less likely to be present. This is, however, thought to be less likely although a combination of the two effects should not be excluded.

4.4.4 Predicted Axial Dispersion on Filtered Data.

The second criterion on the filtering technique applied to the hot-wire anemometer data was to filter the velocity fluctuations until the initial smooth fall of the autocorrelation curve became tangential to the axis as shown in Fig. 37. This was a fairly well-defined point on the time axis, as may also be seen from curves 1 and 2 in Fig. 34. It might be expected that this would then

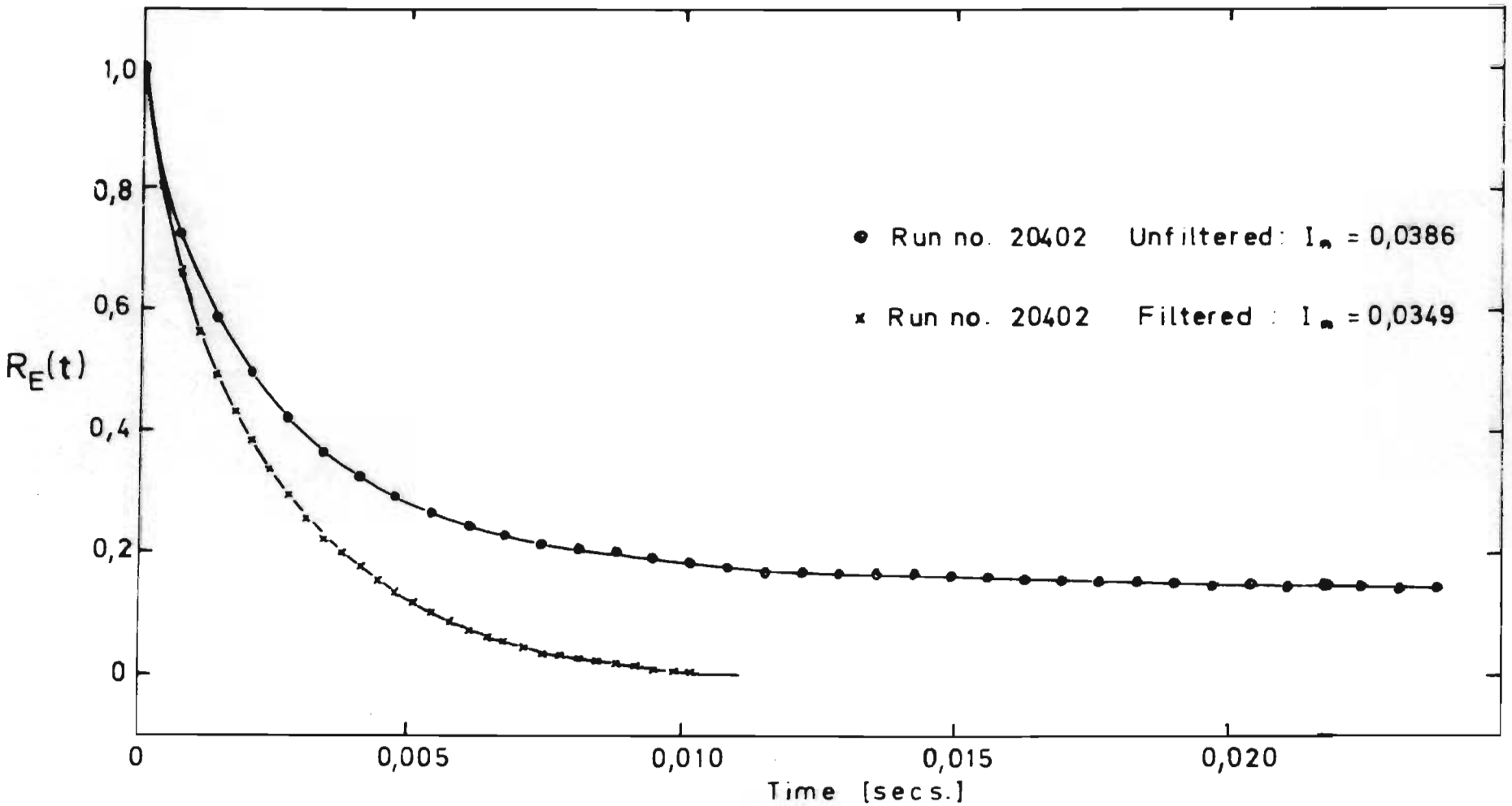

FIG. 37 AUTOCORRELATION ON FILTERED DATA

represent the behavior of the autocorrelation function in the absence of the disturbing low frequency fluctuations.

The Peclet numbers calculated by Philip's method on this data are shown in Table 4.4.4 together with the turbulence intensities obtained.

TABLE 4.4.4

Filtered Hot-wire Anemometer Data.

Run No.	Velocity (m/sec.)	Intensity	Predicted N_{Pe}
22401	13.4	0.0346	353
22402	13.4	0.0337	384
20401	13.4	0.0341	369
20402	13.4	0.0349	329
16040	13.4	0.0346	349
5080	13.4	0.0332	385
24401	29.5	0.0298	343
24402	29.5	0.0310	334
27801	29.5	0.0286	387
27802	29.5	0.0316	336
27803	29.5	0.0314	375

It is seen that there is a very good correspondence between the Peclet numbers at both velocities. A comparison of the individual Peclet numbers in Table 4.2.1 with these predicted Peclet numbers shows that there are quite a few values which lie around the predicted average value of $\sim$ 350, although it is not possible to obtain conclusive proof from the dispersion data that this would be the value obtained in the absence of the low frequency fluctuations, if it were ever possible to eliminate them in a higher capacity apparatus. Some support for this value is found in the

work of Laufer in a two-dimensional channel (57) where Eulerian two-point space correlations were measured. Laufer found that the Eulerian longitudinal integral scale calculated on this data was about 3 to 4 times that in the lateral direction, compared with the value of 2 times for the isotropic turbulence case (4). Hinze (49) has also inferred this approximate relation from Laufer's measurements on the kinetic energy and dissipation in pipe flow to postulate the presence of large elongated eddies in the core of pipe flow (Hinze,p.535).

4.4.5 Filtered Velocity Fluctuation Distribution.

The distribution of the velocity fluctuations about the mean were recalculated after filtering the slow fluctuations and the curves are shown in Figs. 38 and 39, together with the Gaussian curves having the same standard deviation determined after filtering. The approach of the higher wave-number components to a Gaussian distribution is seen to be quite good, although the flatness factors were still consistently greater than 3.0.

4.5 The One-Dimensional Energy Spectrum.

The function $E_1(n)$ is defined in the Appendix. The relationship between the autocorrelation function $R_E(t)$ and $E_1(n)$ shown first by Taylor (47):

$$E_1(n) = 4\overline{u^2} \int_0^\infty R_E(t)\cos(2\pi nt)dt$$

was used to calculate the "normalized" spectrum function $E_1(n)/\overline{u^2}$. It was found that direct numerical evaluation

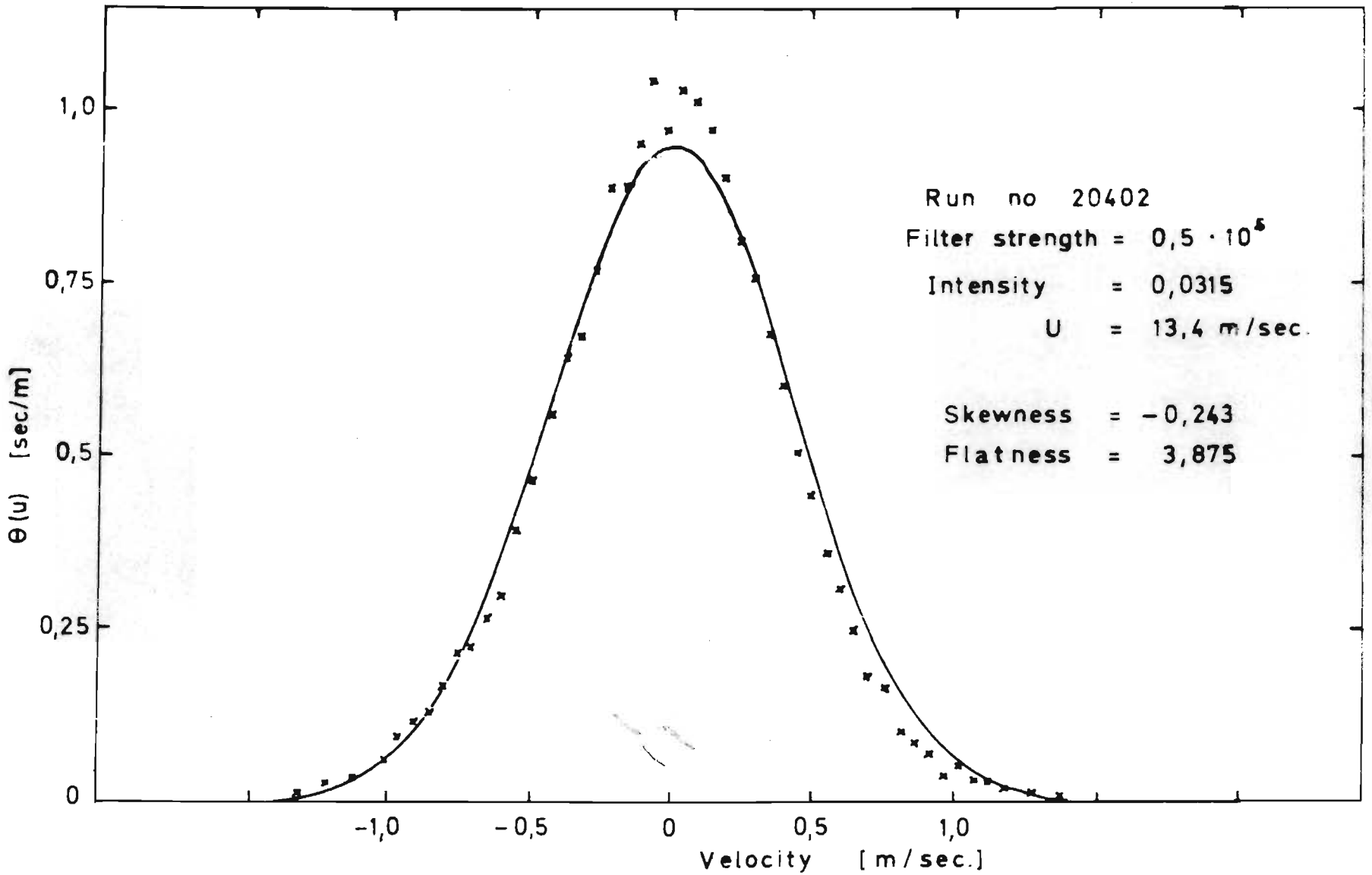

FIG 38 VELOCITY PROBABILITY DENSITY FUNCTION AFTER FILTERING

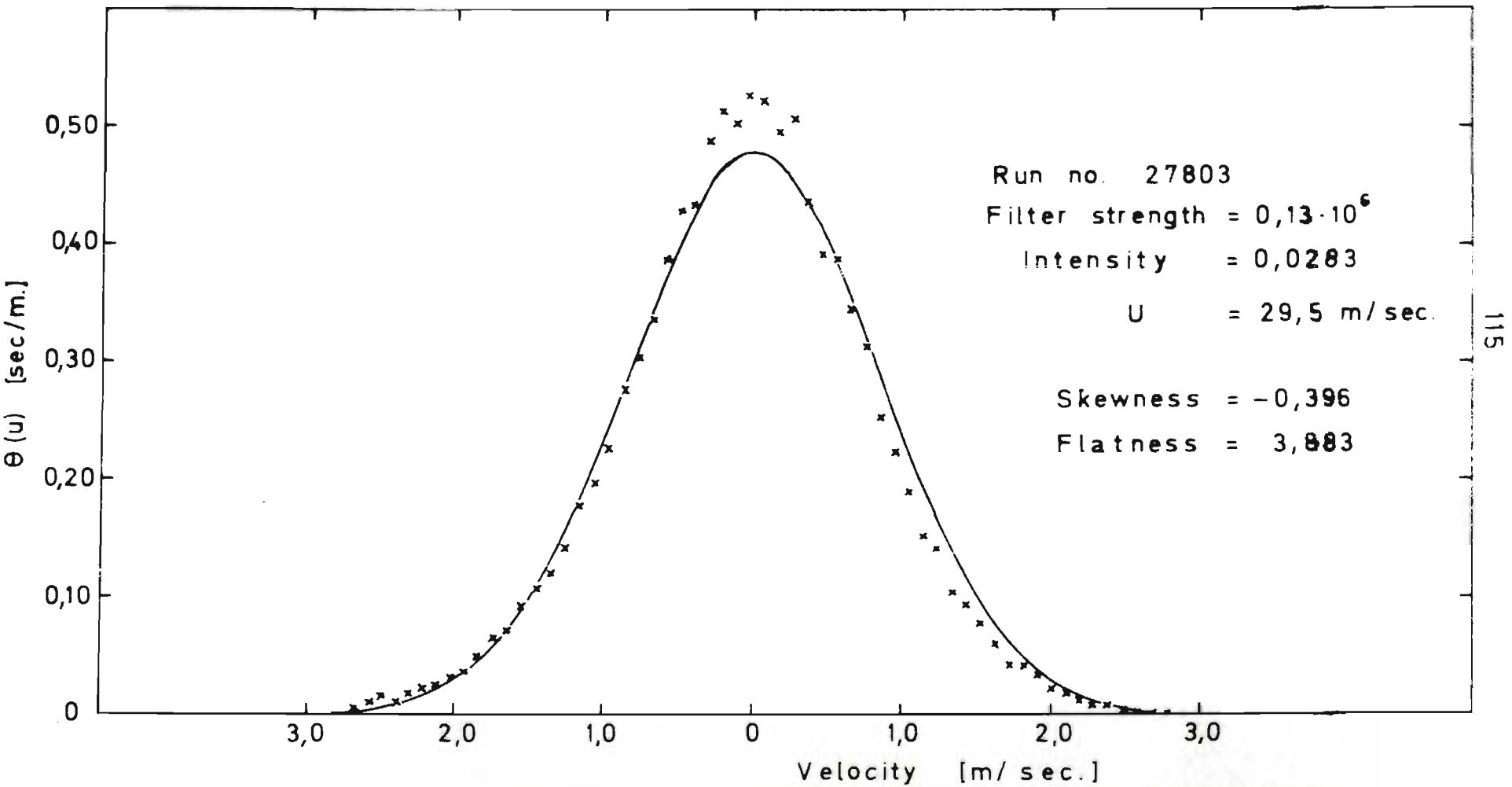

FIG. 39 VELOCITY PROBABILITY DENSITY FUNCTION AFTER FILTERING

on about 25 points making up the autocorrelation curve produced highly erratic results depending on the sample interval chosen. It was decided to approximate the autocorrelation curve by a series of linear time-dependent segments between the digital values; the determination of the equations of these straight-line segments was easily performed on the computer, allowing an analytic evaluation of the integral over each segment for any particular frequency. The computer program FRQAU is included in the Appendix.

Fig. 40 represents the spectrum function evaluated on the autocorrelation functions determined from the unfiltered data for the two mean velocities measured. At higher frequencies instabilities develop which mask the behavior of these curves in this region. The low frequency end of the spectrum is more stable and confirms the idea of low frequency fluctuations being superimposed on the spectrum: this is particularly noticeable at the lower velocity.

Fig. 41 shows the effect of doubling the sample interval on the autocorrelation curve which, besides smoothing the curve at low frequencies as expected, causes instabilities to develop at lower frequencies.

Fig. 42 shows the effect on the energy spectrum function of filtering the hot-wire anemometer data so that the autocorrelation curve just became tangential to the axis. The removal of the low frequency components is obvious.

Fig. 43 shows the effect on the spectrum

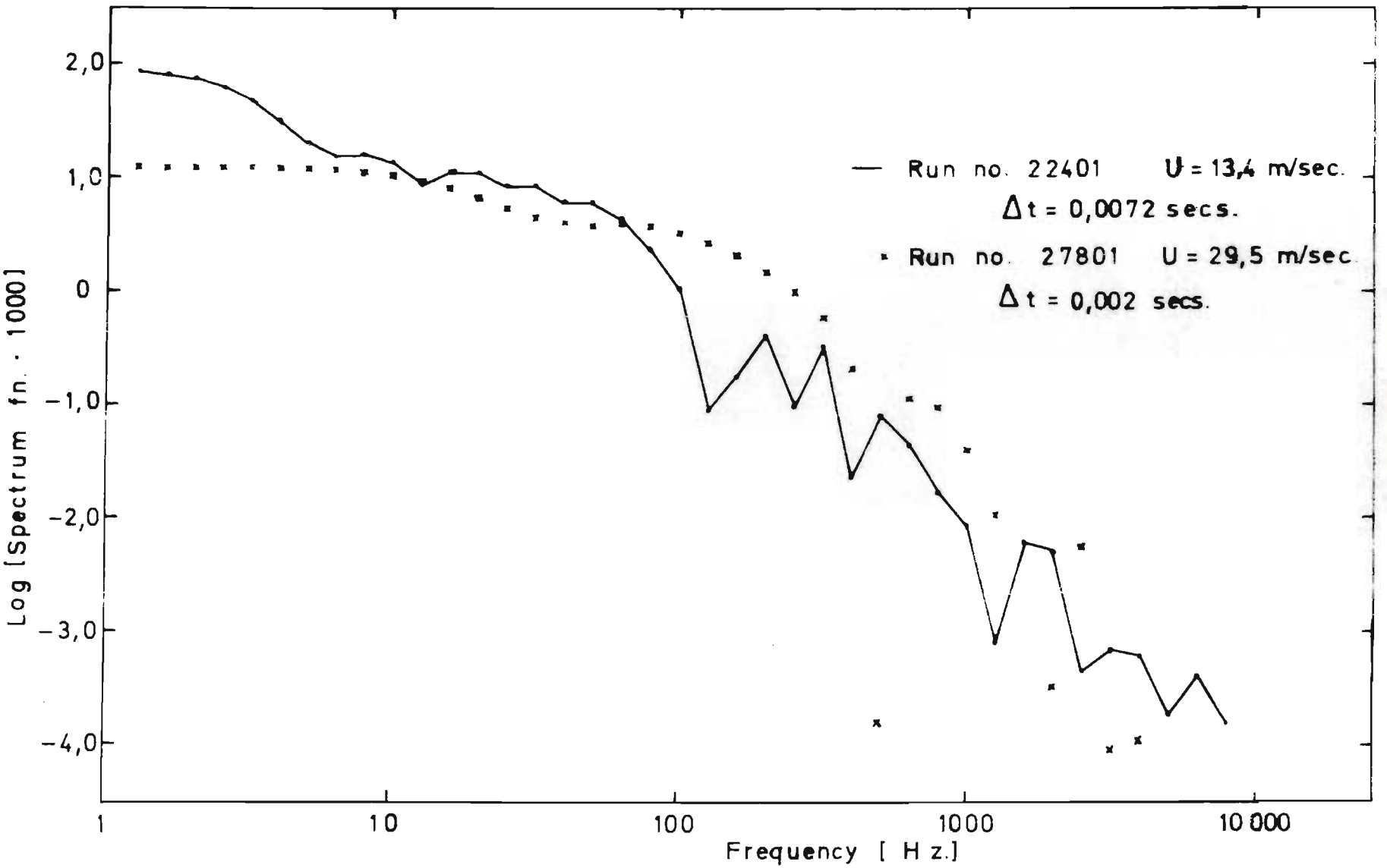

FIG. 40 ENERGY SPECTRUM FUNCTION

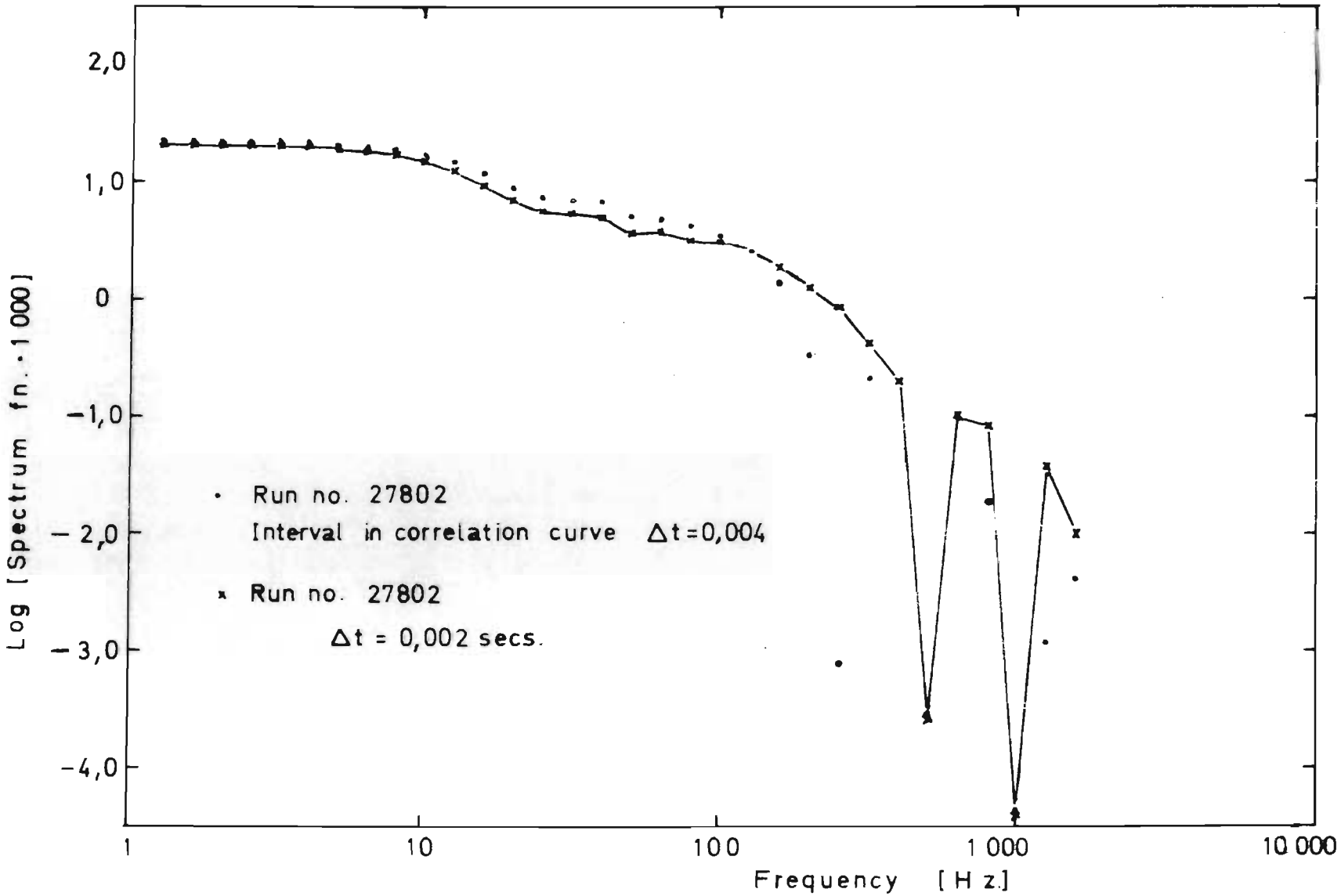

FIG. 41 ENERGY SPECTRUM FUNCTION

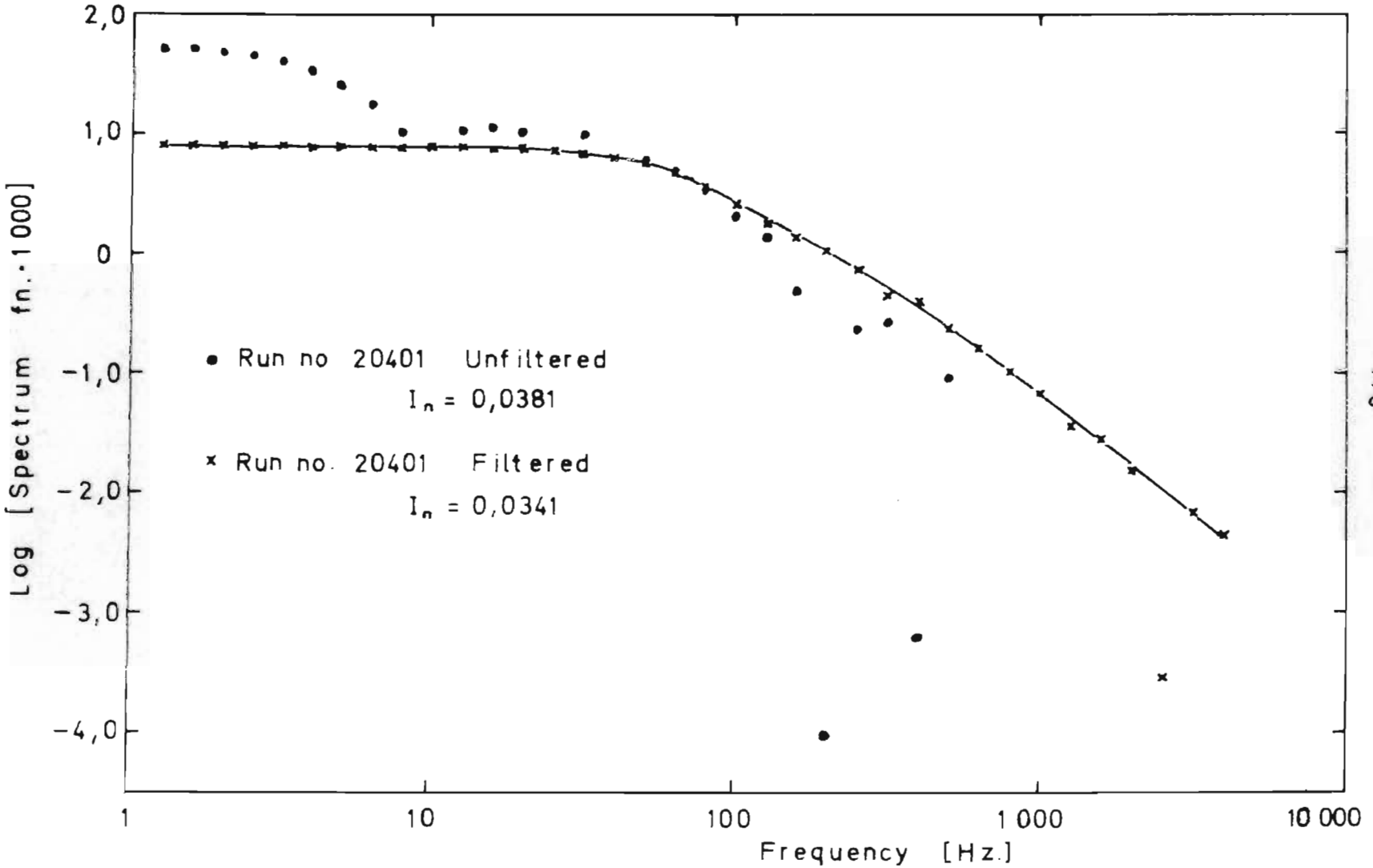

FIG. 42 ENERGY SPECTRUM FUNCTION

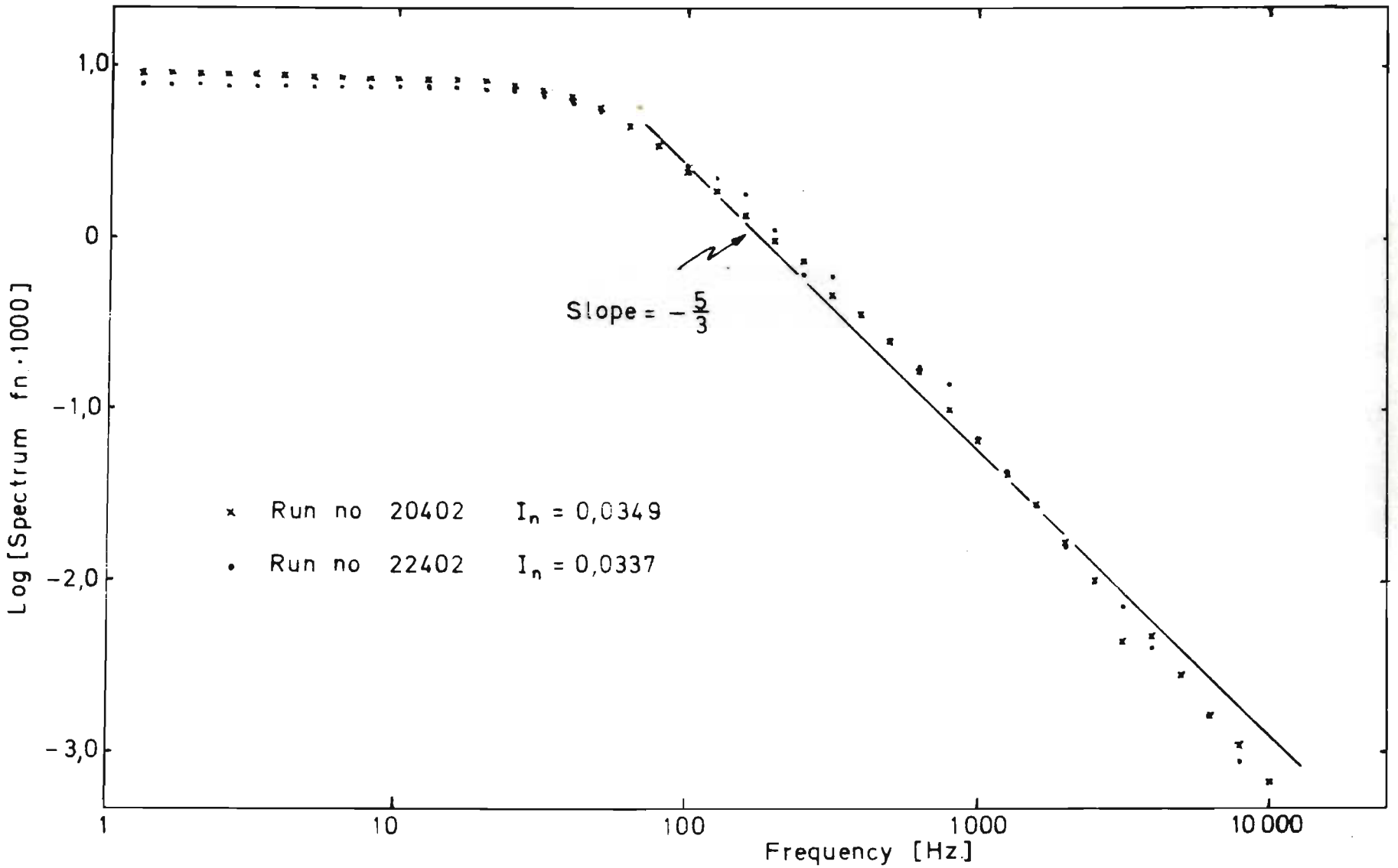

FIG. 43 ENERGY SPECTRUM FUNCTION

function of the sample interval in real time during the recording of the hot-wire signal. As the region of interest is at the high frequency end of the spectrum, the low frequency components were filtered from the velocity data before the autocorrelation was performed, and the spectrum curves in Fig. 43 were calculated on these values. The small difference in these curves shows that there is apparently little aliasing of high frequencies by the digital sampling technique. This was also, perhaps more directly, obvious from the autocorrelation curves on which Fig. 43 was based. Also shown in Fig. 43 is the line of slope $-5/3$ which corresponds to the dependence of the spectrum function on the frequency n according to Kolmogorov's spectrum law in the inertial subrange

$$E_1(n) = \text{const.} \cdot n^{-5/3}$$

The agreement with this law is seen to be quite good.

CHAPTER 5.

CONCLUSIONS.

The conclusions which may be drawn from the hot-wire anemometer and tracer dispersion measurements made in this investigation in the central core of air flowing through a pipe may be summarized:

1) The measurements made at two mean velocities with the hot-wire anemometer with a digital recording technique showed that the longitudinal fluctuating velocity spectrum extends to much lower frequencies than have previously been measured with conventional analog recording techniques. An examination of the energy spectrum function and the autocorrelation curves obtained on the velocity fluctuations indicate that there are low frequency components superimposed on the turbulence field. The distribution of the velocity fluctuations about the mean are shown to deviate from the Gaussian distribution which is normally assumed for this case, although it is considered probable that the short time of the total recording had a deleterious effect on this measurement.

2) The digital filtering of the velocity fluctuation data to remove fluctuations below any desired frequency has been shown to be feasible with the quadratic dynamic programming filter. It has also been shown that the instantaneous velocity fluctuations in the inertial subrange agree well with the Kolmogorov spectrum law.

3) Measurements made of the longitudinal dispersion of radioactive Krypton-85 gas gave Peclet numbers very much

smaller than those previously reported for dispersion in a radial direction. These low Peclet numbers are however not surprising in the presence of the large, slow eddies known to be primarily responsible for causing scalar dispersion. The majority of the dispersion measurements were confined to the lower mean velocity as less dilution of the tracer resulted in well-defined pulse shapes. The values of the mixing coefficient obtained with a regression on pairs of pulses, although individually fairly scattered, appeared to approach an asymptotic value for increasing separation of the two detector stations. The averaging technique used to obtain an average mixing coefficient for each separation resulted in a Peclet number to which a short-time correction was applied. The Peclet number thus obtained represents the average dispersion produced in a longitudinal direction.

4) The method suggested by Philip (4) for the estimation of the Lagrangian autocorrelation function from the Eulerian measurement, when applied to the unfiltered hot-wire anemometer data, gave a Peclet number slightly lower than that measured in the dispersion measurements, although the agreement is probably satisfactory for a working estimation.

The method applied to the hot-wire data filtered to give a turbulence intensity equal to that found by previous workers in radial scalar dispersion measurements, predicted a Peclet number very close to that measured, the value at higher velocity being slightly lower. This tendency was also found when Peclet numbers were predicted

from Baldwin's (17) longitudinal velocity autocorrelation curves. The method was also applied to the present hot-wire data filtered to remove the disturbing low frequency fluctuations. It was found that there were individual Peclet numbers obtained in the tracer dispersion measurements which were distributed around the value of N_{Pe} = 350 found by this method, although full justification is not possible.

5) It may be postulated that the slow, longitudinal fluctuations quantitatively examined here, have also been present in previous investigations to a greater or lesser extent and may partially account for the discrepancies in radial dispersion measurements discussed by Groenhof (28).

BIBLIOGRAPHY.

1. Taylor G.I.:Proc. Lond. Math. Soc. 1921, A20, 196.
2. Laufer J.: NACA Report 1174, 1954.
3. Brier G.W.: J. of Meteorology, 1950,7,283.
4. Philip J.R.:Phys. of Fluids Suppl., 1967,S69
5. Taylor G.I.:Proc. Roy. Soc., 1935, 151, p421.
6. Towle W.L. & Sherwood T.K.:Ind. & Eng. Chem., 1939,31,457.
7. Kalinske A.A. & Pien C.L.:Ind. & Eng. Chem., 1944,36,220.
8. Townsend A.A.:Proc. Roy. Soc., 1951,A209,418.
9. Richardson L.F.:Proc. Roy. Soc., 1926,A110,709.
10. Uberoi M.S. & Corrsin S.: NACA Report 1142, 1953.
11. Townsend A.A.:Proc. Roy.Soc., 1954,A224,487.
12. Saffman P.G.:J. of Fluid Mech., 1960,8,273.
13. Batchelor G.K. & Townsend A.A.: Surveys in Mechanics, Ed. by Batchelor & Davies, C.U.P.,1956,p352.
14. Mickelsen W.R.:J. of Fluid Mech., 1960,7,397.
15. Batchelor G.K.: "The Theory of Homogeneous Turbulence", C.U.P.,1956
16. Mickelsen W.R.: NACA TN 3570, 1955.
17. Baldwin L.V.:Ph.D. thesis, Case Inst. of Tech.,1959.
18. Becker H.A.,Rosensweig R.E. & Gwozdz J.R., J. of Fluid Mech.,1967,30,259.
19. Baldwin L.V. & Mickelsen W.R.:Am. Soc. Civ. Eng. Trans.,1963,128,1595.
20. Baldwin L.V. & Walsh T.J.: A.I.Ch.E.J.,1961,7,53.
21. Corrsin S.: J. of Atmos. Sci., 1963, 20, 115.
22. Kraichnan R.:Phys. of Fluids,1964,7,142
23. Saffman P.G.: Appl. Sci. Res.,1962,A11,245.
24. Corrsin S.: Adv. in Geophysics, 1959,6,441.

25. Flint D.L., Kada H. & Hanratty T.J.: A.I.Ch.E.J.,1960,6,325.

26. Martin G.Q. & Johanson L.N.:A.I.Ch.E.J.,1965,11,29.

27. Malengé J.P. & Gosse J.: Genie Chimique,1965,94,170.

28. Groenhof H.C.: C.E.S., 1970,25,1005.

29. Patterson G.K. & Zakin J.L.: A.I.Ch.E.J.,1967,13,513.

30. Sandborn V.A.: NACA TN 3266, 1955.

31. Frenkiel F.N. & Klebanoff P.S.:Phys. of Fluids, 1967,10,507.

32. Favre A.,Gaviglio J. & Dumas R.: NACA TM 1370,1955.

33. Stewart R.W.:Proc. Cambr. Phil. Soc.,1951,47,146.

34. Boothroyd R.G.:Trans. Inst. Chem. Eng.,1967,45,T297.

35. Hay J.S. & Pasquill F. Adv. in Geophysics,1959,6,345.

36. Pasquill F. "Atmospheric Diffusion", 1962, van Nostrand & Co.

37. Batchelor G.K.:Austr. J. Sci. Res.,1949,A2,437.

38. Batchelor G.K.: Proc. Cambr. Phil. Soc.,1952,48,345.

39. Abramowitz M. & Stegun I.A.:(Ed.) "Handbook of Math. Functions", Dover Publs.,N.Y., 1965.

40. Brown R.G. & Nilsson J.W.:"Introduction to Linear Systems Analysis", Wiley & Sons, 1962.

41. Law V.J. & Bailey R.V.: C.E.S., 1963,18,189.

42. King R.P. & Woodburn E.T.: Dept. of Chem. Eng., Univ. of Natal, Durban.

43. Levenspiel O. & Bischoff K.B.: Adv. in Chem. Eng. 1964,3,95

44. Exall D.I.:M.Sc. thesis, Univ. of Natal, 1966.

45. Hamming R.W.: "Numerical Methods for Scientists & Engineers", McGraw Hill, 1962.

46. Bendat J.S.: "Principles & Applications of Random Noise Theory", Wiley & Sons, 1958.

47. Taylor G.I.: Proc. Roy. Soc., 1938,A164,476.

48. Bradshaw P. & Johnson R.F.:"Turbulence Measurements with Hot-wire Anemometers", NPL Notes on Applied Science No. 33, 1963.

49. Hinze J.O.: "Turbulence", McGraw Hill, 1959.

50. Crank J.: "The Maths. of Diffusion", Oxford U.P.1956.

51. Soo S.L., Ihrig H.K. & El Kouh A.F.: ASME Tr., J. of Basic Eng., Sept., 1960, 609.

52. Friedlander G. & Kennedy J.: "Nuclear and Radiochem." Wiley & Sons, 1957.

53. Dearnaley G. & Whitehead A.B.: Nucl. Instr. & Methods, 1961,12,205.

54. King R.P., Woodburn E.T., Colborn R.P., Edwards R. & Smith W.E., Nucl. Tech. & Min. Res., IAEA, Vienna, 1968, 117.

55. Bellman R.: Quart. Appl. Math., 1957, 14, 353.

56. Hougen J.O. & Walsh R.A.: C.E.P., 1961, 57,69.

57. Laufer J. NACA TN 2123, 1950.

58. Frenkiel F.N.: Aeronaut. Quart., 1954, 5,1.

APPENDIX I

Possible Sources of Error.

There are a number of possible sources of error in the experimental measurements which deserve consideration:

1) The hot-wire anemometer readings were not corrected for the finite length of the sensitive element, which affects the spatial resolution obtained (48,49). This error affects only the high frequency components and at the comparatively low Mach numbers studied, it is not expected that the wire length of approx. 1mm. would introduce much error. At the lower velocity of 13.4 m/sec. and assuming a maximum frequency of 5000 Hz., this corresponds to an eddy size of 3 mm. The main interest in the present investigation was, further, the correct representation of the large eddies which produce scalar dispersion.

2) It has been found that vibration of the prongs of the hot-wire anemometer can introduce spurious signals at high velocities above 70 to 100 m/sec.(48,49). At the velocities examined this should not be the case. Three separate probes were constructed with prong lengths projecting from about 8 to 12 mm. from the ceramic insulator: no marked difference was observed in the slow fluctuations recorded. The probes were also securely fastened to the wall of the pipe with a packing gland and a bracing clamp about 10 cm. from the wall of the pipe so that vibration of the whole probe was not possible.

3) It has been assumed, in the conversion of the fluctuating hot-wire anemometer voltage to velocities, that the instantaneous heat transfer from the wire may be described by the same expression as that describing steady-state heat transfer. It is not known whether this assumption is justified, although Hinze(49,p121) discusses some evidence for it.

4) The correction for molecular diffusion to the mixing coefficient obtained in the tracer measurements was found to be negligible if it may be assumed that the interaction term discussed in Section 1.3 is small. The molecular diffusivity of Krypton-85 in air is approx. $1.2 \cdot 10^{-5}$ m^2/sec. and so no correction was applied.

5) The interference in the turbulent dispersion of the tracer material caused by the first detector is not directly estimable. Indirect evidence is provided by the relatively smooth behavior of the curve in Fig. 31 that the effect is small. One might expect, if this factor were significant, that larger separation between the detectors would result in a lower mean mixing coefficient as the turbulent dispersion became relatively more important. A series of measurements was also made with the small detector at the upstream station replaced by a larger detector mounted on an aerofoil section identical with the downstream detector, with a probe separation of 0.762 m. The results obtained lay in the same range as those in Table 4.2.1. It is thus assumed that, although this effect is probably measurable, it is small compared with the turbulent dispersion.

APPENDIX 2.

DEFINITION OF TURBULENCE TERMS.

The book by Hinze (49) provides a good background discussion of the subject of turbulent flow, together with the measurement techniques available at that time (1959).

Homogeneous Turbulence: implies that the statistical evaluation of the structure of the turbulence field is not affected by a linear space transformation. Turbulence may be homogeneous in one coordinate direction only, as in the longitudinal direction in pipe flow.

Isotropic Turbulence: implies that the statistical parameters of the turbulence are independent of the angular positioning of the coordinate axes at any point. Considering the central core of flow through a pipe, the origin of the axes is taken as moving with the mean velocity U with instantaneous fluctuations u about the mean in the longitudinal direction, and v and w in the orthogonal transverse directions. Isotropy then implies equality of the statistical behavior of u, v and w, including $\overline{u^2} = \overline{v^2} = \overline{w^2}$ and $\overline{uv} = \overline{vw} = \overline{uw}$, where the mean is taken in time.

Stationary Turbulence: implies time stationarity and indicates that the statistical parameters evaluated in a time interval are independent of the time origin.

Intensity of Turbulence: This is usually defined as the root mean square of the fluctuating velocity component in any direction. As used in this investigation

it is defined as the ratio of the rms. velocity fluctuation in any direction to the mean centerline velocity U in the pipe. e.g. $\overline{u^2}/U$.

Eulerian Correlation Coefficient R_E: This function is defined in a general form (in Cartesian coordinates) by:

$$R_E(x,y,z,t) = \frac{\overline{u(0,0,0,0)\,u(x,y,z,t)}}{\overline{u^2}}$$

the mean being taken in time. The measurements made in this investigation correspond to the Eulerian single-point time autocorrelation which follows from the above expression with x=y=z=0.

Lagrangian Correlation Coefficient R_L: This function is obtained by following one particular fluid particle p on its meandering path in the turbulence field, recording its velocity as a function of time and evaluating the function below, where the mean is taken over many individual particle releases:

$$R_L(t) = \frac{\overline{u_p(0)\,u_p(t)}}{\overline{u_p^2}}$$

Integral Scale of Turbulence: This is the area under the Eulerian or Lagrangian correlation curve. It may be defined as an integral length scale L or an integral time scale T, which for the Eulerian case implies use of the correlation functions $R_E(x,0,0,0)$ and $R_E(0,0,0,t)$ resp. The Lagrangian integral scales are given by uT_L and T_L resp., where u is the Lagrangian rms. velocity fluctuation.

Turbulent Spectrum Function $E_1(n)$: This is evaluated on the single-point fluctuating velocity measurements made in the time-stationary turbulence field. $E_1(n)dn$ is then the contribution to the mean square velocity fluctuation $\overline{u^2}$ by the frequencies between n and (n+dn), and satisfies the relationship:

$$\int_0^\infty E_1(n)\,dn = \overline{u^2}$$

APPENDIX 3.

PRINCIPAL SYMBOLS.

c	- Scalar concentration	(kg/m^3)
d	- Pipe diameter	(m)
D	- Molecular diffusivity	(m^2/sec)
E	- Turbulent mixing coefficient	(m^2/sec)
E_1	- One-dimensional spectrum function	(m^2/sec)
H	- Laplace transform of impulse response: units as defined.	
I	- Voltage from hot-wire anemometer	(V)
I_n	- Intensity of turbulence	(-)
L	- Integral length scale	(m)
n	- Frequency	(Hz.)
N_{Nu}	- Nusselt no. for heat transfer from hot-wire	(-)
N_{Pe}	- Peclet no. Ud/E	(-)
N_{Re}	- Reynolds no. $Ud\rho/\mu$	(-)
P	- Probability function	(-)
R	- Correlation coefficient	(-)
r	- Radial displacement coordinate	(m)
s	- Particle displacement from mean position	(m)
t	- Time	(secs)
T	- Integral time scale	(secs)
u^*	- Friction velocity in Blasius equation	(m/sec)
U	- Mean longitudinal velocity (on centerline unless otherwise stated)	(m/sec)
u	- Instantaneous longitudinal velocity deviation from the mean	(m/sec)
v	- Instantaneous vertical velocity	(m/sec)
w	- Instantaneous horizontal transverse velocity	(m/sec)
X	- Longitudinal displacement of tracer about mean	(m)

Y	- Vertical displacement of tracer about mean	(m)
x	- Longitudinal displacement	(m)
y	- Vertical displacement	(m)
z	- Horizontal transverse displacement	(m)
δ	- Dirac delta function	
Θ	- Probability density function	
ξ	- Distance variable	(m)
ρ	- Density	(kg/m^3)
τ	- Time variable	(secs)
τ_w	- Wall shear stress in Blasius equation	($kg/m^2 sec$)
ω	- Vorticity of turbulence	(sec^{-1})

APPENDIX 4.

COMPUTER PROGRAMS.

These were written in Fortran 1V for the IBM 1130 computer.

1. The Fluctuating Velocity Distribution.

The linking between the main programs XBCDT, EXVDT and EVELD, with the subroutines EVCON, QDPF and BREAD, is shown below. The program VPLTF was a plotting routine for a graphical output and will not be included here.

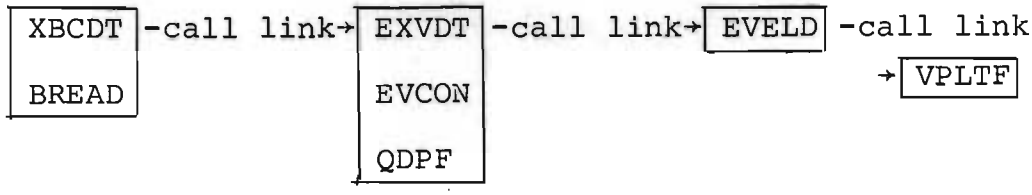

The binary-reading subroutine BREAD read the pseudo-binary data from the cards and this was stored on disk by XBCDT. A link to EXVDT was followed by conversion of the raw data to velocities with EVCON and subsequent filtering, if required, by the quadratic dynamic programming filter QDPF. A link was then performed to EVELD for the evaluation of the velocity distribution.

Input Data EXVDT:

EFILT - filter strength for QDPF if filtering is required.

Input Data EVCON:

Argument list: N,LF1,LF2,LPT1,LPT2,VCAL,V,L

VCAL - calibration velocity

CCAL - DC voltage at calibration velocity

COCAL - DC voltage at zero velocity

AMP - voltage amplification factor

VSUB - mean velocity (=calibration velocity)

TOT - facility for reading in mean of binary counts. If TOT is read as 0.0, the value of TOT is determined in the program.

N - total no. of velocity samples read by BREAD.

LF1 - voltage fluctuation file

LF2 - velocity fluctuation file

LPT1 - file pointer for LF1

LPT2 - file pointer for LF2.

Input Data QDPF:

Argument list: S,R,M,EFILT,F1,THETA

S - vector of reals through which smoothed sequence is returned

R - vector of reals supplying raw data to subroutine

M - number of elements to be filtered

EFILT - vector of reals supplying filter strength to subroutine.

F1 - final value of the function F

THETA - not used

The first and second values of the smoothed data must be provided in the calling program.

This program is a Library Program in the Dept. of Chem. Eng., University of Natal.

Input Data EVELD:

NC - no. of points on which histogram is determined.

VAR - variance of velocity fluctuations (from autocorrelation program)

NPAR - dummy variable not used

NAME - run no.

BREAD is a University of Natal Computer Centre Library Program.

2. The Autocorrelation Programs.

The linking of these programs is shown below:

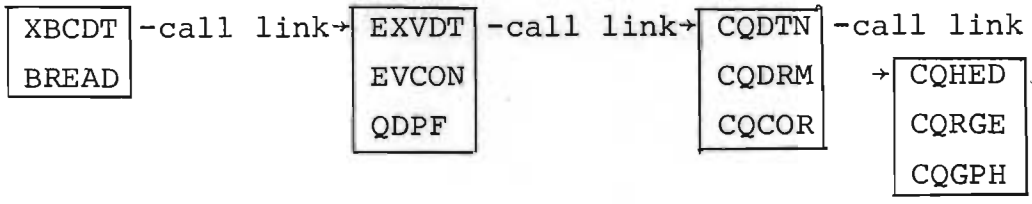

The programs up to CQDTN are the same as for the velocity distribution calculation. CQDTN calls subroutine CQDRM which subtracts either the running mean or a constant mean from the data: control then passes to subroutine CQCOR which calculates the correlation. CQHED is the control program for a plotting sequence which uses subroutines CQRGE and CQGPH. These six programs CQDTN, CQDRM, CQCOR, CQHED, CQRGE, CQGPH are Library Programs in the Dept. of Chem. Eng., Univ. of Natal.

3. The Non-linear Regression on Pulse-test Data.

The linking of these programs is shown below:

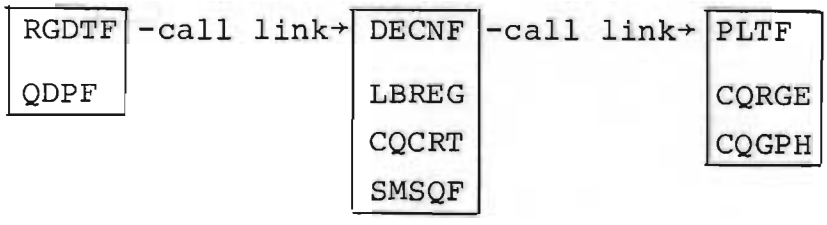

The main program RGDTF reads the pulse-test data from cards and filters the data to give a smooth curve. A link is performed to DECNF which calls the subroutine LBREG which performs a Law and Bailey

regression with a Newton-Raphson search on the data. CQCRT is a matrix-inversion subroutine, solving N linear simultaneous equations using the compact elimination scheme due to Crout (Tewarson R.P., "The Crout Reduction for Sparse Matrices" - Computer J., Vol. 12,No.2,May 1969, p.158). The subroutine SMSQF evaluates the sum of squares and the coefficient matrix for LBREG. PLTF is again a plotting routine with CQRGE and CQGPH.

Input Data for RGDTF:

B(I) - vector of initial estimates for U, E and the normalizing factor, for LBREG

TOL(I) - vector of tolerances on the 3 parameters.

MAX - maximum no. of iterations allowed in LBREG.

Z(1) - tolerance to prevent the division of the matrix by a very small element (less than the value of Z(1)) of the principal diagonal of the auxiliary matrix in CQCRT

NFAC - filter strength for filter program QDPF.

XS1 and XS2 - first and second values in filtered sequence for first pulse.

YS1 and YS2 - first and second values in filtered sequence for second pulse.

NAME - run no.

DEDTX - dead-time from arbitrary source to start of first pulse.

DEDTY - dead-time from the same arbitrary source to the start of the second pulse.

DISTX,DISTY - position of the two detectors from arbitrary source.

DELT,DTY - sample time interval on the first and second pulses resp.

MX, MY - no. of points comprising first and second pulses resp.

WIN, DELW - dummy variables not used.

X(I) - sequence of first pulse data.

Y(I) - sequence of second pulse data.

Input Data for DECNF:

The following parameters are defined internally in DECNF to specify the function of LBREG:

NEWT = 0 for Law and Bailey regression.

BETA = 0.25 A convergence parameter in the Law and Bailey regression

IOPT = -1 specifies Law and Bailey regression

M = 3 No. of parameters

IOUT = 3 Unit no. of output device (printer)

Input Data for LBREG:

Argument list: BETA, B, TOL, CQCRT,SMSQF,IOPT, NEWT, IOUT, MAX

The parameters in the argument list are defined above in the calling program.

Input Data for CQCRT:

Argument list: C, X, N, Z

C - coefficient matrix (equations to be solved)

X - vector of reals (solution to equations)

N - no. of equations to be solved

Z - vector tolerance for CQCRT read by RGDTF.

Input Data for SMSQF:

Argument list: LAB, MATRX, C, SA, B

LAB - label set by LBREG =1, the computed values of the parameters give a satisfactory fit
=0 for other cases.

MATRX - label set by LBREG =1 when both the coefficient matrix and the sum of squares are to be computed.
=0 when only the sum of squares is to be computed.

C - coefficient matrix

SA - sum of squares

B -vector of the parameters of the model

The programs LBREG and CQCRT are Library Programs in the Dept. of Chem. Eng., Univ. of Natal. The program SMSQF was adapted from a program written by Woodburn of this department.

4) Philip's Prediction of the Lagrangian Autocorrelation Function.

This iterative procedure was performed with the program EITER.

Input Data for EITER:

NPB - no. of points calculated in the table of displacement variance as a function of time.

N - no. of points in Eulerian autocorrelation curve.

DELT - time interval in Eulerian autocorrelation curve.

DT - normalized time interval (Δt_*) in double integral.

DTT - normalized time interval (Δt_*) in double integral.

NP - maximum no. of steps allowed in the iteration.

LPLOT - control on print-out of results. Lagrangian correlation function printed if LPLOT$\geq$1, otherwise only graphical output.

S(I) - vector comprising the Eulerian autocorrelation function.

The plotting routine to which EITER links is similar to those previously discussed.

5. Regression on Mean Impulse Response.

The linking of these programs is shown below:

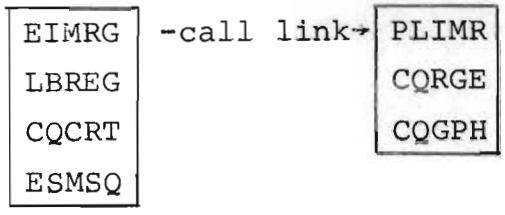

This calculation is similar to the regression discussed previously, but is performed directly on the impulse response and not on an inlet and outlet pulse. The evaluation of the mean impulse response is performed in EIMRG.

Input Data for EIMRG:

The parameters B(I), TOL(I), MAX and Z(1) are as defined previously for the non-linear regression in RGDTF.

NAME - run number

POSX - position of first detector from arbitrary source.

POSY - position of second detector from the same source.

DTX - time interval in evaluation of impulse response.

NREG - no. of sets of regressed data from pulse tests used to establish the mean impulse response.

NDROP - coefficient of DTX giving time at which evaluation of impulse response starts.

NPB - coefficient of DTX giving time at which evaluation of impulse response ends.

D(I) - vector of parameters from regression on pulse tests.

The programs LBREG and CQCRT are the same as used previously, and the subroutine ESMSQ is equivalent to the subroutine SMSQF, the argument lists being identical. The program PLIMR is again a graph-plotting routine.

6. The One-Dimensional Energy Spectrum Evaluation:FRQAU.

The evaluation of this function was performed with the program FRQAU, using the Eulerian autocorrelation data.

This program evaluated in a stepwise procedure, for each frequency, the following expression:

$$A(m) = \text{Area}_{t_1 \to t_2} = \int_{t_1}^{t_2} R(t)\cos(nt)dt$$

$$\simeq \int_{t_1}^{t_2} \{S(m)t + X(m)\}\cos(nt)dt$$

after this had been evaluated analytically. S(m) and X(m) represent the slope and intercept resp. of the m-th segment.

Input Data for FRQAU:

NAME - run no. of autocorrelation

N - no. of samples comprising autocorrelation function.

DELT - time interval of samples comprising autocorrelation function

NDEC - no. of decades over which the evaluation is to be performed

EFILT - filter strength used in filtering original velocity data before autocorrelation.

R(I) - vector comprising the Eulerian autocorrelation function.

A link was performed to the graph-plotting routine FRQPL which used the library subroutines CQRGE and CQGPH.

XBCDT.

```
EXTENDED PRECISION
INTEGER L(81)
COMMON N
DEFINE FILE 1(1600,3,U,KUP),3(400,240,U,LUP),4(4000,8,U,K3)
```

PROGRAM:

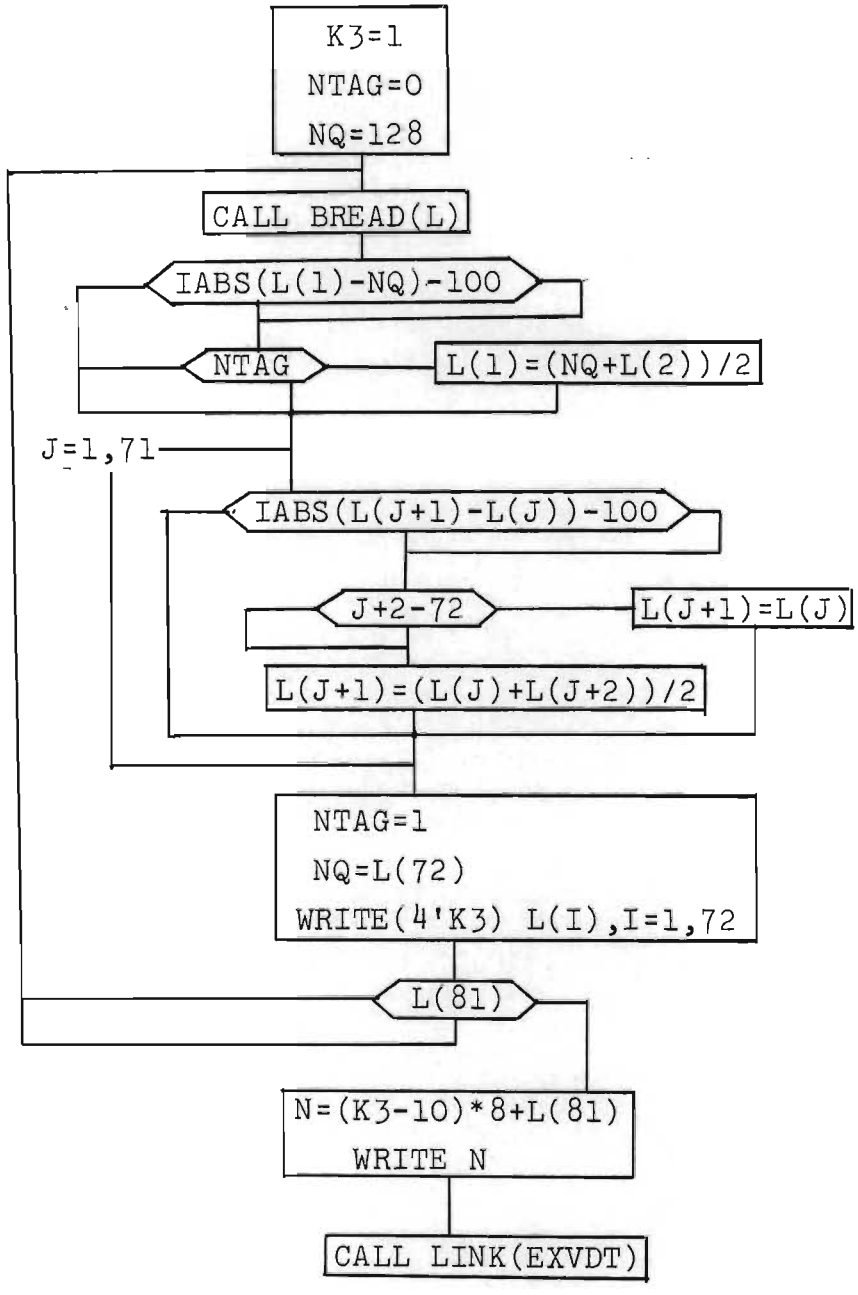

EXVDT.

```
EXTENDED PRECISION
DIMENSION R(85),S(85),L(85),E(85)
COMMON N,NAME,EFILT
DEFINE FILE 1(1600,3,U,KUP),3(400,240,U,LUP),4(4000,8,U,K3)
            ,5(4000,24,U,MUP)
```

PROGRAM:

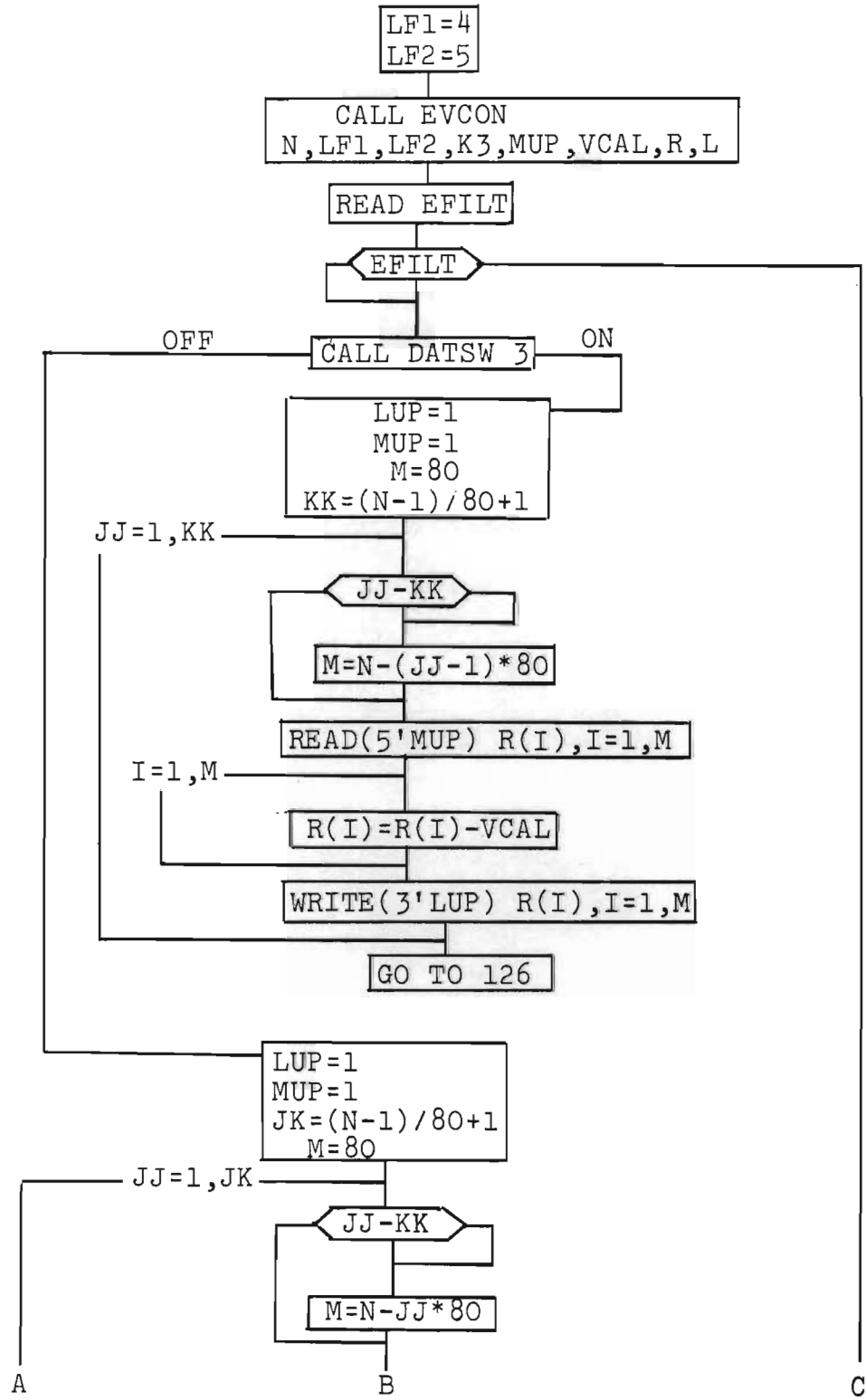

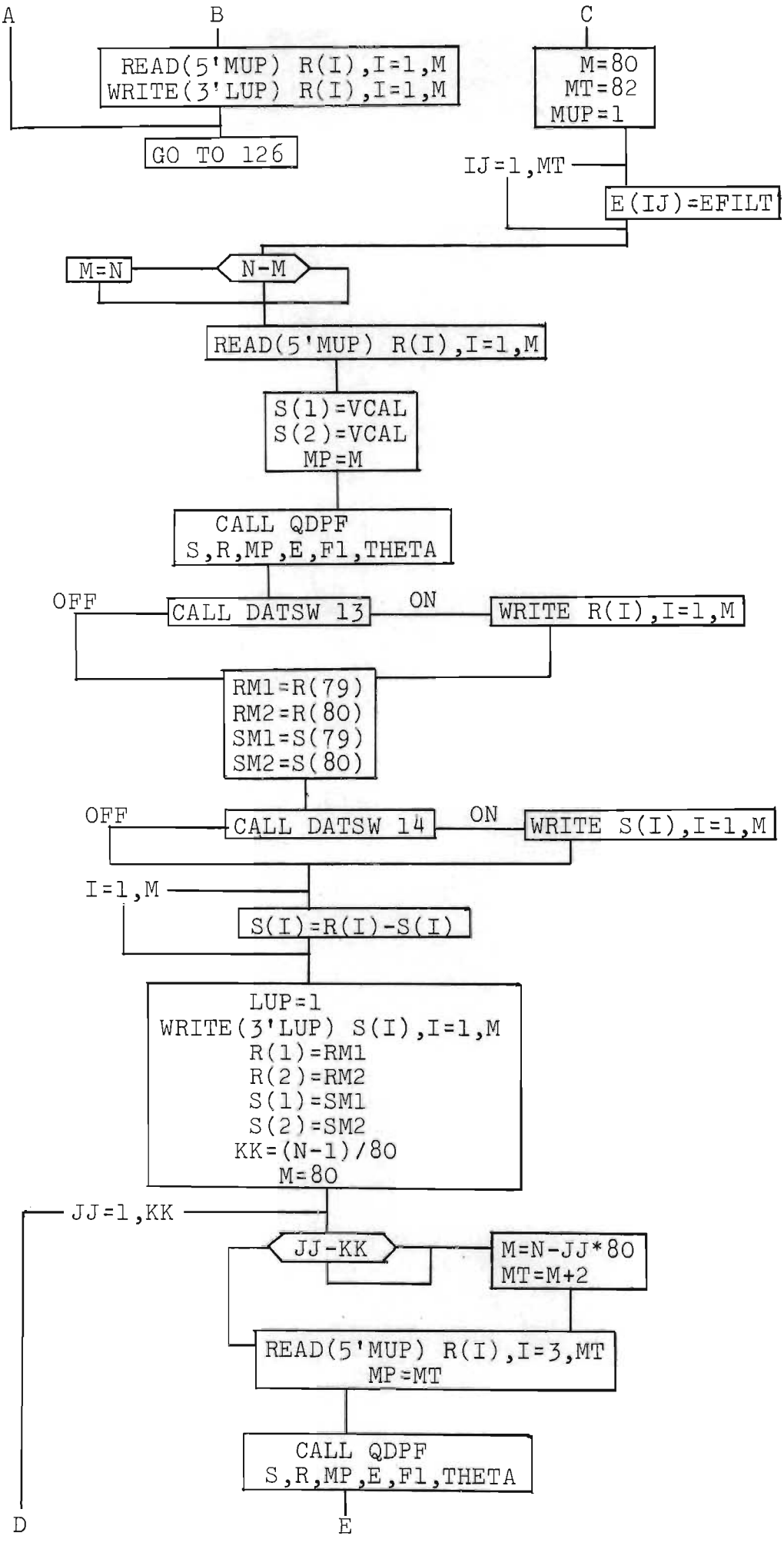
A
B
C
READ(5'MUP) R(I),I=1,M
WRITE(3'LUP) R(I),I=1,M
GO TO 126
M=80
MT=82
MUP=1
IJ=1,MT
E(IJ)=EFILT
M=N
N-M
READ(5'MUP) R(I),I=1,M
S(1)=VCAL
S(2)=VCAL
MP=M
CALL QDPF
S,R,MP,E,F1,THETA
OFF
CALL DATSW 13
ON
WRITE R(I),I=1,M
RM1=R(79)
RM2=R(80)
SM1=S(79)
SM2=S(80)
OFF
CALL DATSW 14
ON
WRITE S(I),I=1,M
I=1,M
S(I)=R(I)-S(I)
LUP=1
WRITE(3'LUP) S(I),I=1,M
R(1)=RM1
R(2)=RM2
S(1)=SM1
S(2)=SM2
KK=(N-1)/80
M=80
JJ=1,KK
JJ-KK
M=N-JJ*80
MT=M+2
READ(5'MUP) R(I),I=3,MT
MP=MT
CALL QDPF
S,R,MP,E,F1,THETA
D
E

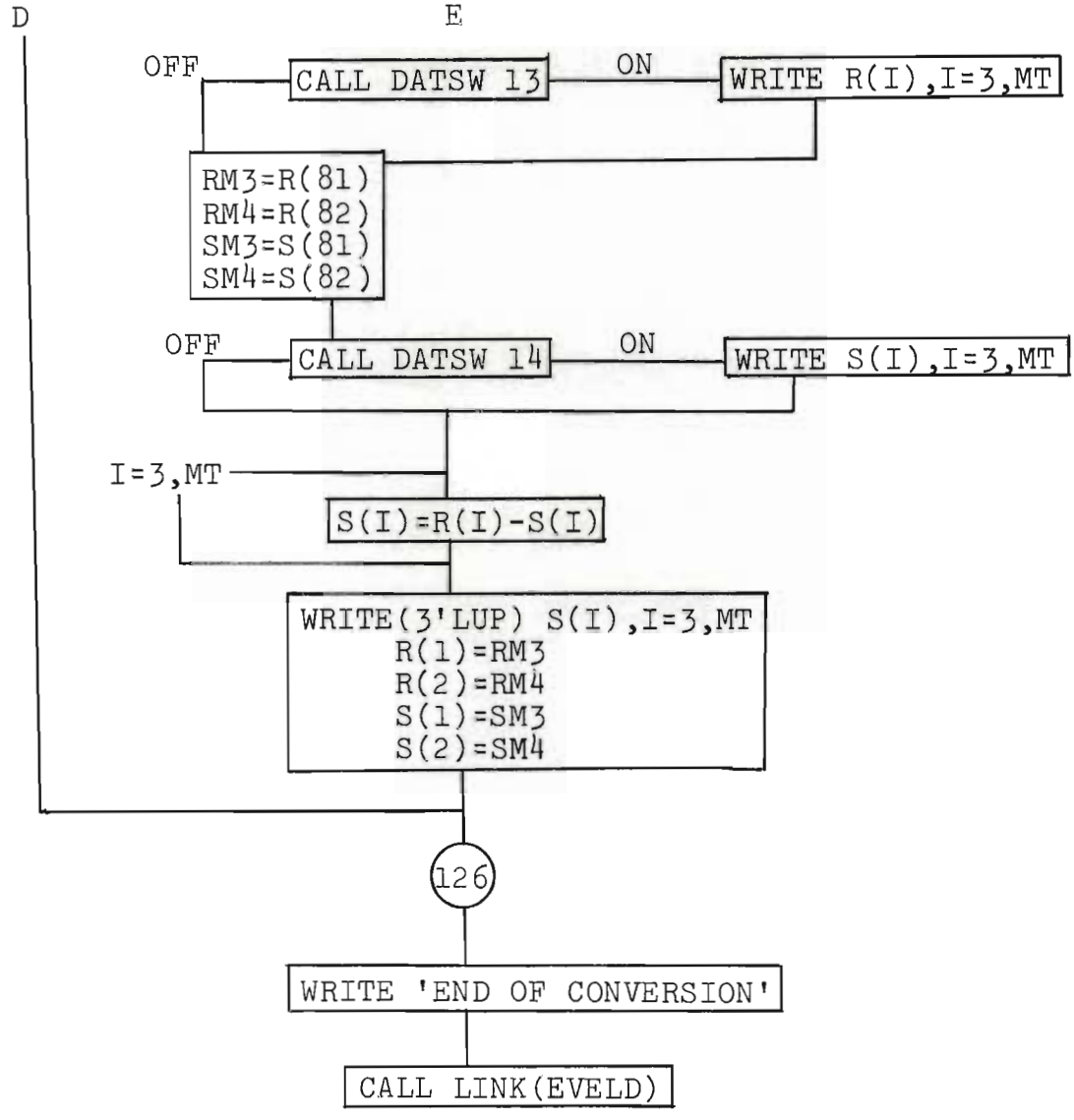
D
E
OFF
CALL DATSW 13
ON
WRITE R(I),I=3,MT
RM3=R(81)
RM4=R(82)
SM3=S(81)
SM4=S(82)
OFF
CALL DATSW 14
ON
WRITE S(I),I=3,MT
I=3,MT
S(I)=R(I)-S(I)
WRITE(3'LUP) S(I),I=3,MT
R(1)=RM3
R(2)=RM4
S(1)=SM3
S(2)=SM4
126
WRITE 'END OF CONVERSION'
CALL LINK(EVELD)

SUBROUTINE EVCON.

DIMENSION V(1),L(1)

PROGRAM:

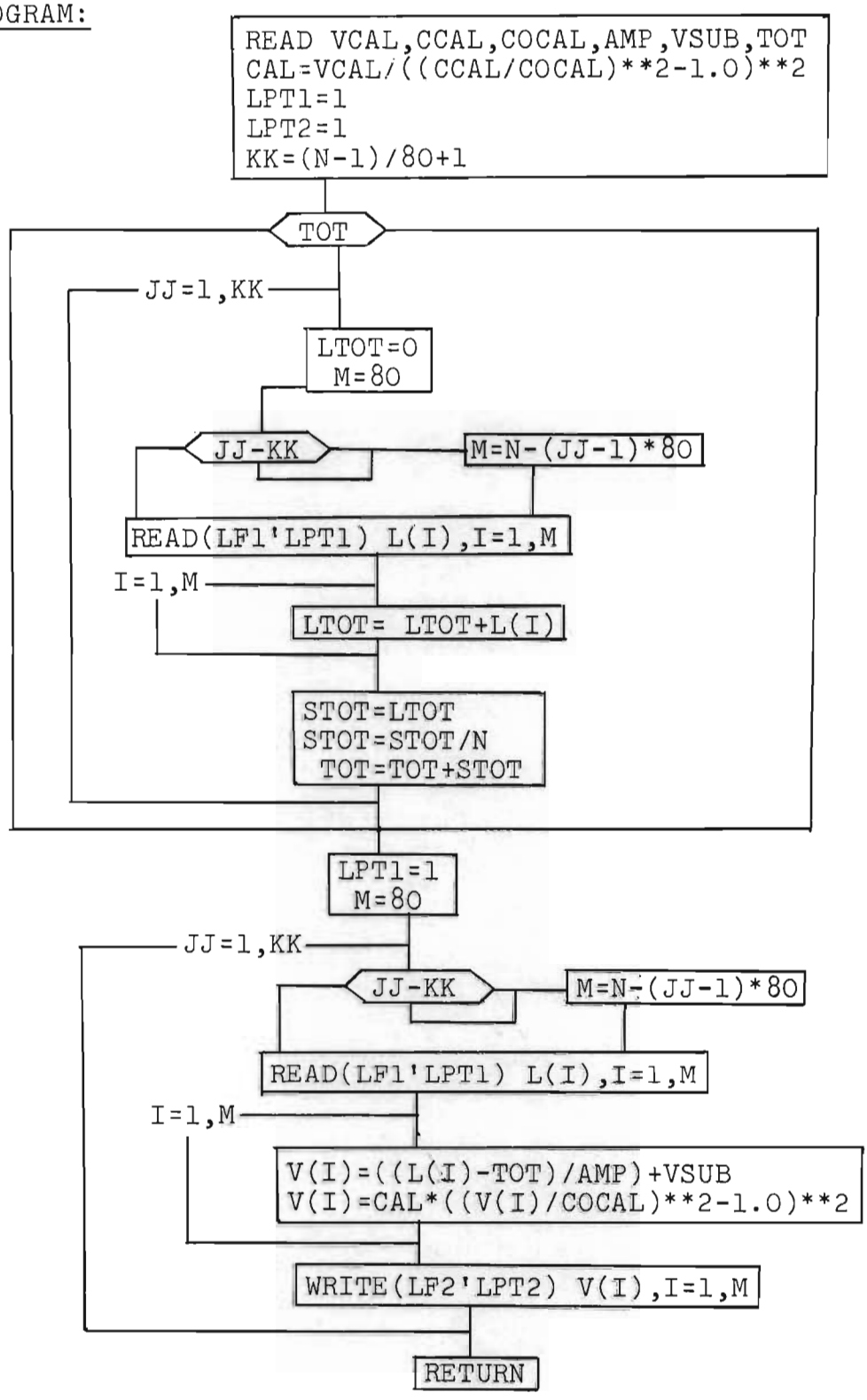

SUBROUTINE QDPF.

```
DIMENSION R(1),S(1),E(1),WS1(300),WS2(300)
```

PROGRAM:

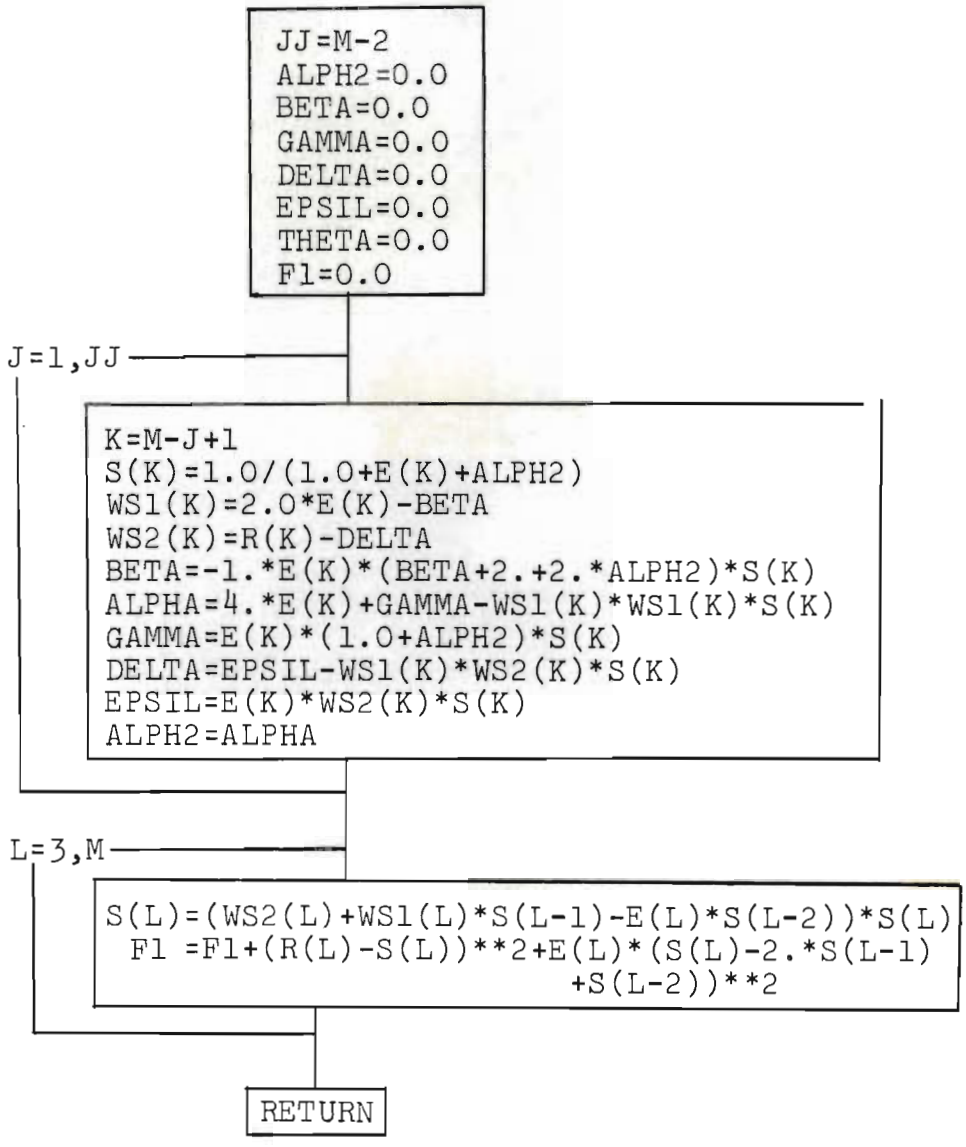

EVELD.

```
DIMENSION J(150),V(150),Y(150)
COMMON NC,NAME,EFILT
DEFINE FILE 1(1600,3,U,KUP),3(400,240,U,LUP),4(6,300,U,LPT)
```

PROGRAM:

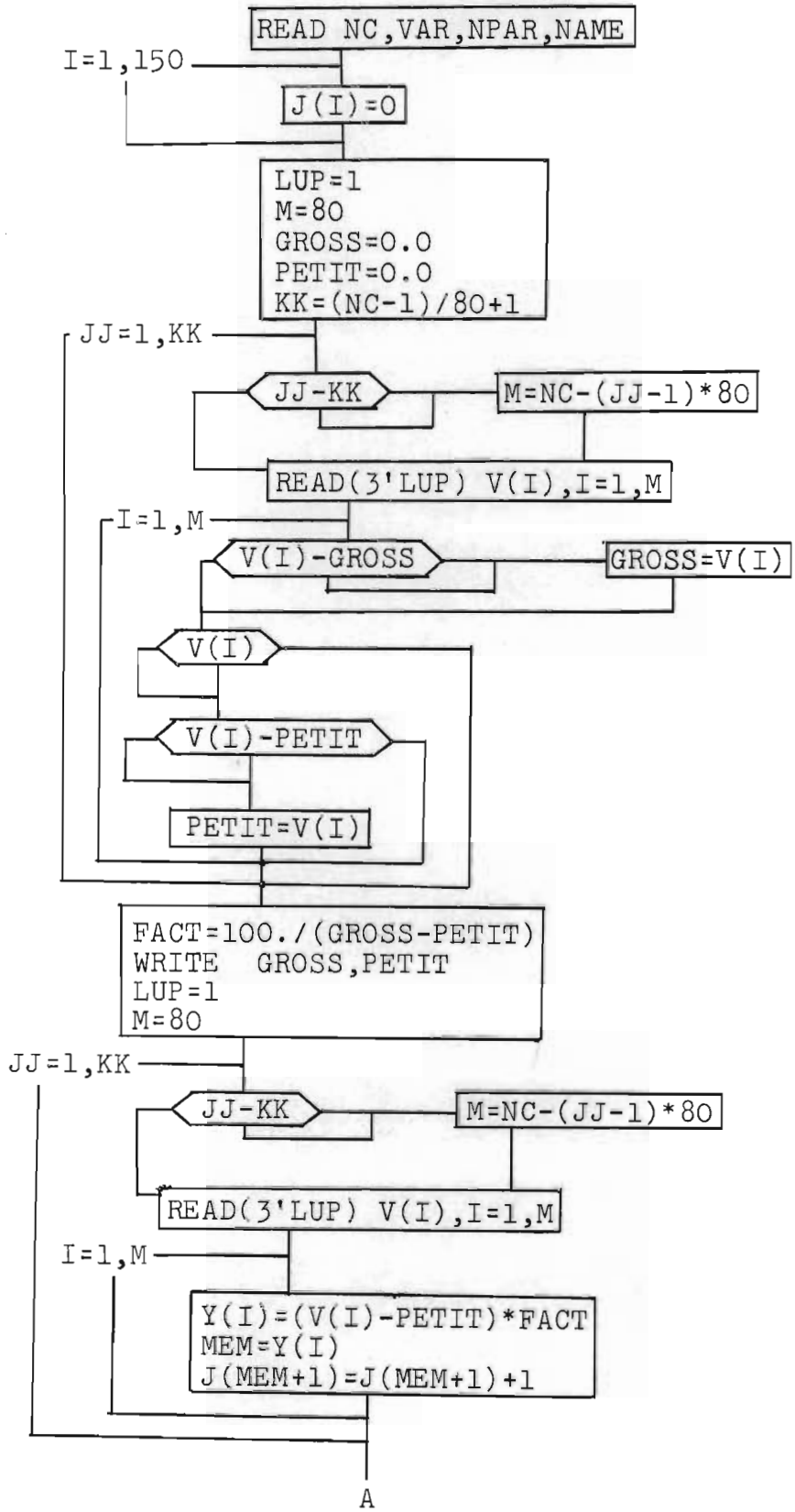

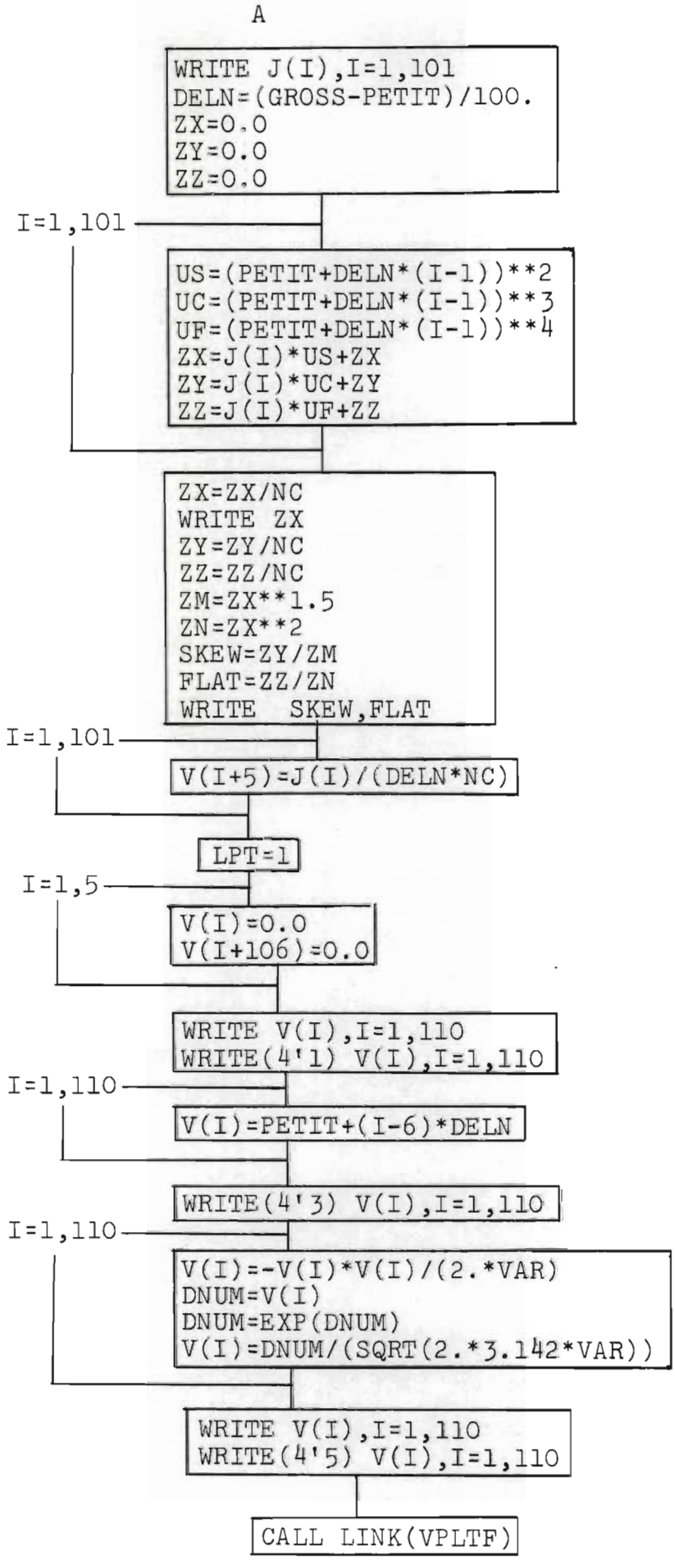
A
WRITE J(I),I=1,101
DELN=(GROSS-PETIT)/100.
ZX=0.0
ZY=0.0
ZZ=0.0
I=1,101
US=(PETIT+DELN*(I-1))**2
UC=(PETIT+DELN*(I-1))**3
UF=(PETIT+DELN*(I-1))**4
ZX=J(I)*US+ZX
ZY=J(I)*UC+ZY
ZZ=J(I)*UF+ZZ
ZX=ZX/NC
WRITE ZX
ZY=ZY/NC
ZZ=ZZ/NC
ZM=ZX**1.5
ZN=ZX**2
SKEW=ZY/ZM
FLAT=ZZ/ZN
WRITE SKEW,FLAT
I=1,101
V(I+5)=J(I)/(DELN*NC)
LPT=1
I=1,5
V(I)=0.0
V(I+106)=0.0
WRITE V(I),I=1,110
WRITE(4'1) V(I),I=1,110
I=1,110
V(I)=PETIT+(I-6)*DELN
WRITE(4'3) V(I),I=1,110
I=1,110
V(I)=-V(I)*V(I)/(2.*VAR)
DNUM=V(I)
DNUM=EXP(DNUM)
V(I)=DNUM/(SQRT(2.*3.142*VAR))
WRITE V(I),I=1,110
WRITE(4'5) V(I),I=1,110
CALL LINK(VPLTF)

RGDTF.

```
DIMENSION X(100),Y(100),E(100)
COMMON XL,DELT,MY,M2,ETD,MX,IOUT,NAME,S(100),Q(100),Z(5),
       TOL(5),DTY,DEDTY,DEDTX,DISTY,DISTX,MAX,B(5)
```

PROGRAM:

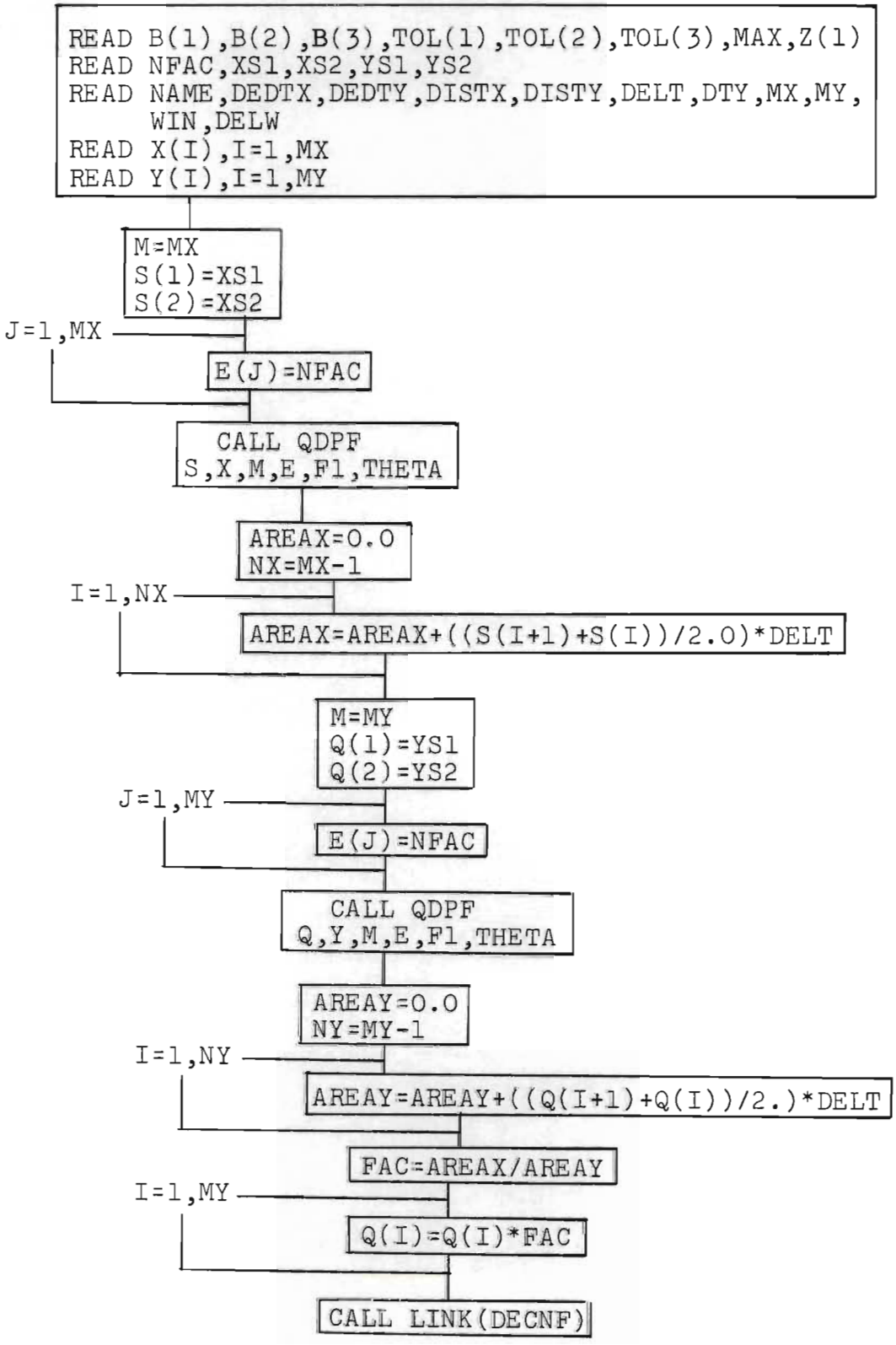

DECNF.

```
INTEGER RATIO
EXTERNAL CQCRT
EXTERNAL SMSQF
COMMON XL,DELT,MY,M2,ETD,MX,IOUT,NAME,X(100),Y(100),Z(5),
       TOL(5),DTY,DEDTY,DEDTX,DISTY,DISTX,MAX,B(5)
```

PROGRAM:

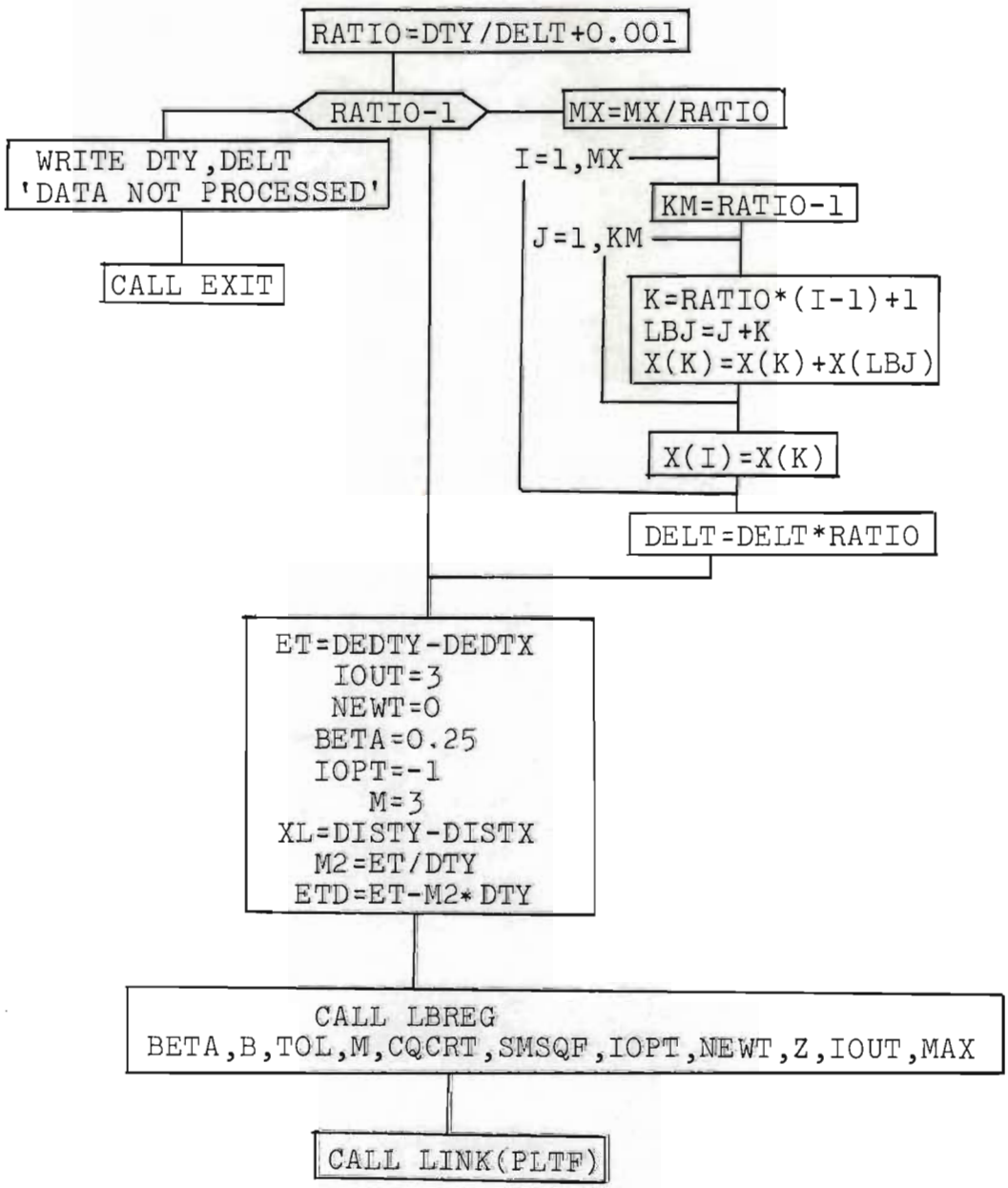

SUBROUTINE SMSQF.

```
DIMENSION B(10),C(10,11),Z(3),U(100),H(100)
COMMON XL,DELT,MY,M2?ETD,MX,IOUT,NAME,R(100),S(100),E(5),
       TOL(5),DTY,DEDTY,DEDTX,DISTY,DISTX,MAX
```

PROGRAM:

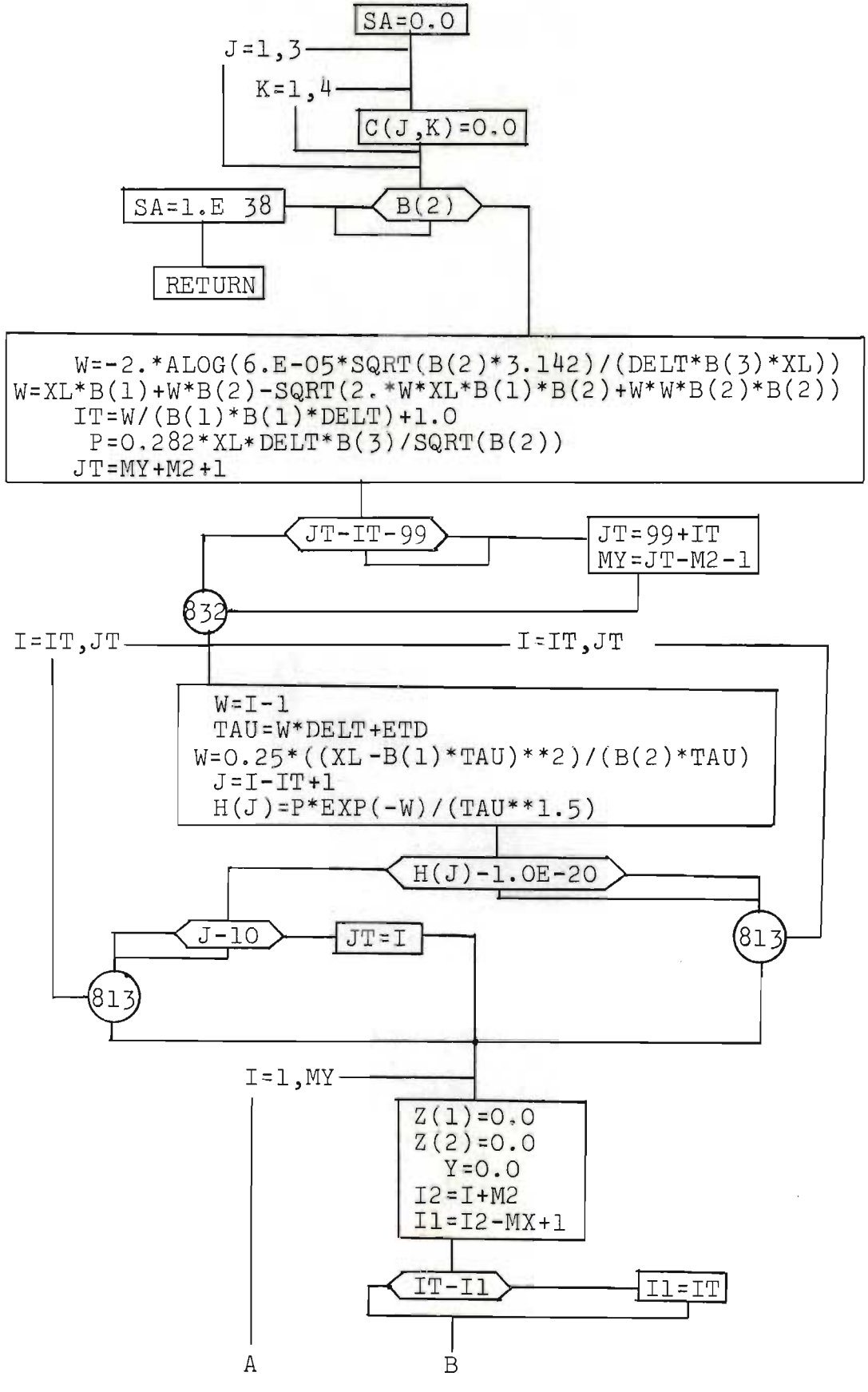

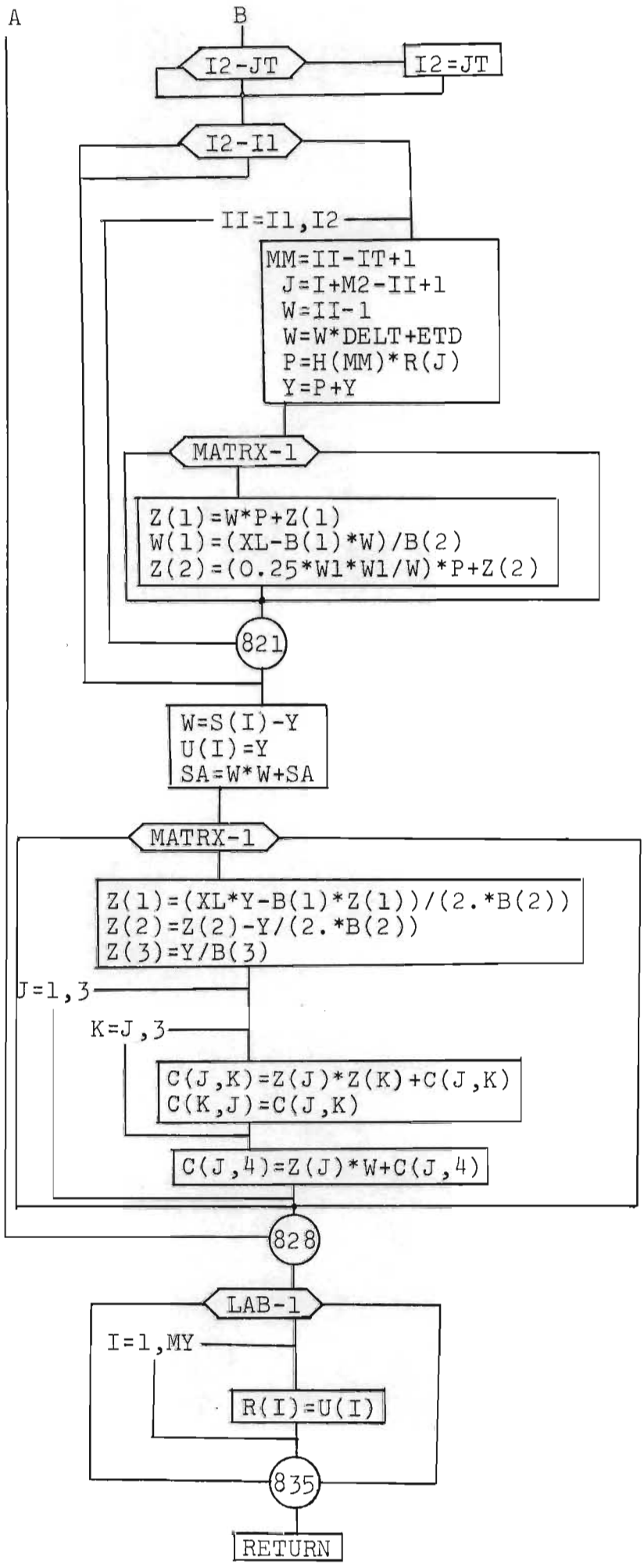
A
B
I2-JT
I2=JT
I2-I1
II=I1,I2
MM=II-IT+1
J=I+M2-II+1
W=II-1
W=W*DELT+ETD
P=H(MM)*R(J)
Y=P+Y
MATRX-1
Z(1)=W*P+Z(1)
W(1)=(XL-B(1)*W)/B(2)
Z(2)=(0.25*W1*W1/W)*P+Z(2)
821
W=S(I)-Y
U(I)=Y
SA=W*W+SA
MATRX-1
Z(1)=(XL*Y-B(1)*Z(1))/(2.*B(2))
Z(2)=Z(2)-Y/(2.*B(2))
Z(3)=Y/B(3)
J=1,3
K=J,3
C(J,K)=Z(J)*Z(K)+C(J,K)
C(K,J)=C(J,K)
C(J,4)=Z(J)*W+C(J,4)
828
LAB-1
I=1,MY
R(I)=U(I)
835
RETURN

EITER.

```
DIMENSION S(150),T(150),R(150),B(150),FAC(150)
DEFINE FILE 4(20,300,U,KK)
```

PROGRAM:

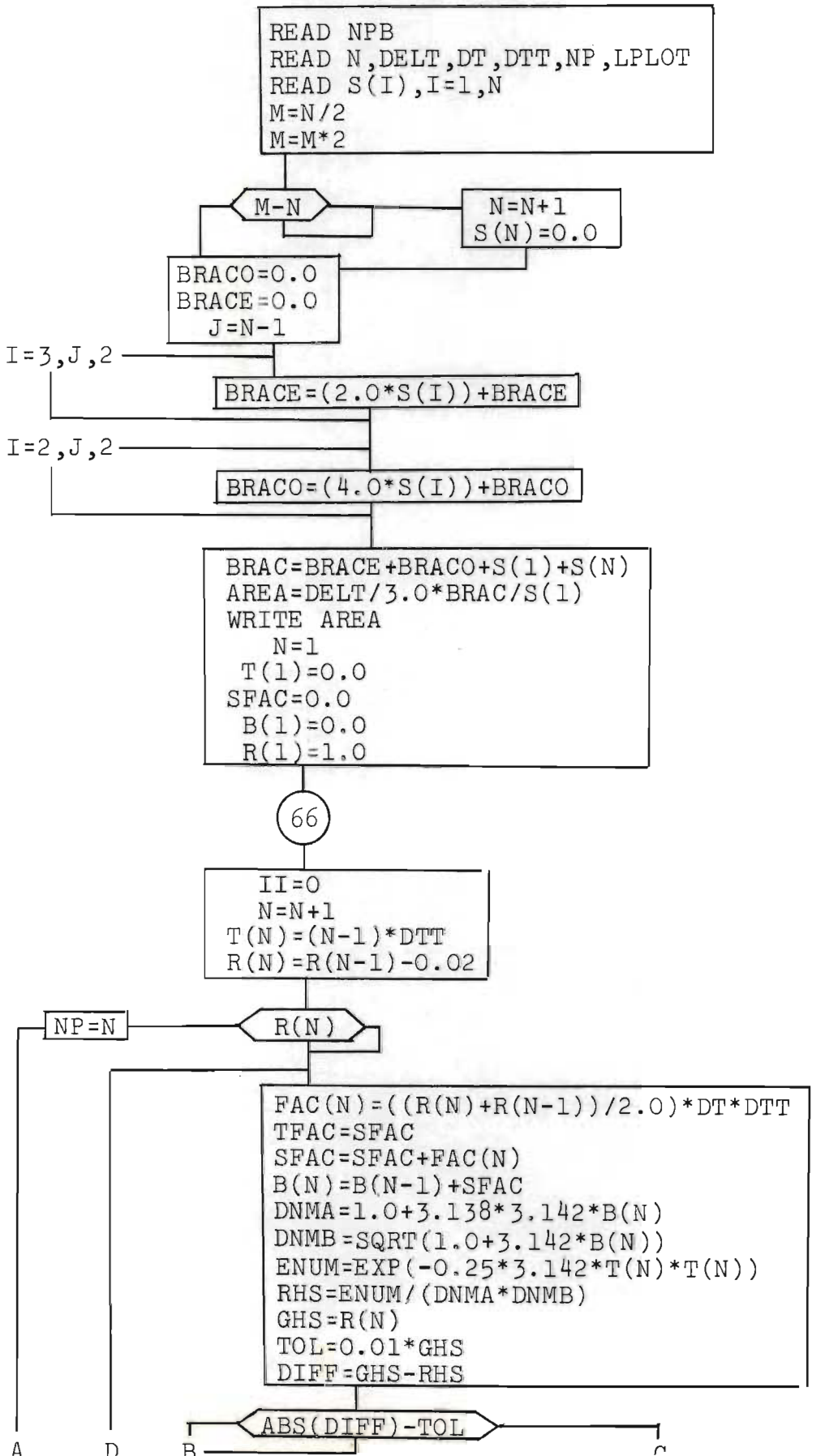

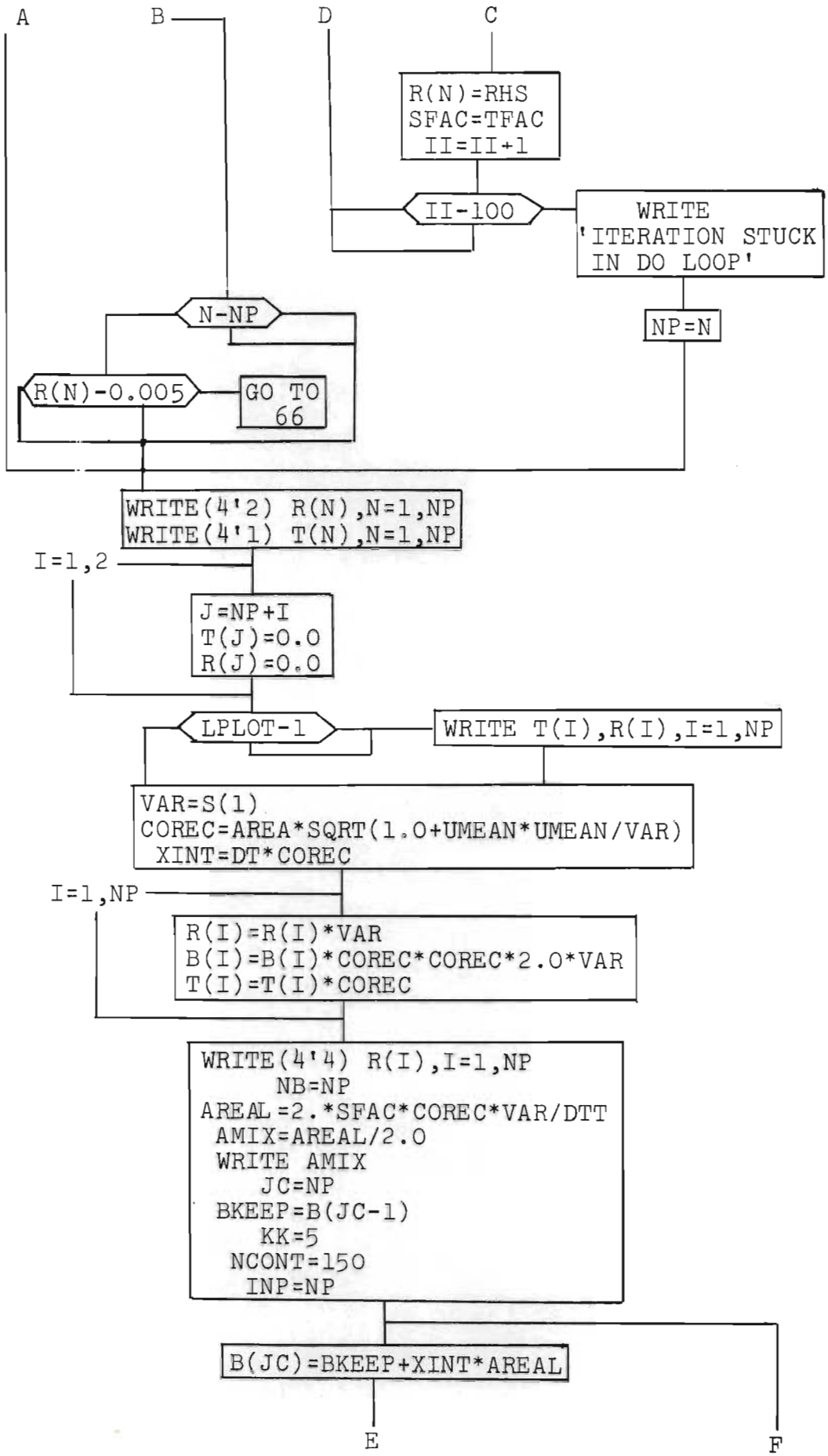
A
B
D
C
R(N)=RHS
SFAC=TFAC
II=II+1
II-100
WRITE
'ITERATION STUCK
IN DO LOOP'
NP=N
N-NP
R(N)-0.005
GO TO
66
WRITE(4'2) R(N),N=1,NP
WRITE(4'1) T(N),N=1,NP
I=1,2
J=NP+I
T(J)=0.0
R(J)=0.0
LPLOT-1
WRITE T(I),R(I),I=1,NP
VAR=S(1)
COREC=AREA*SQRT(1.0+UMEAN*UMEAN/VAR)
XINT=DT*COREC
I=1,NP
R(I)=R(I)*VAR
B(I)=B(I)*COREC*COREC*2.0*VAR
T(I)=T(I)*COREC
WRITE(4'4) R(I),I=1,NP
NB=NP
AREAL=2.*SFAC*COREC*VAR/DTT
AMIX=AREAL/2.0
WRITE AMIX
JC=NP
BKEEP=B(JC-1)
KK=5
NCONT=150
INP=NP
B(JC)=BKEEP+XINT*AREAL
E
F

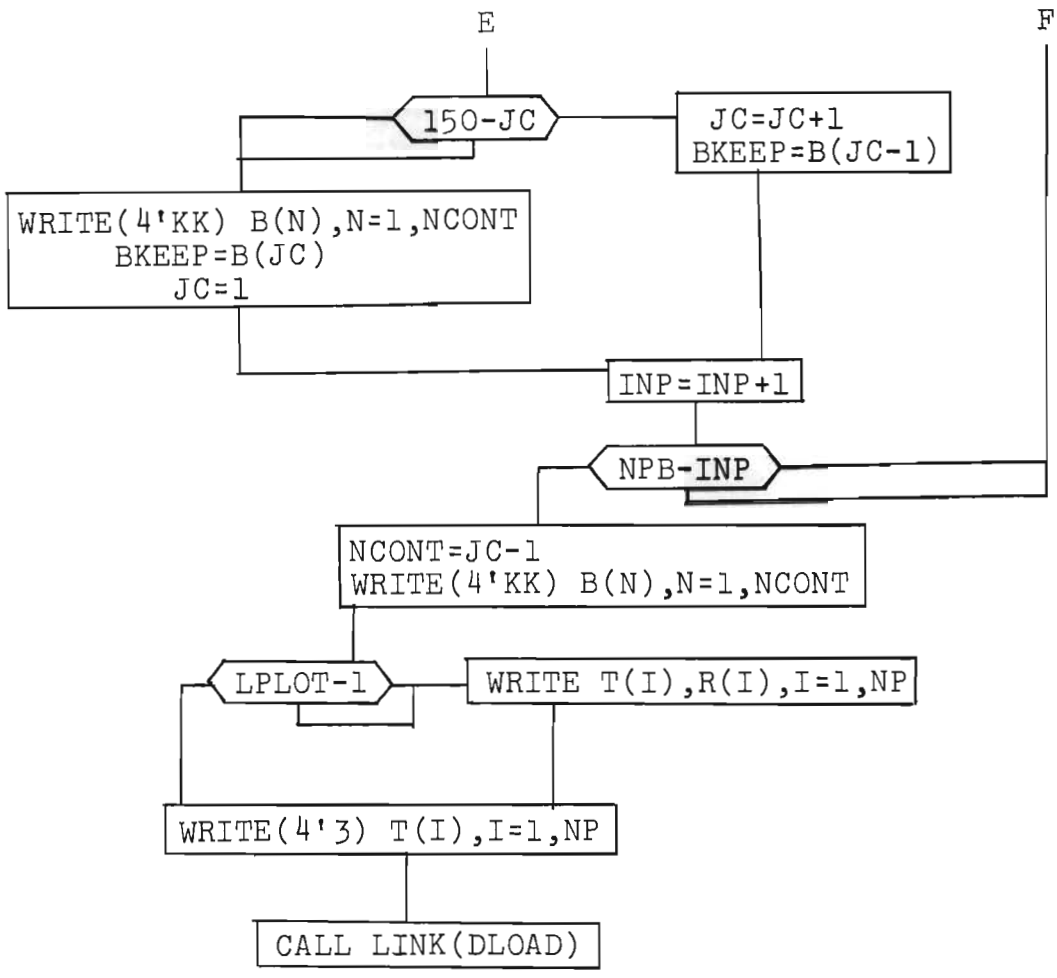
E
F
150-JC
JC=JC+1
BKEEP=B(JC-1)
WRITE(4'KK) B(N),N=1,NCONT
BKEEP=B(JC)
JC=1
INP=INP+1
NPB-INP
NCONT=JC-1
WRITE(4'KK) B(N),N=1,NCONT
LPLOT-1
WRITE T(I),R(I),I=1,NP
WRITE(4'3) T(I),I=1,NP
CALL LINK(DLOAD)

EIMRG.

```
EXTERNAL CQCRT
EXTERNAL ESMSQ
DIMENSION D(45)
COMMON VARI(150),Y(150),Z(5),TOL(5),MAX,B(5),NDROP,DTX,
       POS,NRED,IYPTR,ITPTR,NAME,NREG
DEFINE FILE 4(20,300,U,KK),7(40,300,U,JK)
```

PROGRAM:

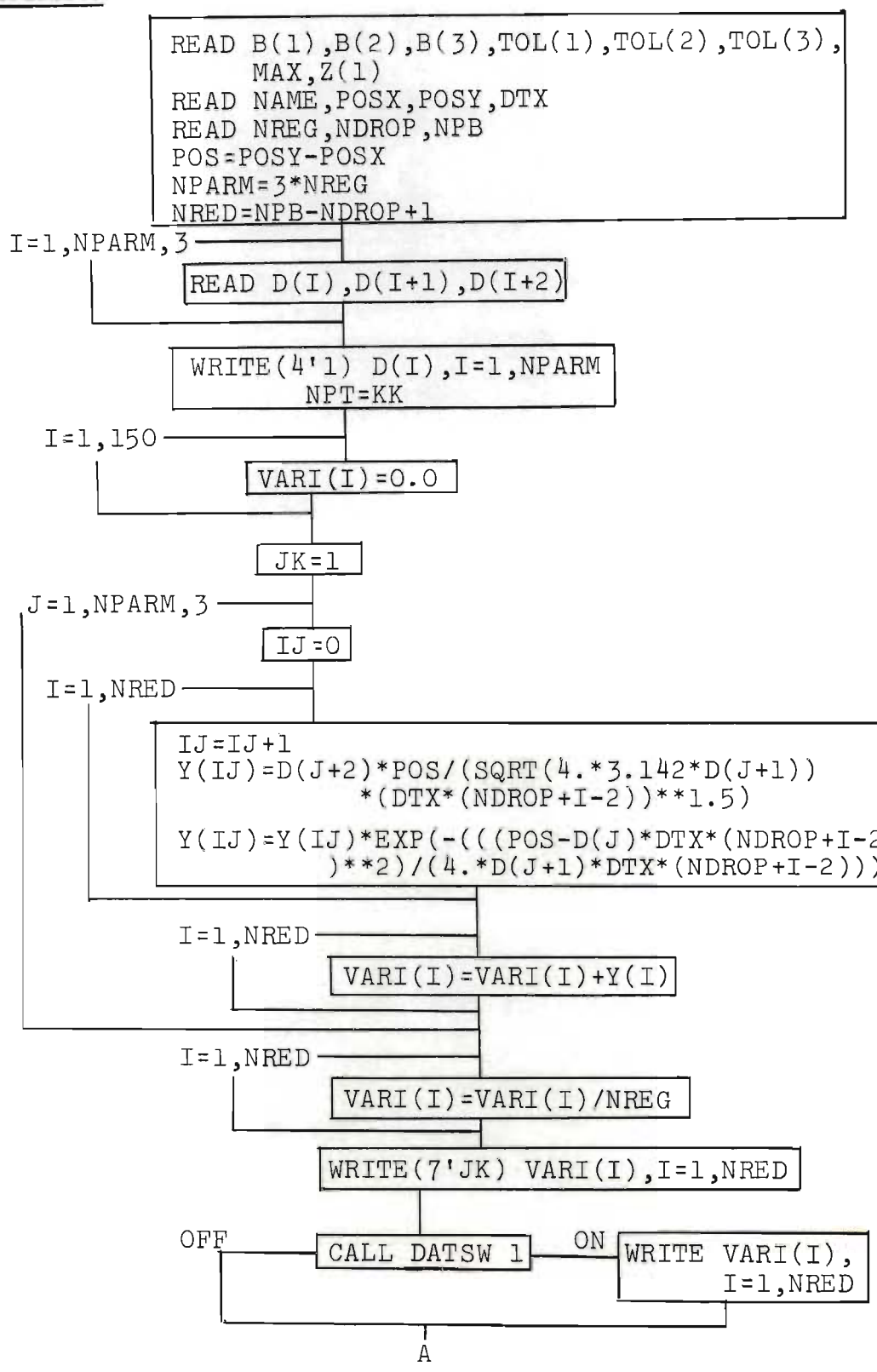

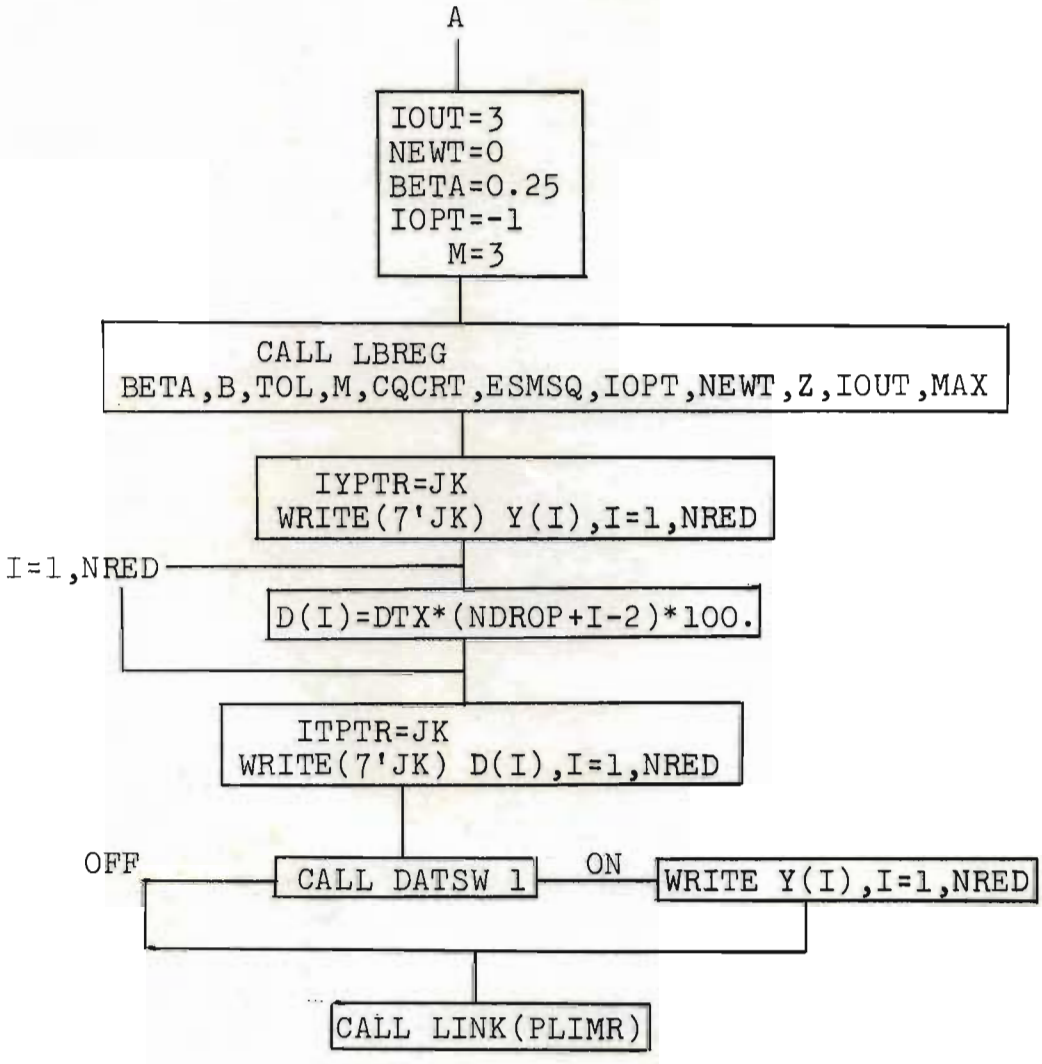
A
IOUT=3
NEWT=0
BETA=0.25
IOPT=-1
M=3
CALL LBREG
BETA,B,TOL,M,CQCRT,ESMSQ,IOPT,NEWT,Z,IOUT,MAX
IYPTR=JK
WRITE(7'JK) Y(I),I=1,NRED
I=1,NRED
D(I)=DTX*(NDROP+I-2)*100.
ITPTR=JK
WRITE(7'JK) D(I),I=1,NRED
OFF
CALL DATSW 1
ON
WRITE Y(I),I=1,NRED
CALL LINK(PLIMR)

SUBROUTINE ESMSQ.

```
DIMENSION C(10,11),Z(3),B(5)
COMMON VARI(150),Y(150),E(5),TOL(5),MAX,S(5),NDROP,DTX,
       POS,NRED,IYPTR,ITPTR,NAME,NREG
```

PROGRAM:

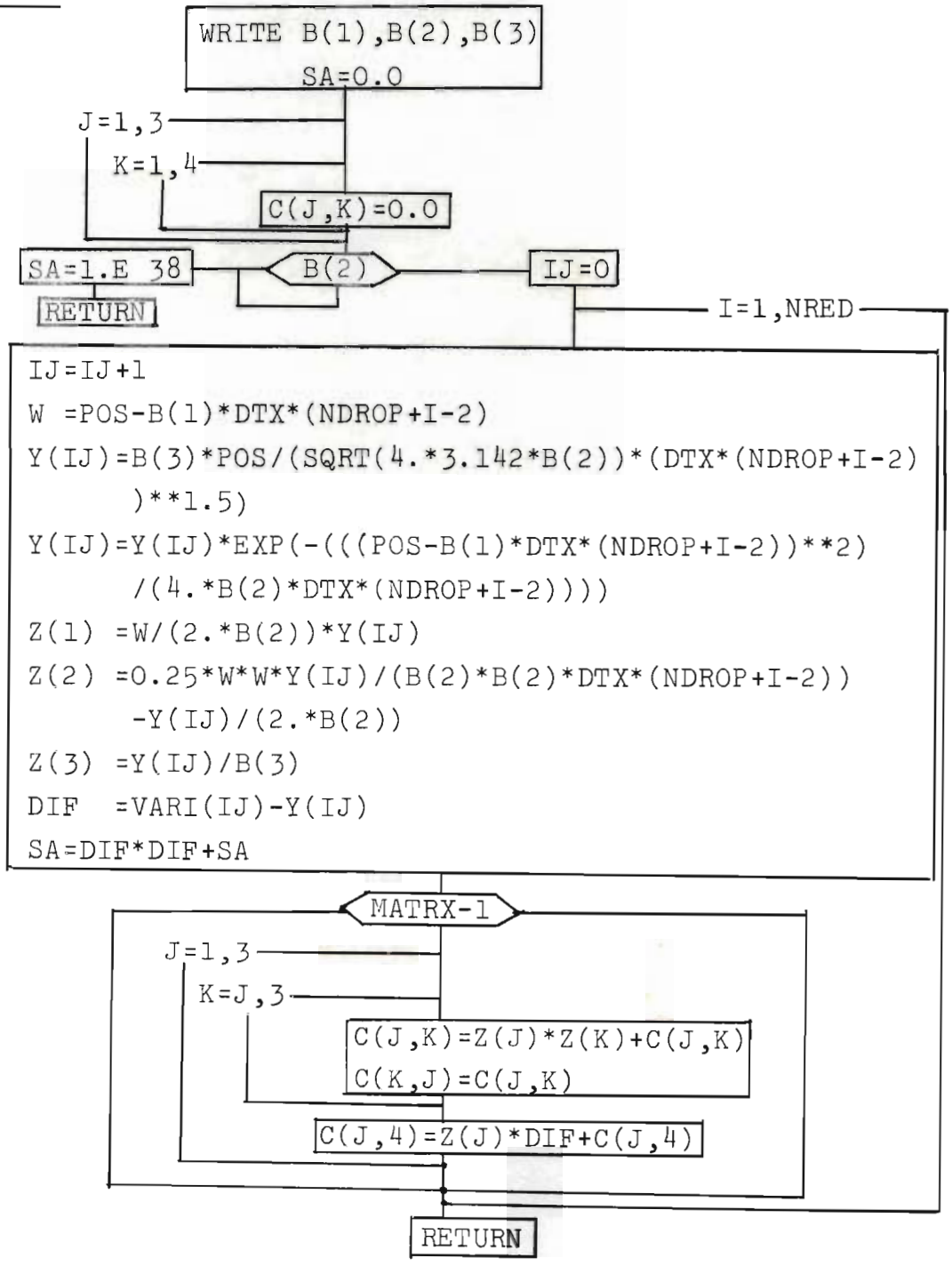

FRQAU.

```
DIMENSION E(100),F(100),G(100),R(100),X(100),S(100)
COMMON NAME,N,DELT,NDEC,EFILT,NPLOT,JA
DEFINE FILE 1(150,20,U,LUP),2(51,111,U,LREC),3(10,200,U,MUP)
```

PROGRAM:

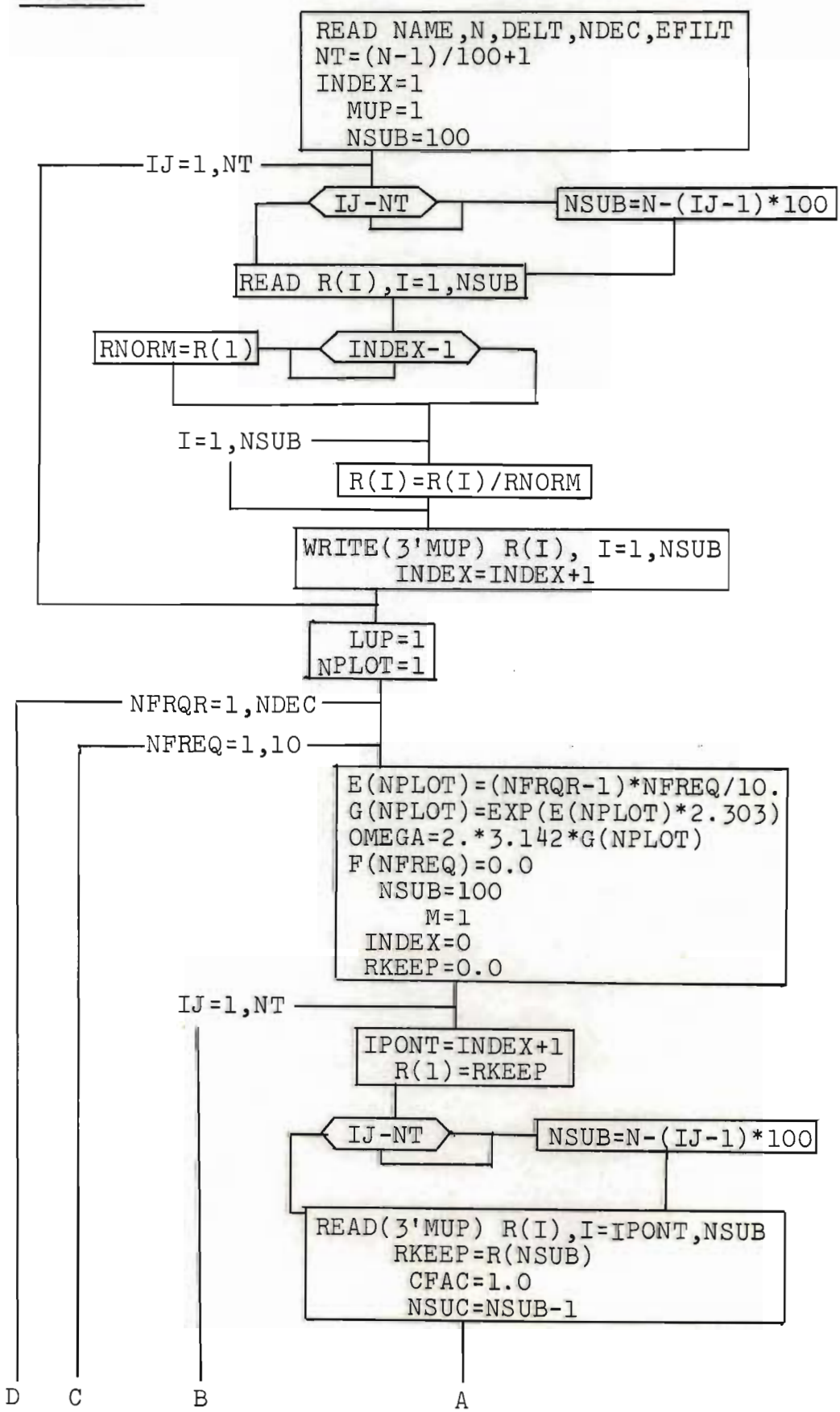

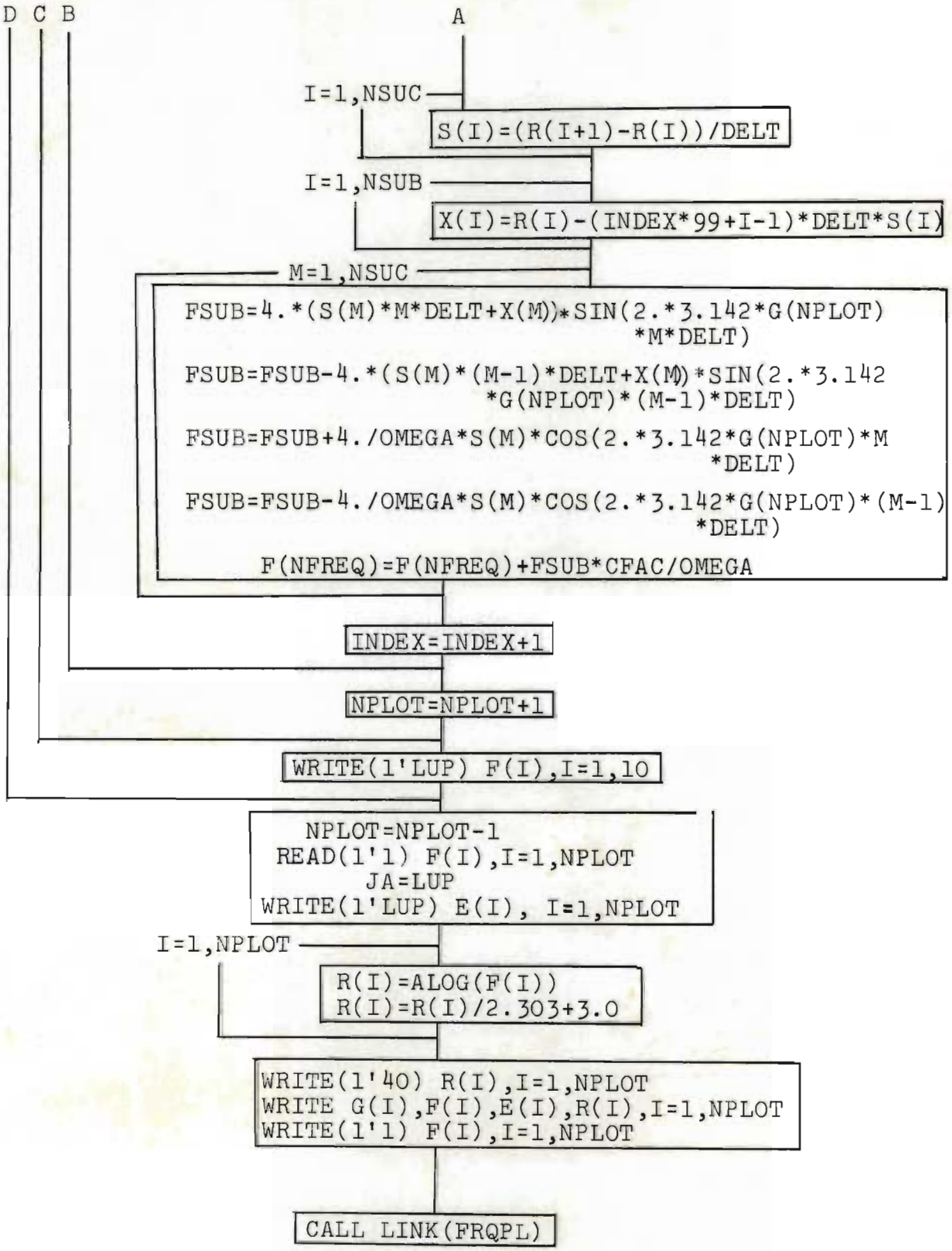
D C B
A
I=1,NSUC
S(I)=(R(I+1)-R(I))/DELT
I=1,NSUB
X(I)=R(I)-(INDEX*99+I-1)*DELT*S(I)
M=1,NSUC
FSUB=4.*(S(M)*M*DELT+X(M))*SIN(2.*3.142*G(NPLOT)*M*DELT)
FSUB=FSUB-4.*(S(M)*(M-1)*DELT+X(M))*SIN(2.*3.142*G(NPLOT)*(M-1)*DELT)
FSUB=FSUB+4./OMEGA*S(M)*COS(2.*3.142*G(NPLOT)*M*DELT)
FSUB=FSUB-4./OMEGA*S(M)*COS(2.*3.142*G(NPLOT)*(M-1)*DELT)
F(NFREQ)=F(NFREQ)+FSUB*CFAC/OMEGA
INDEX=INDEX+1
NPLOT=NPLOT+1
WRITE(1'LUP) F(I),I=1,10
NPLOT=NPLOT-1
READ(1'1) F(I),I=1,NPLOT
JA=LUP
WRITE(1'LUP) E(I), I=1,NPLOT
I=1,NPLOT
R(I)=ALOG(F(I))
R(I)=R(I)/2.303+3.0
WRITE(1'40) R(I),I=1,NPLOT
WRITE G(I),F(I),E(I),R(I),I=1,NPLOT
WRITE(1'1) F(I),I=1,NPLOT
CALL LINK(FRQPL)

APPENDIX 5.

INSTRUMENT SPECIFICATIONS.

1.) Hot-wire Anemometer Measurements.

(i) Flow Corporation Model 900, Constant-temperature hot-wire anemometer instrument.

Bridge circuit Model 900-1

Power Supply Model 900-2 fitted with Weston multirange voltmeter.

(ii) Amplifier and zero offset unit constructed in Electronics Dept., University of Natal.

(iii) Analog to digital convertor constructed in Electronics Dept., University of Natal.

(iv) Computer drum storage device for digital recording adapted from an ICT Model 1202 computer by the Electronics Dept., Univ. of Natal.

2.) The Tracer Dispersion Measurements.

(i) Beckman gas chromatograph valve from a Model GC-2A unit.

(ii) Surface-barrier detector electronic circuits:
R.I.D.L. Model 40-14 Bias supply & noise meter.
R.I.D.L. Model 30-21 Amplifier
R.I.D.L. Model 31-18 Charge-sensitive preamp.

(iii) Wavetek Model III signal generator for producing sawtooth wave.

(iv) Tektronix Model 535A Oscilloscope with an algebraic summing facility on the two input channels.

(v) Wollensak Fastax Model WF6, high-speed 16 mm. camera.

Wollensak Goose Control Unit, Model WF-358.

Kodak Tri-X film, developed for 30 mins. at 30°C in Kodak D-11 developer.

The velocity calibrations were performed with a Lambrecht Pitot tube (ca. 2.5 mm.O.D.,0.8 mm. dia. impaction area) and a Casella water micromanometer reading to within 0.05 mm. H_2O.

All computer programs were written for the IBM 1130 computer with approximately 4000 word available core storage.